SIGGRAPH 2001 COURSE 15

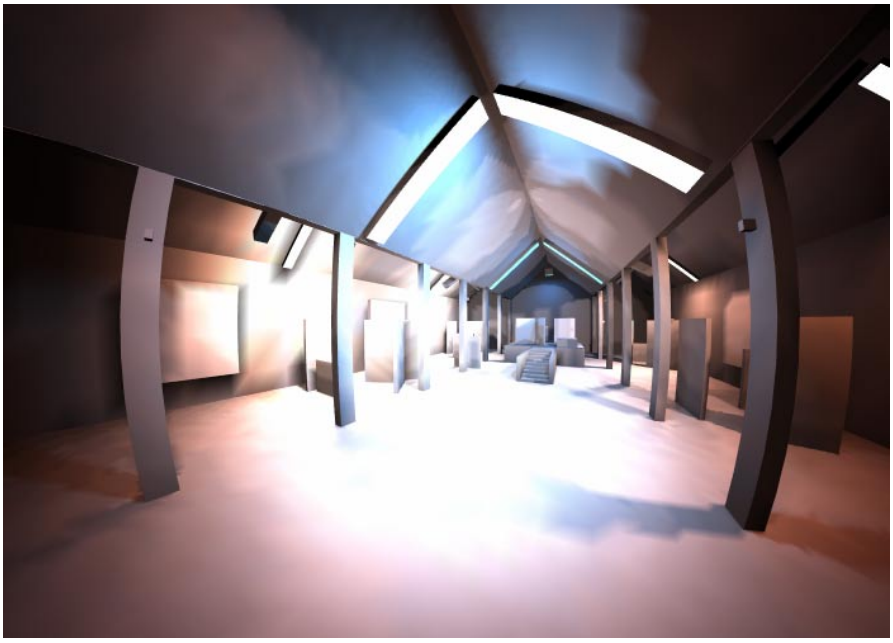

Visualizing Relativity

Course Speakers

1. **Andrew J. Hanson**
   hanson@cs.indiana.edu
2. **Daniel Weiskopf**
   weiskopf@informatik.uni-stuttgart.de

Abstract

This course is intended for attendees with simultaneous interests in the concepts of relativistic physics and in the practical extension of computer graphics methods to relativity. The first half of the course will focus on how relativistic effects can be intuitively understood starting from extremely simple Euclidean 2D geometry. The concept of object vertices as world-lines moving in a space that can be mixed with time is explained first in this context. Relativistic imaging is then explained in three dimensions, two space plus one time, exploiting analogies with Euclidean 3D geometry. Finally, four-dimensional spacetime is introduced to make the transition to the real world simulations treated in the final part of the course.

The second half will concentrate on recent advances in visualization and photorealistic simulation of relativistic scenes and phenomena using computer graphics to show features that could never be seen in real life at human time and space scales. Properties of light under the extreme conditions of both special and general relativity will be discussed, including changes of color, intensity, and direction of light, and gravitational light bending. A survey of state-of-the-art rendering techniques will be presented and selected animations produced using recently developed methods for relativistic rendering will be shown. An introduction to user interaction in special relativistic virtual environments will conclude the presentation.

Speaker Contact Information

1. **Andrew J. Hanson**
   Department of Computer Science
   Lindley Hall 215
   Indiana University
   Bloomington, Indiana 47405
   hanson@cs.indiana.edu
   http://www.cs.indiana.edu/~hanson

2. **Daniel Weiskopf**
   University of Stuttgart
   Visualization and Interactive Systems Group
   Breitwiesenstr. 20-22
   70565 Stuttgart
   Germany
   weiskopf@informatik.uni-stuttgart.de
   http://wwwvis.informatik.uni-stuttgart.de/~weiskopf

Speaker Biographies

Andrew J. Hanson is a professor of computer science at Indiana University, and has regularly taught courses in computer graphics, computer vision, and scientific visualization. He received a BA in chemistry and physics from Harvard College in 1966 and a PhD in theoretical physics from MIT in 1971. Before coming to Indiana University, he did research in theoretical physics at the Institute for Advanced Study, Stanford, and Berkeley, and then in computer vision at the SRI Artificial Intelligence Center in Menlo Park, CA. He has published in IEEE Computer, CG&A, TVCG, ACM Computing Surveys, and has over a dozen papers in the IEEE Visualization Proceedings. He has also contributed three articles to the Graphics Gems series dealing with user interfaces for rotations and with techniques of N-dimensional geometry. Previous experience with conference tutorials includes a Siggraph '98 tutorial on N-dimensional graphics, a Visualization '98 course on Clifford Algebras and Quaternions, and a tutorial on Visualizing Quaternions presented at both Siggraph '99 and Siggraph 2000. Major research interests include scientific visualization, machine vision, computer graphics, perception, and the design of interactive user interfaces for virtual reality and visualization applications. Particular visualization applications currently being studied include an astrophysical treatment of the local galactic neighborhood of the sun, the exploitation of constrained navigation for visualization environments, and applications of graphics in dimensions greater than three to mathematics and theoretical physics.

Daniel Weiskopf is researcher and teacher of computer science at the Visualization Group (led by Prof. Thomas Ertl) at the University of Stuttgart (Germany). He studied physics at the University of Tübingen (Germany), San Francisco State University, and the University of California at Berkeley. He received a Diplom (M.S.) in physics from the University of Tübingen in 1997 and a Ph.D. in theoretical astrophysics in 2001. Daniel Weiskopf authored several articles on special and general relativistic visualization. In addition to his research on relativistic visualization, he is interested in communicating complex physical concepts to the public via visualization: several of his films were featured at major European festivals of scientific animations and TV broadcasts; he is a scientific collaborator in a couple of film projects; his visualizations have been included in a number of popular-science publications. Major research interests include scientific visualization, virtual reality, interaction techniques, special and general relativity.

Course Schedule

1. **13:30–14:20 Introduction (Hanson)**
   (a) Motivation
   (b) 2D Euclidean vs Minkowski: Build Relativity concepts from 2D Graphics
   (c) Spacetime points and the twin paradox
   (d) Relativistic objects, cameras, and imaging
2. **14:20–15:00 Visualization Methods in 3D and 4D (Hanson)**
   (a) 3D = 2 Space + 1 Time: Transformations
   (b) Multiple transformations and Thomas Precession
   (c) Aberration of Light
   (d) Object Viewing: Occlusion, IBR, Terrell effect
   (e) 4D = 3 space + 1 time
3. **15:00–15:15 Break**
4. **15:15–15:50 Light (Weiskopf)**
   (a) Fundamentals (electromagnetic wave, photons, plenoptic function)
   (b) Relativistic effects on light (aberration, Doppler and searchlight effects, transformation of the plenoptic function)
   (c) General relativistic effects (bending light by gravity, gravitational lensing)
5. **15:50–16:35 Rendering (Weiskopf)**
   (a) Special relativistic rendering methods (polygon rendering, radiosity, ray tracing, image-based rendering, texture-based rendering)
   (b) General relativistic rendering (ray tracing, image-based rendering)
6. **16:35–16:45 Interaction Techniques (Weiskopf)**
   (a) Accelerated motion of an observer in special relativity
   (b) Interactive virtual environment
7. **16:45–16:50 Conclusion (Weiskopf)**
8. **16:50–17:00 Questions and Answers (Hanson, Weiskopf)**

Table of Contents

Visualizing Relativity

Andrew J. Hanson
Indiana University
and
Daniel Weiskopf
University of Stuttgart

Siggraph 2001 Tutorial

GRAND PLAN

I: Introduction: *Hanson, 50 min*
II: Visualization Methods: *Hanson, 40 min*
< 15 minute Break >
III: Light: *Weiskopf, 30 min*
IV: Rendering: *Weiskopf, 30 min*
V: Interaction Techniques: *Weiskopf, 30 min*
VI: Conclusion and Questions: *15 min*

I: Introduction to Special Relativity

- **Motivation**
- **2D Euclidean vs Minkowski:** Build Relativity concepts from 2D Graphics concepts.
- **Spacetime Points and the Twin Paradox.**
- **Relativistic Objects and Cameras:** What happens to graphics modeling near the speed of light.

II: Visualization Methods in 3D and 4D

- **2 Space + 1 Time:** Transformations.
- **Rolling the Relativistic Ball**: Thomas Precession
- **Aberration of Light:**
- **Object Viewing:** Occlusion, IBR, and the Terrell Cube
- **4D = 3 space + 1 time:**

III: Light

- **Directions in Relativity**
- **Frequency Transformations**
- **Relativistic Radiance Transforms**
- **Bending Light with General Relativity**

IV: Rendering

- **From the Z buffer to the T buffer**
- **Special Relativistic Ray Tracing**
- **Texture and Relativistic IBR**
- **Gravitational Lensing**

V: Interaction Techniques

VI: Conclusion

Visualizing Relativity

Part I: Introduction to Special Relativity

Andrew J. Hanson
Indiana University

I: Introduction to Special Relativity

- **Motivation**
- **2D Euclidean vs Minkowski:** Build Relativity concepts from 2D Graphics concepts.
- **Spacetime Points and the Twin Paradox.**
- **Relativistic Objects and Cameras:** What happens to graphics modeling near the speed of light.

Motivation

WHY ARE YOU HERE? Let's guess:

⇒ You know about Graphics

⇒ You know about Visualization

⇒ You DO NOT know much about Relativity.

∗ You WOULD LIKE to know how these three things are CONNECTED. . .

Motivation, contd.

What is Graphics?

- **Graphics:** is the art of *simulating* the *physics* of the interaction of material and light.

Motivation, contd.

What is Visualization?

- **Visualization:** is the art of *creating insights* into non-self-explanatory data and geometry using graphics.

Motivation, contd.

What is Relativity?

- **Relativity:** is the mathematics describing the interaction of material and light UNDER EXTREME PHYSICAL CONDITIONS.

Therefore, this course is the logical extension of everything graphicists and visualizers *already do!*

Euclidean Transformations

We begin with what we all know — 2D Rotations.

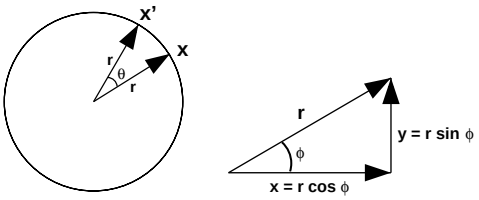

$$x' = x\cos\theta - y\sin\theta$$
$$y' = x\sin\theta + y\cos\theta$$

Euclidean Transformations, contd.

Explicit 2D rotations are realized by a 2D matrix

$$R(\theta) = \begin{bmatrix} \cos\theta & -\sin\theta \\ \sin\theta & \cos\theta \end{bmatrix}$$

where $R(\theta)\begin{bmatrix} 1 & 0 \\ 0 & 1 \end{bmatrix} R(\theta)^t = \begin{bmatrix} 1 & 0 \\ 0 & 1 \end{bmatrix}$

because $\boxed{(\cos\theta)^2 + (\sin\theta)^2 = 1}$

Euclidean Transformations, contd.

Main feature: The *Radius* is unchanged under $[\mathrm{x}'] = R(\theta)\cdot[\mathrm{x}]$:

$$r = \sqrt{x^2 + y^2} = \sqrt{x'^2 + y'^2}$$

In other words, Euclidean distances do not vary under the action of rotations.

Euclidean Transformations, contd.

Similarly, the *Euclidean Inner Product* is unchanged under $[\mathrm{x}'] = R(\theta)\cdot[\mathrm{x}]$, $[\tilde{\mathrm{x}}'] = R(\theta)\cdot[\tilde{\mathrm{x}}]$

$$\mathrm{x}\cdot\tilde{\mathrm{x}} = \mathrm{x}'\cdot\tilde{\mathrm{x}}' = \begin{bmatrix} x & y \end{bmatrix}\begin{bmatrix} 1 & 0 \\ 0 & 1 \end{bmatrix}\begin{bmatrix} \tilde{x} \\ \tilde{y} \end{bmatrix}$$
$$= x\tilde{x} + y\tilde{y} = r\tilde{r}\cos(\phi - \tilde{\phi})$$

In other words, Euclidean angles do not vary under the action of rotations.

Euclidean Transformations, contd.

Properties we know and love:

- Rotations have a **fixed point** at origin.
- Rotations leave **segment lengths and inner products** unchanged.
- Rotations are **orthogonal** $\Rightarrow\ R\,I\,R^t = I$
- **NOTE:** The PROJECTIONS may change, yet we "know" the segment length is constant.

Lorentz Transformations

Special Relativity is just "Rotations with hyperboloids instead of circles."

Euclidean Rotations $\Rightarrow$ Lorentz Transformations.

Let x be a space interval and t be a time interval:

$$\begin{aligned} x' &= x\cosh\xi + t\sinh\xi \\ t' &= x\sinh\xi + t\cosh\xi \end{aligned}$$

Lorentz Transformations, contd.

When we apply this transform to a vector from the origin to a point (x,t), the new point (x',t') lies on a hyperboloid instead of a circle!

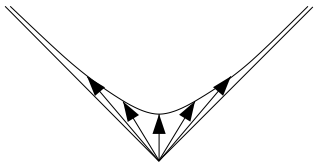

Lorentz Transformations, contd.

Explicit 1-space + 1-time Lorentz transformations are realized by a 2D "boost" matrix

$$B(\xi) = \begin{bmatrix} \cosh\xi & \sinh\xi \\ \sinh\xi & \cosh\xi \end{bmatrix} .$$

where

$$B(\xi)\begin{bmatrix} 1 & 0 \\ 0 & -1 \end{bmatrix}B(\xi)^t = \begin{bmatrix} 1 & 0 \\ 0 & -1 \end{bmatrix}$$

$B(\xi)$ preserves the length of **proper time** due to $(\cosh\xi)^2 - (\sinh\xi)^2 = 1$

Lorentz Transformations, contd.

Compare Euclidean and Lorentz functions:

$$\cos\theta = \frac{1}{2}\left(e^{i\theta} + e^{-i\theta}\right) \qquad \sin\theta = \frac{1}{2i}\left(e^{i\theta} - e^{-i\theta}\right)$$

$$\cos^2 + \sin^2 = 1$$

$$\cosh\xi = \frac{1}{2}\left(e^{\xi} + e^{-\xi}\right) \qquad \sinh\xi = \frac{1}{2}\left(e^{\xi} - e^{-\xi}\right)$$

$$\cosh^2 - \sinh^2 = 1$$

where the MINUS SIGN is all-important!

Lorentz Transformations, contd.

Main feature of Lorentz-transformed vectors is very close to rotations: Instead of the *Radius*, depending on sign inside root,

- THE PROPER TIME is unchanged.

$$\tau = \sqrt{t^2 - x^2} = \sqrt{t'^2 - x'^2}$$

- Alternatively, THE PROPER DISTANCE is unchanged.

$$\delta = \sqrt{x^2 - t^2} = \sqrt{x'^2 - t'^2}$$

Lorentz Transformations, contd.

- . . . and instead of the *Euclidean dot product*, the THE MINKOWSKI SPACE INNER PRODUCT

$$\mathrm{x}\cdot\tilde{\mathrm{x}} = \begin{bmatrix} x & t \end{bmatrix}\begin{bmatrix} 1 & 0 \\ 0 & -1 \end{bmatrix}\begin{bmatrix} \tilde{x} \\ \tilde{t} \end{bmatrix} = x\tilde{x} - t\tilde{t}$$

IS UNCHANGED.

Lorentz Transformations, contd.

Now let's visualize a typical invariant:

$$\tau^2 = t^2 - x^2 = t'^2 - x'^2$$

describes a hyperbola, $x = 0 \Rightarrow t = \tau$:

$$x \neq 0 \;\Rightarrow\; t = \sqrt{\tau^2 + x^2}$$

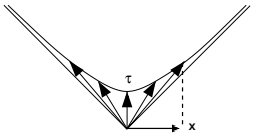

Lorentz Transformations, contd.

An alternative view showing geometry of proper time, emphasizing *interval property*.

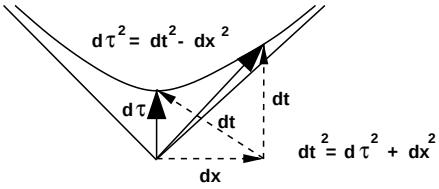

Lorentz Transformations, contd.

What *are* $\cosh\xi$ and $\sinh\xi$ anyway?

Suppose $t_0 = 1.0$ and $x_0 = 0$:

$$\begin{aligned} dx &= x_0\cosh\xi + t_0\sinh\xi = \sinh\xi \\ dt &= x_0\sinh\xi + t_0\cosh\xi = \cosh\xi. \end{aligned}$$

Lorentz Transformations, contd.

Thus $(dx/dt) = \sinh\xi/\cosh\xi$ is the *inverse slope* of the interval $(0.0, d\tau)$ after the transformation:

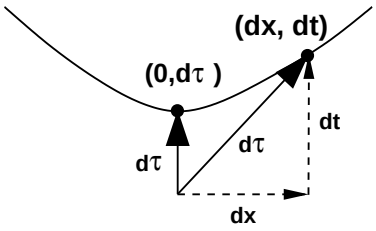

Lorentz Transformations, contd.

We identify this slope as the

$$\text{velocity} = v = \frac{\sinh\xi}{\cosh\xi} = \tanh\xi$$

Simple algebra and $\cosh^2 - \sinh^2 = 1$ give us:

$$\begin{aligned} \cosh\xi &= \frac{1.0}{\sqrt{1.0 - v^2}} \\ \sinh\xi &= \frac{v}{\sqrt{1.0 - v^2}} \end{aligned}$$

Lorentz Transformations and velocity of light

OOps! Where did the velocity of light go?

Simple answer: we set it to unity to make (x, t) plots work!

Better answer: Replace $v \Rightarrow v/c$ whenever you need it.

What happens as $c \Rightarrow \infty$?? This is ORDINARY GALILEAN SPACETIME, where NO mixing of space and time can occur!

Lorentz Transformations and velocity of light

Check Galilean limit: as $\boxed{c \Rightarrow \infty}$

$$\cosh\xi = \frac{1.0}{\sqrt{1.0-(v/c)^2}} \Rightarrow 1$$

$$\sinh\xi = \frac{v/c}{\sqrt{1.0-(v/c)^2}} \Rightarrow 0$$

So we get $B(\xi) \Rightarrow$ **identity matrix** and the effects of the Lorentz transform disappear!

Lorentz Transformations, contd

Note: Euclidean intervals do not care if you start with $(x,\ y) = (r,\ 0)$ or $(x,\ y) = (0,\ r)$ before you rotate: $\Rightarrow$ r is always positive.

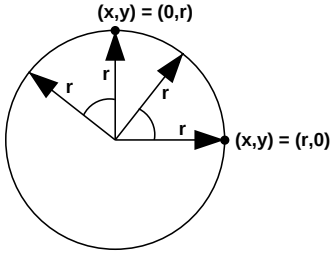

Lorentz Transformations, contd

Relativistic intervals **do care**:

$(x,\ t) = (0,\ \tau),\ \ t^2 - x^2 > 0$ **= Timelike interval**
$(x,\ t) = (\tau,\ \tau),\ \ t^2 - x^2 \equiv 0$ **= Lightlike interval**
$(x,\ t) = (\delta,\ 0),\ \ t^2 - x^2 < 0$ **= Spacelike interval**

Furthermore, these distinctions are **invariant** under the Lorentz transform!

$x' = x\cosh\xi + t\sinh\xi \qquad t' = x\sinh\xi + t\cosh\xi$

Lorentz Transformations for timelike intervals

Define a **timelike interval**, with $x = 0.0$ and $t = 1.0$, and transform:

$x' = x\cosh\xi + t\sinh\xi \qquad t' = x\sinh\xi + t\cosh\xi$

$x' = \sinh\xi \qquad t' = \cosh\xi$

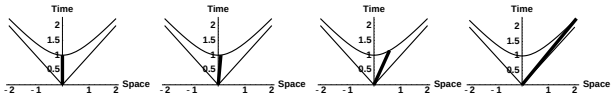

$v = 0.0$ $v = 0.1$ $v = 0.5$ $v = 0.9$

Lorentz Transformations for time-like intervals

Let $t = 1.0$, $x = 0.0$ as before, but let **velocity be negative:**

$x' = x\cosh\xi - t\sinh\xi \qquad t' = -x\sinh\xi + t\cosh\xi$

$x' = -\sinh\xi \qquad t' = \cosh\xi$

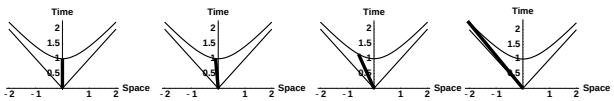

$v = 0.0$ $v = -0.1$ $v = -0.5$ $v = -0.9$

Lorentz Transformations: different velocity signs

You already know this difference:

Euclidean: **angle** > 0 means	**object interval is rotated**
Euclidean: **angle** < 0 means	**viewer is rotated**
Lorentz: **velocity** > 0 means	**object interval is boosted**
Lorentz: **velocity** < 0 means	**viewer is boosted**

Lorentz Transformations for lightlike intervals

Define a lightlike interval,
with $x = 1.0$ and $t = 1.0$,
and observe that $x^2 - t^2 = x'^2 - t'^2 \equiv 0$:

$$x' = \cosh\xi + \sinh\xi \qquad t' = \sinh\xi + \cosh\xi$$

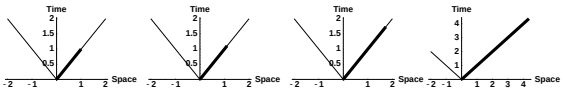

$v = 0.0$ $v = 0.1$ $v = 0.5$ $v = 0.9$

Lorentz Transformations for spacelike intervals

Define a spacelike interval:
with $(x = 1.0,\ t = 0) \Rightarrow x^2 - t^2 > 0$
so $x' = \cosh\xi,\ t' = \sinh\xi$.

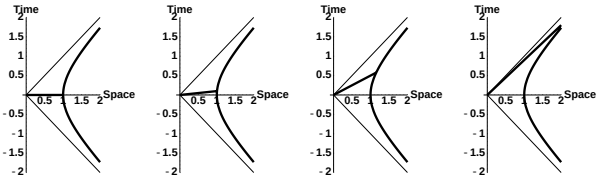

$v = 0.0$ $v = 0.1$ $v = 0.5$ $v = 0.9$

Lorentz Transformations: fixed points

Every graphicist knows that $\boxed{x' = R \cdot x}$ has a
fixed point at $x = 0$.

Relativity is the same: translate to $t = 0.0$ and $x = 0.0$ before transforming:

$$x' = x_0 + (x - x_0)\cosh\xi + (t - t_0)\sinh\xi$$
$$t' = t_0 + (x - x_0)\sinh\xi + (t - t_0)\cosh\xi$$

Lorentz Transformations: fixed points

Transform with **Lorentz Fixed Point at** $x_0 = (x_0,\ t_0)$:

$$\begin{bmatrix} x' \\ t' \end{bmatrix} = T(+x_0, +t_0) \cdot B(\xi) \cdot T(-x_0, -t_0) \cdot \begin{bmatrix} x \\ t \end{bmatrix}$$

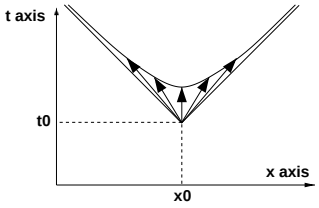

Lorentz Transformations: whole plane

Every point in the (x, t) plane Lorentz transforms to one light cone or the other along a hyperboloid as $v \to \pm 1$:

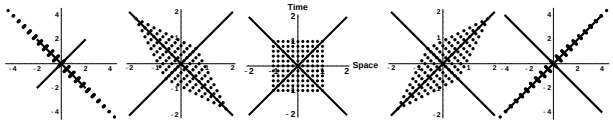

$v = -0.9$ $v = -0.5$ $v = 0.0$ $v = 0.5$ $v = 0.9$

Lorentz Transformations: world lines

Every timelike line in the (x, t) plane Lorentz transforms to a slanted line as $v \to 1$:

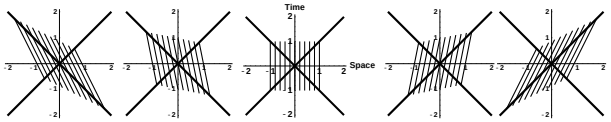

$v = -0.5$ $v = -0.2$ $v = 0.0$ $v = 0.2$ $v = 0.5$

What is a Minkowski frame?

Let $\hat{\mathrm{x}}_0, \hat{\mathrm{t}}_0$ be the basis vectors of a Minkowski-space frame:

- **Space-Like:** $\hat{\mathrm{x}}_0 = (1, 0)$ whose *length* is $\hat{\mathrm{x}}_0 \cdot \hat{\mathrm{x}}_0 = 1$.
- **Time-Like:** $\hat{\mathrm{t}}_0 = (0, 1)$ whose *length* is $\hat{\mathrm{t}}_0 \cdot \hat{\mathrm{t}}_0 = -1$.

What is a Minkowski frame?

Compare a Euclidean frame to a Minkowski frame:

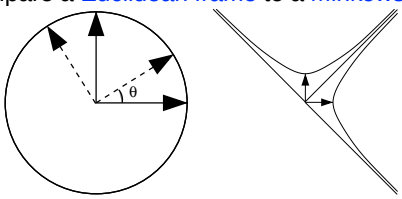

The Euclidean axes stay at right angles under rotations. What happens to the Minkowski axes under Lorentz transforms??

How do the frame axes transform?

The usual **Three Othonormality Conditions** are preserved **in any coord system.**

- **Space-Like:** $\hat{\mathrm{x}}_0 = (1, 0)$ has *unit length*: $\hat{\mathrm{x}}_0 \cdot \hat{\mathrm{x}}_0 = 1$.
- **Time-Like:** $\hat{\mathrm{t}}_0 = (0, 1)$ has *unit length*: $\hat{\mathrm{t}}_0 \cdot \hat{\mathrm{t}}_0 = -1$.
- **Orthogonality:** $\hat{\mathrm{x}}_0 = (1, 0)$ and $\hat{\mathrm{t}}_0 = (0, 1)$ have *vanishing inner product*: $\hat{\mathrm{t}}_0 \cdot \hat{\mathrm{x}}_0 = 0$.

Frame axis transforms, contd

The **picture** seems to show axes coming together, but **orthonormality** is automatically **preserved**:

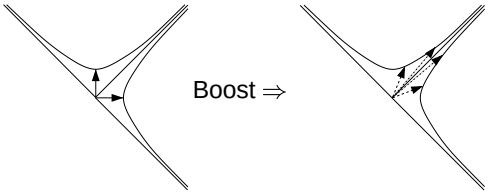

Lorentz Frame Axes

If we did not know about $\cosh^2 \xi - \sinh^2 \xi = 1$, we might represent the frame differently, e.g., as:

$$\begin{bmatrix} \hat{\mathrm{x}}_0 & \hat{\mathrm{t}}_0 \end{bmatrix} = \begin{bmatrix} A & B \\ B & A \end{bmatrix} .$$

where the constraint $A^2 - B^2 = 1$ guarantees orthonormality in the the Minkowski space; the columns are orthogonal, and of length +1 and -1, respectively.

Lorentz Frame axes, contd

As for 2D rotations, we can define a **double-valued** parameterization (a, b) of the frame:

$$\begin{bmatrix} \hat{\mathrm{x}}_0 & \hat{\mathrm{t}}_0 \end{bmatrix} = \begin{bmatrix} A & B \\ B & A \end{bmatrix} = \begin{bmatrix} a^2 + b^2 & 2ab \\ 2ab & a^2 + b^2 \end{bmatrix} .$$

where $A^2 - B^2 = 1$ IF $a^2 - b^2 = 1$, and (a, b) is precisely the *same frame* as $(-a, -b)$.

These are *hyperbolic half angle* formulas, $a = \cosh(\xi/2)$, $b = \sinh(\xi/2)$!

1+1 "Quaternion" Frames!

Differentiating *both* $\dot{\bar{x}}_0$ and $\dot{\bar{t}}_0$, our eqns reduce to

$$\begin{bmatrix} \dot{a} \\ \dot{b} \end{bmatrix} = \frac{1}{2} \begin{bmatrix} 0 & \kappa \\ \kappa & 0 \end{bmatrix} \cdot \begin{bmatrix} a \\ b \end{bmatrix}$$

This is the square root *of Lorentz frame equations.*

(Quaternion frame equations have $\begin{bmatrix} 0 & -\kappa \\ \kappa & 0 \end{bmatrix}$.)

Lorentz Transformations, summarized.

Properties we **will** know and love:

- Boosts have **fixed point** at origin.
- Boosts leave **proper times, proper lengths, and Minkowski inner products** unchanged.
- Boosts are **orthogonal on a negative signature identity matrix** $\Rightarrow B \begin{bmatrix} 1 & 0 \\ 0 & -1 \end{bmatrix} B^t = \begin{bmatrix} 1 & 0 \\ 0 & -1 \end{bmatrix}$
- **As in Euclidean space:** The PROJECTED PARTS OF A VECTOR may change, yet we know the inner product lengths are CONSTANT.

What is an object?

In Relativity, a point object is a **world line**.

- *Standing still* at one point: world line still ticks away: Equation $\Rightarrow$ $(\delta = \text{const},\ t)$.
- *Moving curve* $x(t)$ must obey $|dx/dt| < 1$.
- **Communication** can only occur using light or slower media.
- So all possibility of **image data** is restricted essentially to rays with paths having $|dx/dt| = 1$.

Point Objects . . .

What do point objects look like in spacetime?

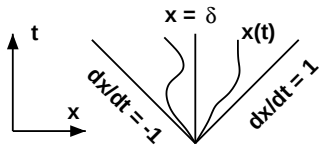

Relativistic equations have **space and time** components, so think of a **static point** as the **parametric line** $(\delta,\ t)$.

Twin Paradox

A **world line** represents an object, e.g., a person, evolving in time, possibly moving through space.

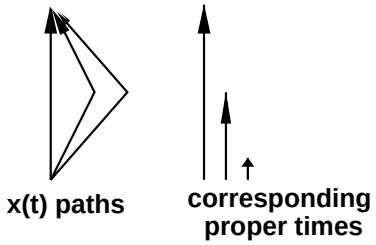

Twin Paradox, contd.

Consider **two twins**, one living on path P_1, the other on path P_2. Their ages **in any frame** are the *proper lengths* of their world lines:

$$\textbf{Age 1} = T_1 = \int_{P_1} d\tau$$
$$\textbf{Age 2} = T_2 = \int_{P_2} d\tau$$

Twin Paradox, contd.

Graphical picture of twin ages: go to rest frame of each leg of journey to visualize true proper time:

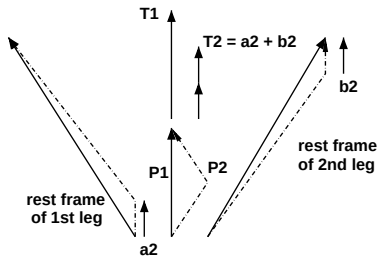

Time Dilation of Point Clocks

Since the point $(0, \tau)$ is transformed to $x = \tau \sinh \xi$, $t = \tau \cosh \xi$, we can solve for τ, yielding $x = vt$, so the **invariant proper time** can be written:

$$\tau = \sqrt{t^2 - x^2} = t\sqrt{1 - v^2}$$

Since the measured time $t = \tau/\sqrt{1 - v^2} > \tau$, this is **Time Dilation**.

Time Dilation, contd.

Now visualize change in apparent tick rate of **moving clock**, as well as **how you would measure it**:

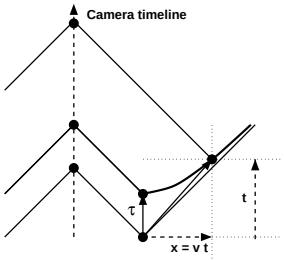

Lorentz Contraction of Spacelike Intervals

For spacelike intervals, the situation is trickier. Let

$$x_1(t) = (0, t)$$
$$x_2(t) = (\delta, t)$$

be the ends of a line segment.

Lorentz Contraction, contd.

Under a Lorentz transform, the origin stays fixed, but

$$x_2'(t) = (X(t), T(t))$$
$$= (\delta \cosh \xi + t \sinh \xi, \delta \sinh \xi + t \cosh \xi)$$

becomes a curve with the old $(\delta, 0)$ pushed far up the hyperboloid to

$$X(0) = \delta \cosh \xi \qquad T(0) = \delta \sinh \xi$$

for large $v = \sinh \xi / \cosh \xi$.

Lorentz Contraction, contd.

We must take the line $(X(t), T(t)$ and **extrapolate backwards to** $T(t) = 0$ to find the new interval as seen by the observer. Solving

$$T(t) = \delta \sinh \xi + t \cosh \xi = 0$$

for $t = t_0$, we find

$$t_0 = -\delta \sinh \xi / \cosh \xi$$

Lorentz Contraction, contd.

Thus t_0 is **negative** and we must have a **length reduction**.

The numbers come out to be:

$$\begin{aligned} X(t_0) &= \delta\cosh\xi + t_0\sinh\xi \\ &= \delta\cosh\xi - \delta\frac{\sinh^2\xi}{\cosh\xi} \\ &= \frac{\delta}{\cosh\xi}\left(\cosh^2\xi - \sinh^2\xi\right) \\ &= \frac{\delta}{\cosh\xi} = \delta\sqrt{1-v^2} \end{aligned}$$

Therefore the observed interval $X(t_0) - \textbf{origin} = \delta\sqrt{1-v^2}$ is **Lorentz Contracted** in the moving frame relative to the rest frame interval δ.

Lorentz Contraction, contd.

We may visualize the Lorentz contraction as a backwards sliding of the intercept of the Lorentz transformed worldline, $X(t_0) = \delta/\cosh\xi = \delta\sqrt{1-v^2}$:

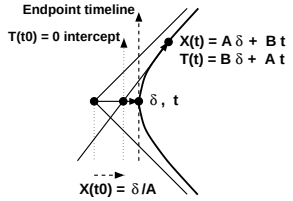

What is a solid object?

In 2D relativity, a solid object is a **line segment**.

- Each end tracks **timelike world line.**
- Segment itself is **spacelike interval.**
- **Simultaneity** is tricky; after Lorentz transform, observer time cuts a skewed slice.

What is an object, contd

Watch the points — spacelike and unable to communicate sideways — as they each evolve on a timelike worldline.

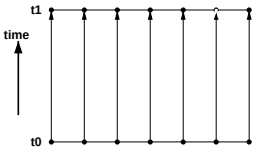

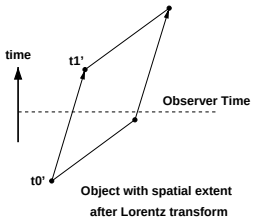

After Lorentz transform, **Simultaneity** is modified.

What is an observation?

Observation of object is only possible via lightlike rays striking **CAMERA.**

These rays must strike observing camera's **world line** at SAME TIME!

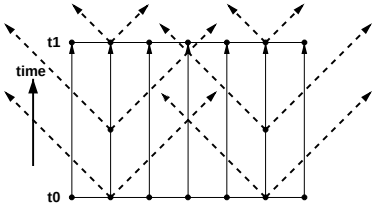

What is an observation, contd.

Since emitted rays must arrive simultaneously at camera on forward light cone to create a snapshot, we have an alternate method:

Shoot a light cone of rays **backwards** from camera

All relativistic pictures then come from time-reversed ray tracing:

What is an observation, contd

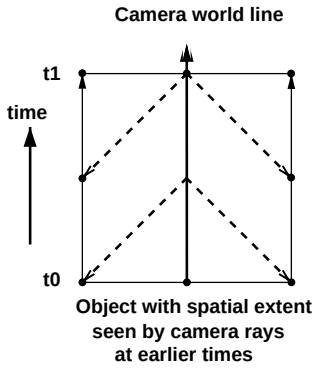

Summary So Far:

- cos **to** cosh and sin **to** sinh make rotations change to Lorentz transformations.
- **Invariants** are inner products with minus sign.
- **Slope** $=$ tan **to Velocity** $=$ tanh**:** helps visualize the meaning of the Lorentz parameters.
- **Objects:** spacelike intervals, endpoints track timelike worldlines, emitting lightlike signals.
- **Cameras:** construct images by back-tracing light rays to intersect object worldlines.

Visualizing Relativity

Part II: Visualization Methods for Special Relativity in 3D and 4D

Andrew J. Hanson
Indiana University

Part II: Visualization Methods for Special Relativity in 3D and 4D

- **2 Space + 1 Time:** Transformations.
- **Rolling the Relativistic Ball**: Thomas Precession
- **Aberration of Light**
- **Object Viewing:** Occlusion, IBR, Terrell
- **4D = 3 space + 1 time**

From 2D (1+1) to 3D (2+1)

We need at least **two space dimensions** to make interesting pictures. In 2 space + 1 time:

- **Objects** are polygons (at one time)
- Polygon **vertices** sweep out proper-time lines.
- Whole **spacetime object** is **tube-like.**
- **Cameras** see **cones** intersecting these tubes.

$\Longrightarrow$ First, revisit transforms:

2 + 1 Spacetime Boost Matrices

What happens to good old $\begin{bmatrix} \cosh & \sinh \\ \sinh & \cosh \end{bmatrix}$ in 2+1?

$$B(\mathbf{v}) = \begin{bmatrix} 1 + {v_x}^2(\cosh\xi - 1) & v_x v_y(\cosh\xi - 1) & v_x \sinh\xi \\ v_x v_y(\cosh\xi - 1) & 1 + {v_y}^2(\cosh\xi - 1) & v_y \sinh\xi \\ v_x \sinh\xi & v_y \sinh\xi & \cosh\xi \end{bmatrix}$$

Note: $\hat{\mathbf{v}} \cdot \hat{\mathbf{v}} = v_x v_x + v_y v_y = 1$ and we define velocity as $\boxed{\mathbf{v} = \hat{\mathbf{v}} \tanh\xi}$ (units: velocity of light = 1), and $\det B = 1$.

Pursue 3D space analogy:

Interesting things happen when you perform *sequences of rotations* in Euclidean 3D space:

$$R(\epsilon,\hat{\mathrm{x}})R(\epsilon,\hat{\mathrm{y}}) - R(\epsilon,\hat{\mathrm{y}})R(\epsilon,\hat{\mathrm{x}}) =$$
$$(\epsilon^2 + \mathcal{O}(\epsilon^3)) \begin{bmatrix} 0 & -1 & 0 \\ 1 & 0 & 0 \\ 0 & 0 & 0 \end{bmatrix}$$

This generates an infinitesimal Z**-axis rotation!**

3D space analogy:

Sequences of rotations in Euclidean 3D space
counter-rotate:

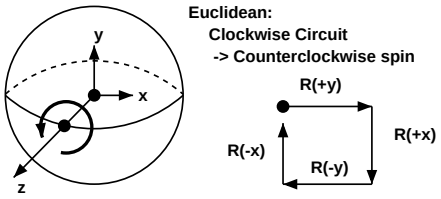

This is the **Rolling Ball** effect.

2 + 1 spacetime: properties

Very Interesting things happen when you perform *sequences of Boosts* in 2 space + 1 time:

$$B(\hat{\mathrm{x}})B(\hat{\mathrm{y}}) - B(\hat{\mathrm{y}})B(\hat{\mathrm{x}}) \;=\; (\epsilon^2 + \mathcal{O}(\epsilon^3)) \begin{bmatrix} 0 & 1 & 0 \\ -1 & 0 & 0 \\ 0 & 0 & 0 \end{bmatrix}$$

This is an infinitesimal **negative Z-axis rotation!**

2 + 1 spacetime: Thomas Precession

This observed **Spatial Rotation** is the origin of *Thomas precession:* in 3D:

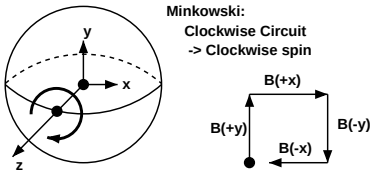

This is a Relativistic Rolling Ball Effect.

Thomas Precession, contd.

Thomas Precession is the exact analog of the Euclidean 3D "Rolling Ball" effect.

This relativistic effect modifies magnetic coupling of atomic electrons in accelerated circular motion by causing an angular velocity

$$\omega = -(\cosh\xi - 1)\frac{v \times \dot{v}}{v^2} \approx -\frac{1}{2} v \times \dot{v}$$

to be applied to the rest frame of an orbiting electron.

. . . recall 3D Euclidean Quaternion Frames . . .

- **Quaternion Correspondence.** The unit quaternions q and $-q$ correspond to a single 3D rotation $R_3(q)$:

$$\begin{bmatrix} q_0^2 + q_1^2 - q_2^2 - q_3^2 & 2q_1q_2 - 2q_0q_3 & 2q_1q_3 + 2q_0q_2 \\ 2q_1q_2 + 2q_0q_3 & q_0^2 - q_1^2 + q_2^2 - q_3^2 & 2q_2q_3 - 2q_0q_1 \\ 2q_1q_3 - 2q_0q_2 & 2q_2q_3 + 2q_0q_1 & q_0^2 - q_1^2 - q_2^2 + q_3^2 \end{bmatrix}$$

- **Rotation Correspondence.**
  If $q = (\cos\frac{\theta}{2}, \hat{\mathrm{n}}\sin\frac{\theta}{2})$, with $\hat{\mathrm{n}}$ a unit 3-vector, $\hat{\mathrm{n}} \cdot \hat{\mathrm{n}} = 1$, then $R(\theta, \hat{\mathrm{n}})$ is usual 3D rotation by θ in the plane perpendicular to $\hat{\mathrm{n}}$.

2 + 1 spacetime quaternion-like form

In 2 space + 1 time, we can construct exactly the same type of quadratic form for the **boost**:

$$B(\mathrm{v}) \;=\; \begin{bmatrix} h_0^2 + h_x^2 - h_y^2 & 2h_xh_y & 2h_0h_x \\ 2h_xh_y & h_0^2 + h_y^2 - h_x^2 & 2h_0h_y \\ 2h_0h_x & 2h_0h_y & h_0^2 + h_x^2 + h_y^2 \end{bmatrix}.$$

If $\mathrm{h} = (h_0, h_x, h_y) = (\cosh\xi/2, \bar{\mathrm{v}}\sinh\xi/2)$
with $v = \sinh\xi/\cosh\xi$ and $|\bar{\mathrm{v}}| = 1$, then this is exactly the standard 2+1 Lorentz transformation!

2 + 1 spacetime quaternion-like form

Caveat: Because of the Thomas Precession, even though $\mathrm{h} = (\cosh\xi/2, \bar{\mathrm{v}}\sinh\xi/2)$ generates $B(\mathrm{v})$, the full group of 2+1 transformations is not quite there, and the algebra is incomplete.

No time for details here, but the full treatment is straightforward using Clifford Algebra to generate $\mathbf{Spin}(2,1)$.

Features of Light in 2+1 Spacetime

Lorentz transforming a light ray can **change its direction.** Let

$x' = x\cosh\xi + t\sinh\xi \qquad t' = x\sinh\xi + t\cosh\xi$

Thus even if $x < 0$,

$$\boxed{x' > 0 \ \text{ if } \ t\sinh\xi > x\cosh\xi!}$$

Light in 2+1, contd

Let θ describe an isotropic distribution of light-like vectors with $(x, y, t) = (\cos\theta,\ \sin\theta,\ 1)$, and Boost with $\hat{\mathrm{v}}$ in x direction:

$$\begin{aligned} x' &= \cos\theta\cosh\xi + \sinh\xi \\ y' &= \sin\theta \\ t' &= \cos\theta\sinh\xi + \cosh\xi \end{aligned}$$

Slice t in *observer frame*, so observed $\boxed{\tan\theta' = y'/x'.}$

Light Aberration: summary

Aberration Formulas we know and love:

After boosting to $v = \sinh/\cosh$ in units of $c = 1$, the isotropic light ray distribution $(x, y, t) = (\cos\theta,\ \sin\theta,\ 1)$ deforms to:

$$\begin{aligned} \sin\theta' &= \frac{\sin\theta}{(1 + v\cos\theta)\cosh\xi} \\ \cos\theta' &= \frac{v + \cos\theta}{1 + v\cos\theta} \\ \tan\theta' &= \frac{\sin\theta}{(v + \cos\theta)\cosh\xi} \end{aligned}$$

Light in 2+1, contd

Observations on relativistic light distortion:

- $\tan\theta' \propto 1/\cosh\xi = \sqrt{1 - v^2}$.
- So, as $v = \sinh/\cosh \to 1 \ldots$
- $\ldots$ the **aberration of light** (resembling a **searchlight**) swings all the rays to the **forward direction!**

Visualizing aberration: light cones

Looking down on boosted spacetime cones representing symmetric Light Ray distributions:

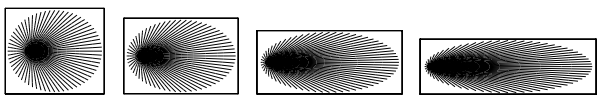

$v = 0.5c$ $v = 0.75c$ $v = 0.9c$ $v = 0.95c$

Visualizing aberration: circular distrib.

Looking down on boosted 2D symmetric Light Ray distributions:

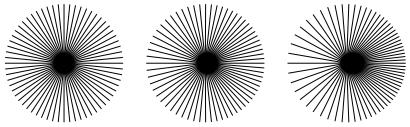

$v = 0.0c$ $v = 0.20c$ $v = 0.50c$

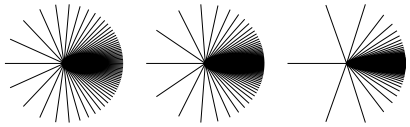

$v = 0.90c$ $v = 0.95c$ $v = 0.99c$

Seeing 2+1 Spacetime

- Points: Still World Lines tracing Proper Time
- Objects: Segments (slabs) $\Rightarrow$ Polygons (tubes)
- Light: Diagonals $\Rightarrow$ Cones
- Images/Cameras: Trace inverse Cones
- Transformations: Completely new features, analogous to 3D rotations

2 + 1 Spacetime Image Construction

At one instant, camera receives back-traced light from a single inverted cone in 2+1 spacetime:

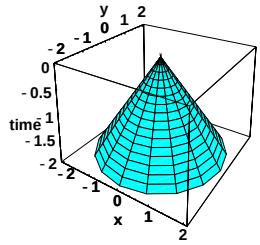

TIME advances UP to zero at the apex, the camera focal point.

2 + 1 Spacetime Object Viewing

How front and back of polygon side emit light towards camera:

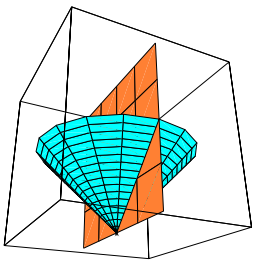

Now vary velocity . . .

2 + 1 spacetime object viewing

When velocity is **0.90** times the speed of light, light escapes from back side in a **almost a full circle:**

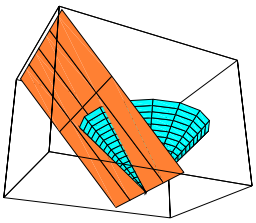

2 + 1 Spacetime Object Viewing

How is light from a moving slab distributed to the camera?

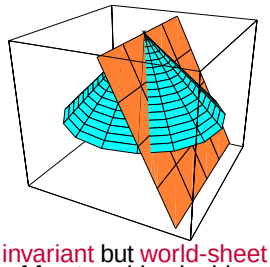

Light cone is invariant but world-sheet of a polygon tilts: visibility of front and back sides varies drastically with velocity.

2 + 1 Spacetime Object Viewing

How face's light distribution changes with velocity:

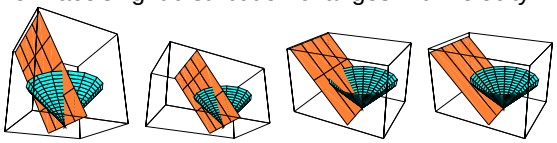

$v = 0.50$ $v = 0.75$ $v = 0.90$ $v = 0.99$

The front side is visible only under more and more restricted conditions.
The back side becomes visible from practically EVERYWHERE as $v \rightarrow 1$!

2 + 1 spacetime object viewing

Simple model: square in 2+1 spacetime: with one side removed so we can see inside:

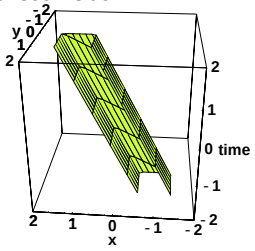

Here, velocity $v = 0.50$ times the speed of light.

2 + 1 spacetime object viewing

Simple model: square in 2+1 spacetime: with one side removed so we can see inside:

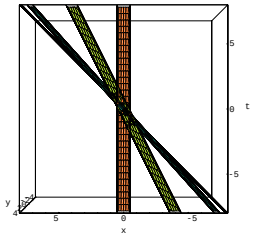

Velocities: **0.00, 0.50, 0.90, 0.99** times the speed of light.
Note Lorentz Contraction.

2 + 1 spacetime object viewing

Looking down from the camera's spacetime viewpoint:

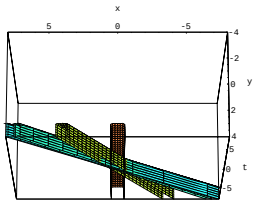

Velocities: **0.00, 0.50, 0.90, 0.99** times the speed of light.

2 + 1 spacetime object viewing

Add a stationary camera: at each time step, the camera sees what the cone intersects:

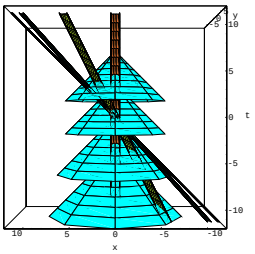

Velocities: **0.00, 0.50, 0.90, 0.99** times the speed of light.

2 + 1 spacetime object viewing

Stationary camera, looking down on the camera's spacetime viewpoint:

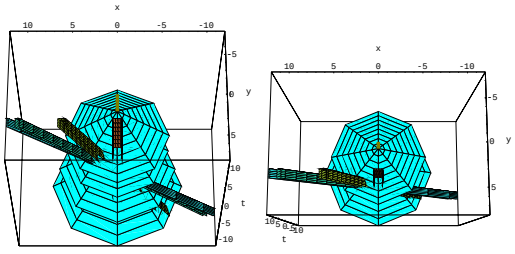

Velocities: **0.00, 0.50, 0.90, 0.99** times the speed of light.

Occlusion in Relativistic Scenes

Study **occlusion** using polygons **aligned with camera rays:**

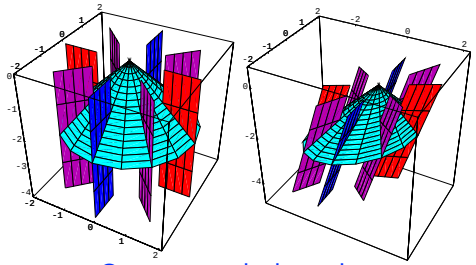

Observe: Once an occlusion edge, ALWAYS an occlusion edge!

2 + 1 occlusion, contd

Even at extreme velocities, occluding edges persist, so boosts will never add face material to a static scene.

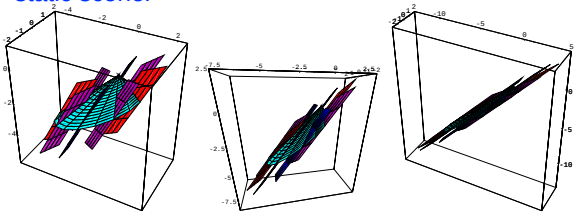

Velocity: **0.50, 0.75, 0.90** times the speed of light.

Static Scenes and Image-Based Rendering

As long as a scene is STATIC, you can take the light distribution in any frame, and use that to make a relativistically distorted scene.

THIS IS THE BASIS OF RELATIVISTIC IMAGE-BASED RENDERING! (See later in Weiskopf lectures).

- The angles and frequencies may change, but the geometric transformations conspire to keep all invisible polygon faces perpetually invisible.

2 + 1 Moving Scenes and the Terrell Effect

In **moving scenes**, the **delay** of light rays reaching us from a rapidly moving object causes bizarre effects

Only the back side of a cube moving towards us at $v \approx 1$ is seen under normal conditions.

Moving Scenes and the Terrell Effect

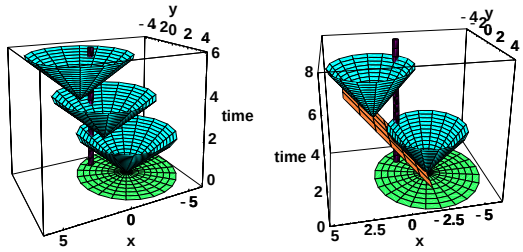

Tube: camera world line.
Disk: ∞ light velocity would make **FRONT** visible.
Cones: finite light velocity shows only BACK.

2 + 1 Moving Scenes and the Terrell Effect

This effect went virtually unnoticed until Terrell (1959) pointed it out. Intuitively, it arises as follows:

- As $v \Rightarrow 1$, aberration reduces the visibility of front edge to a **single ray**.
- Simultaneously, back edge becomes visible *at some time* to any camera in the world.

2 + 1 Moving Scenes and the Terrell Effect

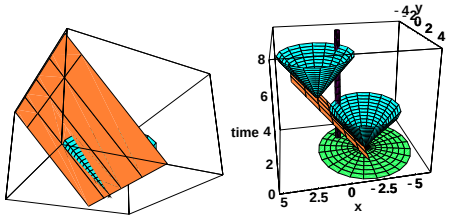

Front only visible along single ray for finite light velocity.

Would be visible everywhere in a half-plane with infinitelight velocity!

3 Space + 1 Time: The Real World!

Goal so far: build intuition in 1+1 and 2+1 dimensions of spacetime. Now do 3 Space and 1 Time:

- **Transformations:** SIX Parameters: 3 boosts (v), 3 Euler angles ($\theta, \hat{\mathrm{n}}$). Most significant features occurred already in 2+1.
- **Aberration:** Same form, spun about boost axis.

3 Space + 1 Time: The Real World!

- **Imaging:** Still the light cone, but now harder to draw; think of as a growing sphere surrounding light source.
- **IBR, Terrell effect, etc:** All just about the same as in 2 space + 1 time, only **objects are like swept spheres** instead of tubes = swept circles.

3 + 1 spacetime Full Boost

In real-world spacetime, a Lorentz transform with velocity $\mathrm{v} = \hat{\mathrm{v}}(\sinh\xi/\cosh\xi)$ becomes:

$$B(\mathrm{v}) = \begin{bmatrix} 1+v_x^2\,\mathrm{C} & v_x v_y\,\mathrm{C} & v_x v_z\,\mathrm{C} & v_x \sinh\xi \\ v_x v_y\,\mathrm{C} & 1+v_y^2\,\mathrm{C} & v_y v_z \mathrm{C} & v_y \sinh\xi \\ v_x v_z\,\mathrm{C} & v_y v_z\,\mathrm{C} & 1+v_z^2\,\mathrm{C} & v_z \sinh\xi \\ v_x \sinh\xi & v_y \sinh\xi & v_z \sinh\xi & \cosh\xi \end{bmatrix}$$

where $\mathrm{C} = (\cosh\xi - 1)$. Here $\det[B] = 1$ and $B(\mathrm{v})$ leaves the matrix $\mathrm{diag}(1,\,1,\,1,\,-1)$ invariant.

3 + 1 spacetime quaternion-like form

Defining $D_x = h_0^2 + h_x^2 - h_y^2 - h_z^2$, cyclic, 4D boosts acquire a quaternion-like form:

$$B(\mathrm{v}) = \begin{bmatrix} D_x & 2h_xh_y & 2h_xh_z & 2h_0h_x \\ 2h_xh_y & D_y & 2h_yh_z & 2h_0h_y \\ 2h_xh_z & 2h_yh_z & D_z & 2h_0h_z \\ 2h_0h_x & 2h_0h_y & 2h_0h_z & h_0^2+h_x^2+h_y^2+h_z^2 \end{bmatrix}$$

where $\mathbf{h} = (h_0, h_x, h_y, h_z) = (\cosh\xi/2, \hat{\mathrm{v}}\sinh\xi/2)$ with $|\hat{\mathrm{v}}| = 1$ generates a standard Lorentz transformation!
Note: $\det[B] = (\cosh^2 - \sinh^2)^4 \equiv 1$.

3 + 1 spacetime quaternion-like form

Caveat: Even though $\mathbf{h} = (\cosh\xi/2, \hat{\mathrm{v}}\sinh\xi/2)$ generates $B(\mathrm{v})$, this is also incomplete, since rotations (e.g., Thomas precession) must be merged in with boosts in the full theory of 3+1 spacetime.

Footnote: The full group $\mathbf{SO}(3,1)$ has a quadratic form corresponding to its "double covering group." This group is directly derivable from Clifford algebra methods, and is written $\mathbf{Spin}(3,1)$. It corresponds to the six parameter group of complex 2×2 matrices $\mathbf{SL}(2,\mathrm{C})$, and eventually leads to the Dirac Equation for the relativistic spin 1/2 electron.

Seeing 3+1 Spacetime

3D **spatial** light ray distributions for a symmetric source are very similar to the 2D spatial distributions:

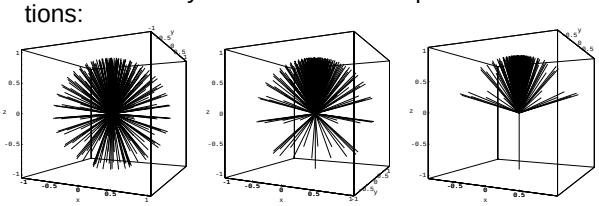

$v = 0.5c$ $v = 0.90c$ $v = 0.99c$

Seeing 3+1 Spacetime

Alternative Visualization: Solid sphere plot of 3D space light ray distributions for symmetric source:

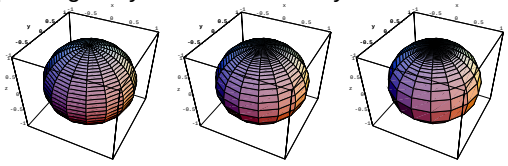

$v = 0.5c$ $v = 0.90c$ $v = 0.99c$

Texture Maps on these distorted spheres provide an implementation of **Relativistic IBR**.

Summary of 3+1 effects:

- $B(\mathbf{v})$ is an orthogonal 4×4 matrix, mostly cosh's and sinh's as usual!
- Quaternion-like forms exist, rigorously corresponding to the representations and algebra of $\mathbf{SL}(2, \mathbf{C})$.
- Occlusion invariance and light aberration allow relativistic IBR to be implemented.
- Objects are made up of vertices tracing world lines, linked into edges, polygons, and polyhedra.
- Camera images can be formed by tracing light rays backward in time on negative light cone until they hit scene objects.

Intuition Overview

- **Orthogonal Matrices:** Did you understand that cos, sin matrices leave dot products unchanged?
  If so, NOW you understand that cosh, sinh matrices leave proper-time dot products unchanged!
- **Rigidity:** Did you understand that 3D rotations change 2D length of projected components, yet radius is constant?
  If so, NOW you understand that Lorentz matrices change $(\mathbf{x}, t)$ coordinate components, yet proper-lengths are unchanged!

Intuition Overview, contd.

- **Non-Commuting Matrices:** Did you understand that x, y 3D rotation matrices generate *extra z-spin*?
  If so, NOW you understand that circular Lorentz transformations generate *Thomas Precession.*
- **Relativistic IBR Theorem:** Did you understand that occlusion of light rays by polygons is *relativistically invariant* due to invariance of dot product?
  If so, NOW you understand how relativistic IBR is possible with **real world image sources.**

Transition:

- **Algebraic thinking** was the focus of the course so far, learning to understand **behavior of light, geometry, and matter** under relativistic conditions.
- **Rendering Virtual Relativistic Reality** will be demonstrated in the final part of the course.
- Together, the two techniques combine to let you **SEE and UNDERSTAND** how Relativity works.

Time for a 15 minute break!

Visualizing Relativity

Daniel Weiskopf
University of Stuttgart

Part III:

LIGHT

Outline

- Physical fundamentals
- Plenoptic function
- Directions and relativistic aberration
- Frequencies and the Doppler shift
- Radiance transformation & Searchlight effect
- Bending light with gravity

Light

- Wave-particle dualism
  - Electromagnetic wave
  - Photons
- Carries all visual information on our surrounding environment

Wave

- Amplitude, Phase, Wavelength

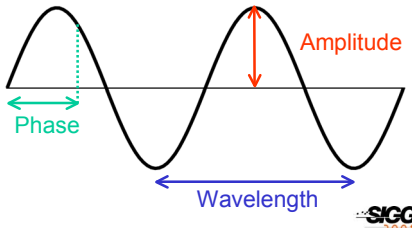

Electromagnetic Wave

- Continuous electric and magnetic fields (perpendicular)
- Amplitude → energy
- Direction
- (Polarization)

Radiance

$$L = \frac{d\Phi}{dt\, dA\, d\Omega_\perp}$$

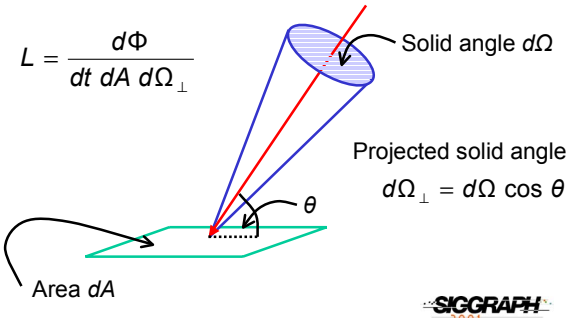

Radiance

- $L = \frac{d\Phi}{dt\, dA\, d\Omega_\perp} = \frac{d\Phi}{dt\, dA\, d\Omega \cos\theta}$
- Energy per
  - Time
  - Projected solid angle
  - Area
- Constant along light ray in vacuum (in Newtonian physics)

Wavelength-Dependent Radiance

- Spectral distribution
- Depends on wavelength
- $L_\lambda = \frac{d\Phi}{dt\, dA\, d\Omega_\perp\, d\lambda}$

Plenoptic Function

- Photon field
- Particle picture

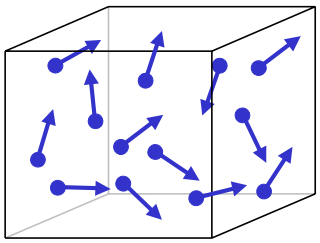

Plenoptic Function

- Compact description of photon field
- Radiance depending on:
  - position
  - time
  - direction
  - wavelength

$P(x,y,z,\theta,\varphi,\lambda)$

Color from Spectral Power Distribution

- Color vision: psychophysics
- Standards by CIE
- Measurement of spectral sensitivity of the human eye
- $C_i = \int f_i(\lambda) P(\lambda)\, d\lambda, \quad i = R,G,B$ (colors)

Color matching function

Special Relativity

- Einstein 1905
- Basis for all modern physical theories
- No gravitation
- Spacetime structure
- Flat spacetime
- Light travels along straight lines

Lorentz Transformation

- Transformation between inertial frames of reference

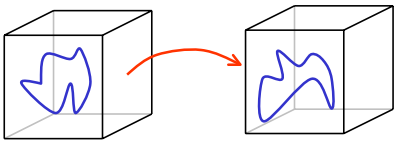

Frame S Frame S'

Relativistic Aberration of Light

- Change of direction of light
- Apparent geometry
- Motion along z axis
- Spherical coordinates (θ,φ)
- $\cos\theta' = \frac{\cos\theta - \beta}{1 - \beta\cos\theta}$

$\varphi' = \varphi$

Velocity

$\beta = \frac{v}{c}$

Speed of light

Relativistic Aberration of Light

Relativistic Aberration of Light

- Non-relativistic (for comparison)

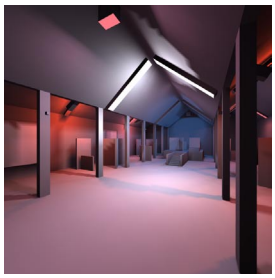

Relativistic Aberration of Light

- v=0.6c
- Increased field of view
- Distortion to hyperbolae

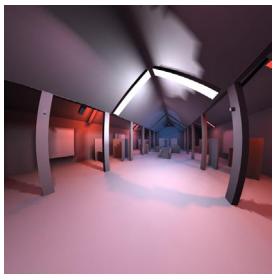

Doppler Effect

- Changes wavelength
- Affects color
- Red or blue shift

Doppler Effect

- $\lambda' = D\lambda$
- Doppler factor: $D = \frac{1}{\gamma(1-\beta\cos\theta)}$

Doppler Effect

- v=0.6c
- Blue shift

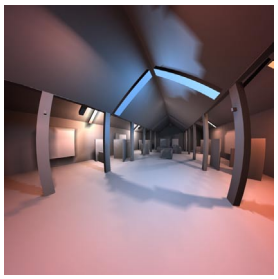

Doppler Effect

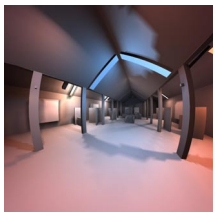

Doppler shift

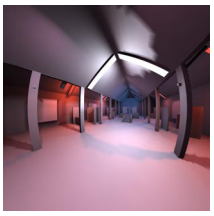

No color shift (comparison)

Searchlight Effect

- Searchlight or headlight effect
- Changes radiance
- Affects brightness

Searchlight Effect

- $L'_\lambda(\lambda',\theta',\varphi') = D^{-5}L_\lambda(\lambda,\theta,\varphi)$
- Highly non-linear
- Extremely bright objects ahead

Searchlight Effect

- v=0.6c
- Overall brightness: 10%
- Objects ahead become brighter

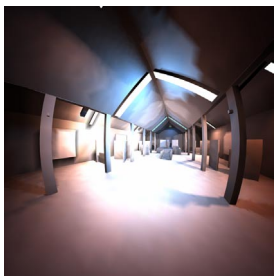

Searchlight Effect

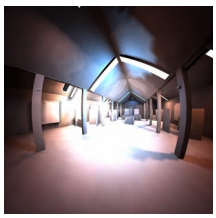

Searchlight effect (brightness: 10%)

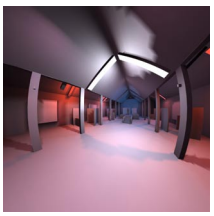

No color/brightness shift (comparison)

Searchlight Effect

- Combining
  - Aberration of light
  - Sweeping effect
  - Doppler effect
  - Time dilation
- $L'_{\lambda}(\lambda',\theta',\varphi') = D^{-5} L_{\lambda}(\lambda,\theta,\varphi)$

Lorentz Transformation of the Plenoptic Function

- Combination of aberration, Doppler & searchlight effects

$$P'(\theta',\varphi',\lambda') = D^{-5} P\left(\arccos\frac{\cos\theta'+\beta}{1+\beta\cos\theta'},\varphi',\frac{\lambda'}{D}\right)$$

- Additional rotations allow for a direction of motion different from z axis

General Relativity

- Einstein 1915
- Theory of gravitation
- Curved spacetime
- Differential geometry

General Relativity

- Light is influenced by gravitation
- Bending of light rays
- Experimental confirmation: solar eclipse expedition (Eddington 1919)
- Gravitational lensing in astronomy

Gravitational Lensing

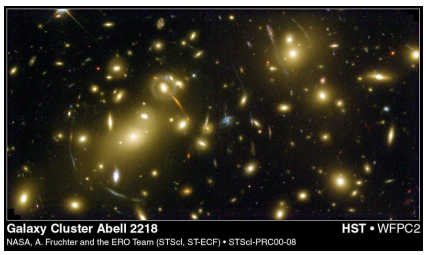

Credits: NASA, STScI (A. Fruchter, ERO Team)

Gravitational Lensing

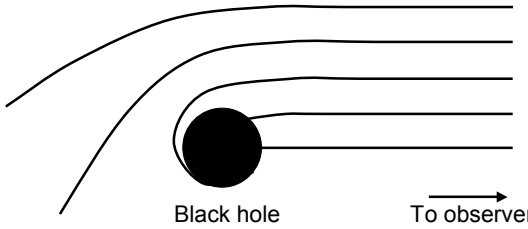

Curved Manifold

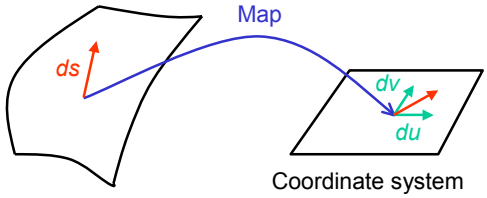

Coordinate system

Curved manifold

Curvature of Spacetime

- Metric $g_{kl}(\mathbf{x})$, $k,l = 0,1,2,3$
- Line element

$$ds^2 = \sum_{k,l=0}^{3} g_{kl}(\mathbf{x}) dx^k dx^l$$

- Local measurement of distances
- Fundamental, intrinsic description of curvature

Geodesics

- Photons (and particles) travel along geodesic lines in 4D spacetime
- Geodesic: “straightest line” in curved manifold

Geodesics

- Geodesic equation

$$\frac{d^2 x^\mu(\zeta)}{d\zeta^2} + \sum_{\nu,\rho=0}^{3} \Gamma^\mu_{\nu\rho}(\mathbf{x}) \frac{dx^\nu(\zeta)}{d\zeta} \frac{dx^\rho(\zeta)}{d\zeta} = 0$$

Christoffel symbols (calculated from metric)

Affine parameter

Geodesics

- Initial value problem for ordinary differential equations (ODE)

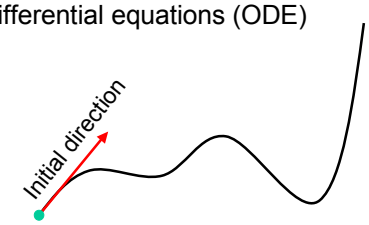

Geodesics

- Initial values:
  - Camera parameters
  - Time component fixed by null-condition (for light rays):

$$\sum_{\mu,\nu=0}^{3} g_{\mu\nu}(\mathbf{x}) \frac{dx^{\mu}(\zeta)}{d\zeta} \frac{dx^{\nu}(\zeta)}{d\zeta} = 0$$

- Numerical integration (e.g. Runge-Kutta)

What Else?

- Shift of wavelength in general relativity:
  - Gravitational redshift
  - Cosmological redshift
  - Doppler redshift
  - Unified treatment of all these
- Transformation of radiance
- (More in the references/literature)

Summary

- Special relativity:
  - Lorentz transformation
  - Aberration of light
  - Doppler effect
  - Searchlight effect
  - Transformation of the plenoptic function

Summary

- General relativity:
  - Light bending
  - Gravitational lensing
  - Geodesic equation
  - (Transformation of wavelength and radiance)

Part IV:

RENDERING

Outline

- Special relativistic rendering:
  - Polygon rendering (T-buffer)
  - Relativistic radiosity
  - Ray tracing
  - Image-based rendering
  - Texture-based rendering

Outline

- General relativistic rendering:
  - Ray tracing
  - Image-based rendering

Relativistic Polygon Rendering (T-Buffer)

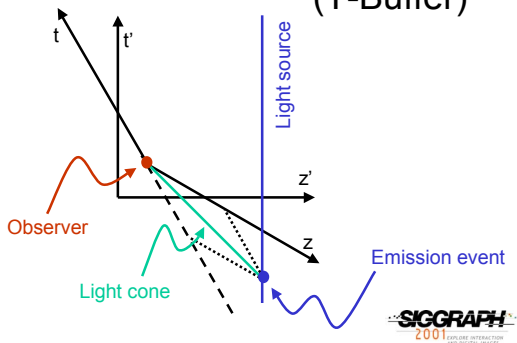

Relativistic Polygon Rendering

- Compute intersection
- Lorentz transformation of the emission event
- Projection onto image plane
- Transformation for each vertex
  ⇒ “photo-surface”

Polygon Rendering: Rendering Pipeline

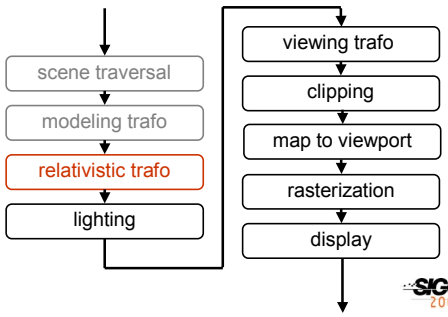

Polygon Rendering: Cube

v=0.95c

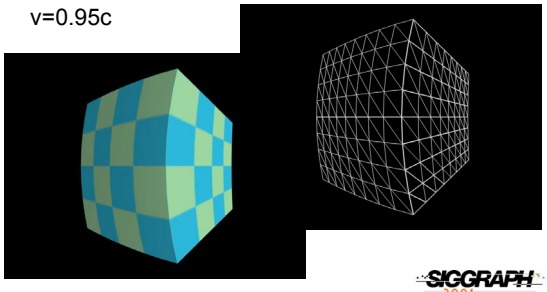

Polygon Rendering: Cube

v=0.95c

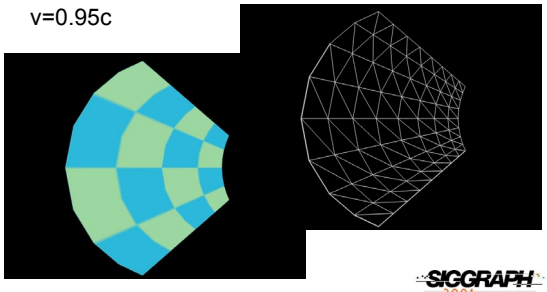

Polygon Rendering: Cube

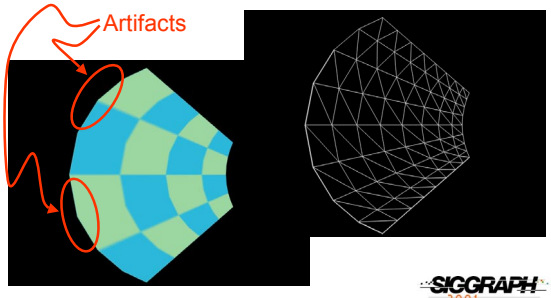

Polygon Rendering: Caveats

- "Flatten" scene graph:
  - Remove shared instancing
  - Remove transformation nodes
- Reduce geometric artifacts by:
  - Fine remeshing in preprocessing step
  - Adaptive subdivision

Polygon Rendering: Hardware Update…

- Exploit state-of-the-art graphics hardware:
- Vertex programs (vertex shaders) for relativistic transformation

Polygon Rendering: What else?

- Secondary processes
- Reflections
- Shadows
- Extension: relativistic radiosity

- (Further information in the references/ literature)

T-Buffer: Key Features & Issues

- Adapted to rendering-pipeline of current hardware
- Fast
- Problems:
  - Geometric artifacts
  - Illumination?

Relativistic Ray Tracing

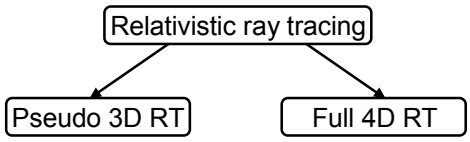

3D Relativistic Ray Tracing

- Transforms moving observer into rest frame of the scene
- Relativistic aberration
- Performs standard non-relativistic ray tracing
- Only static scenes (unless special modifications)

3D Relativistic Ray Tracing

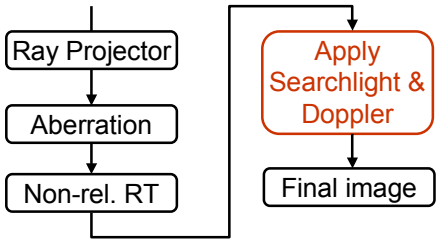

3D Relativistic Ray Tracing: Example – Chain of Cubes

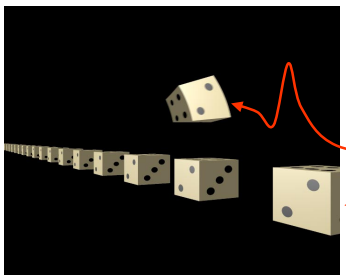

- Apparent geometry
- Penrose-Terrell rotation
- v = 0.95c

4D Relativistic Ray Tracing

- Keep track of different frames of reference
- Perform Lorentz transformation of all relevant light properties when changing frames
- Moving objects

Relativistic Ray Tracing: Key Features

- High image quality
- High computational costs
- Static scene (3D RT), Moving objects (4D RT)

Image-Based Rendering (IBR)

- Lorentz transformation of plenoptic function
- Extension of all non-relativistic IBR methods
- Static scene
- Reconstruction of power spectrum from RGB input data

Image-Based Rendering (IBR)

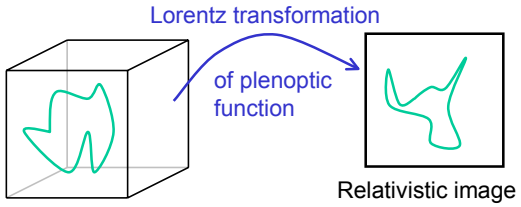

IBR: Magnification and Anti-Aliasing

- Scaling due to aberration
- Higher resolution for back view
- Anti-aliasing for front view
  - Supersampling
  - Texture filtering

IBR: Data acquisition

Fork arm construction

IBR: Data acquisition

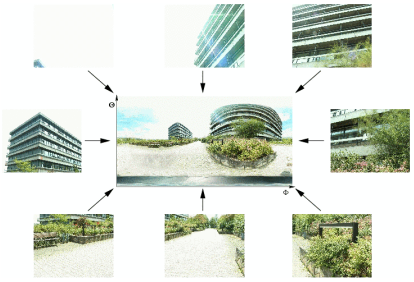

IBR: Example

- Non-relativistic

IBR: Example

- Apparent geometry
- v=0.9c

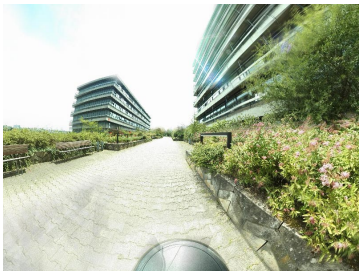

IBR: Example

- Relativistic illumination
- v=0.2c
- Overall brightness: 10 %

IBR: Relativistic Movie

IBR: Movie Production

IBR: Key Features

- Relativistic transformation of plenoptic function
- All IBR methods can be modified
- All relativistic effects on visual perception
- No geometric modeling needed
- Photo-realism

IBR: Issues

- Data (image) acquisition with
  - Wide field of view
  - High resolution
- Acquisition of full power spectrum?
- Moving objects?

Texture-Based Rendering

- Based on aberration of light and searchlight & Doppler effects
- Exploits graphics hardware

TBR: Rendering Steps

1. Generation of non-relativistic panorama
2. Apparent geometry by texture-warping
3. Color and brightness via LUT

TBR: Non-Relativistic Panorama

- Sampling of plenoptic function $P(\theta,\varphi,\lambda)$
- Wavelength-dependent radiance wrt. n basis functions:

$$P(\theta,\varphi,\lambda) = \sum_{i=1}^{n} b_i(\theta,\varphi) B_i(\lambda)$$

- Image projected onto unit sphere $\Rightarrow$ radiance map

TBR: Non-Relativistic Panorama

- Covering of sphere by several images
- Similar to environment or reflection mapping

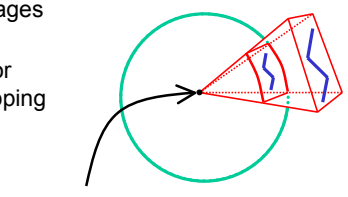

TBR: Apparent Geometry

- Aberration of light
- Texture-warping by modified texture coordinates

TBR: Color & Brightness

- Parameters for final RGB color:
  - Doppler factor D
  - Coefficient b_i

$$P(\lambda) = \sum_{i=1}^{n} b_i B_i(\lambda)$$

TBR: Color & Brightness

- Parameters for final RGB color:
  - Doppler factor D
  - Coefficient b_i

$$P(\lambda) = \sum_{i=1}^{n} b_i B_i(\lambda)$$

$$c_j' = \sum_{i=1}^{n} \int f_j(\lambda') b_i B_i'(\lambda')\, d\lambda' = \sum_{i=1}^{n} X_{j,i}(b_i, D)$$

TBR: Color & Brightness

- Parameters for final RGB color:
  - Doppler factor D
  - Coefficient b_i

$$P(\lambda) = \sum_{i=1}^{n} b_i B_i(\lambda)$$

$$c_j' = \sum_{i=1}^{n} \int f_j(\lambda') b_i B_i'(\lambda')\, d\lambda' = \sum_{i=1}^{n} X_{j,i}(b_i, D)$$

TBR: Color & Brightness

- Non-linear function via LUT
- Pixel textures (SGI)
- Dependent textures (GeForce)
  - Texture coordinates on per-pixel basis
  - Generated in preprocessing step
  - 2 Parameters: D , b_i
  - Output: Final RGB
- Sum over n basis function B_i

TBR: Rendering Pipeline

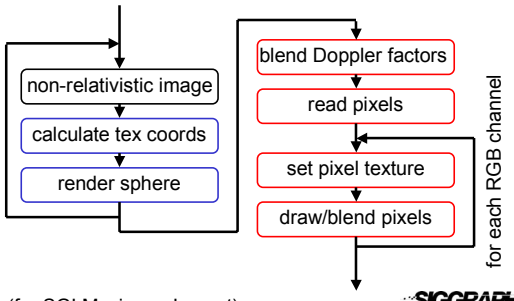

(for SGI Maximum Impact)

General Relativistic Ray Tracing

- 4D curved spacetime
- Photons travel along geodesic lines
- 3D straight light rays
  → 4D bent ray (polygonal approx.)

General Relativistic Ray Tracing

- Initial value problem for ODE
- Initial values:
  - Camera parameters
  - Time component fixed by null-condition
- Numerical integration (e.g. RK4)
- Ray projector: integration of geodesic equations

Structure of the System

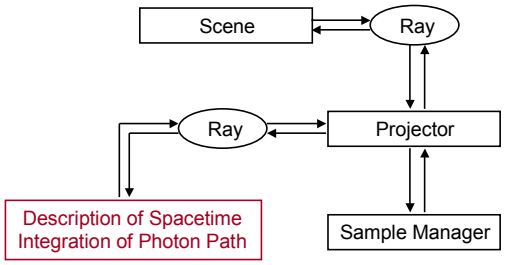

Example: Schwarzschild

- Spherically symmetric
- Static
- Vacuum solution (outer space)
- Example: Non-rotating, non-charged black hole

Schwarzschild: Einstein Ring

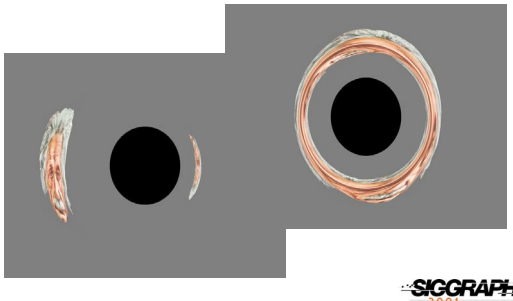

Schwarzschild: Einstein Ring

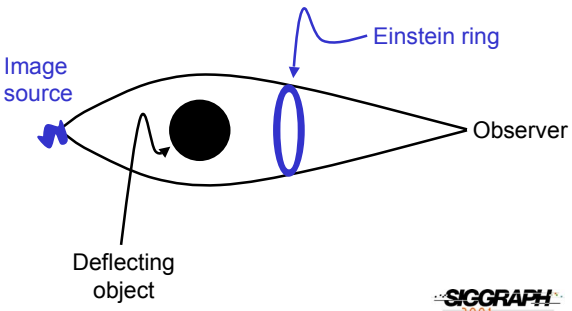

Example: Warp Metric

- Super-fast travel
- Spaceship is at rest in warp bubble
- Dynamic metric

Example: Warp Metric

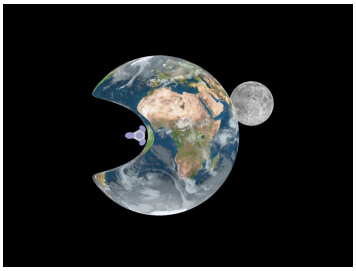

General Relativistic IBR

- Can image-based methods be applied to general relativistic rendering?
- Problem:
  - Plenoptic function is local to each point in spacetime
  - Rendering needs information about emission/absorption

Reduce Complexity: Space Confinement

- Curved region confined within closed area around observer
- Use ray-tracing inside curved area
- Approximate plenoptic function at boundary by plenoptic function taken at one selected location
- Static scenes

General Aberration

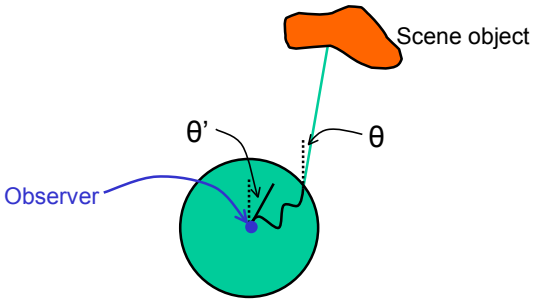

General Aberration

- Changes in apparent geometry between flat and curved spacetimes: $(\theta',\varphi') = f(\theta,\varphi)$
- For rotational symmetry: $\theta' = f(\theta)$
- Analogous to special relativistic IBR
- Generation of LUT for general aberration in preprocessing step

Warp (Inside): Example

- Front view
- At rest

Warp (Inside): Example

- Front view
- Warp 0.8c

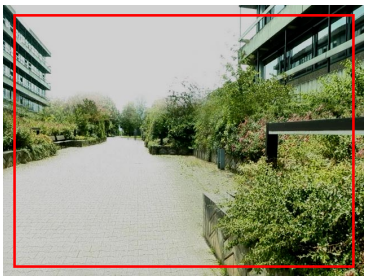

Warp (Inside): Example

- Front view
- Warp 10c

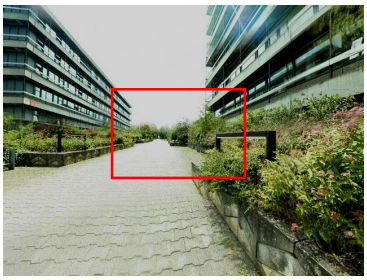

Warp (Inside): Example

- Back view
- At rest

Warp (Inside): Example

- Back view
- Warp –0.8c

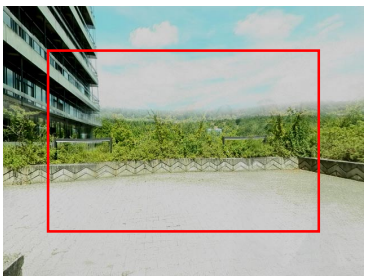

Warp (Inside): Example

- Back view
- Warp –1c

Warp (Inside): Example

- Back view
- Warp –1.2c

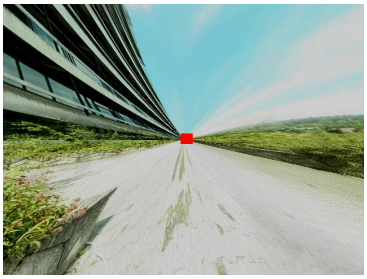

Part V:

INTERACTION TECHNIQUES

Outline

- Accelerated observer
- User interaction model
- Virtual reality/virtual environment for special relativity

Motivation

- So far: only uniform motion within special relativistic visualization
- Goal: navigation by user interaction
- Prerequisite: acceleration of the observer

Accelerated Observer

- Equation of motion

$$a^{\mu} = \frac{du^{\mu}}{d\tau} = \frac{d^2 x^{\mu}}{d\tau^2}$$

- User interaction → acceleration

Accelerated Observer

- Coupled system of ordinary differential equations
- Initial value problem

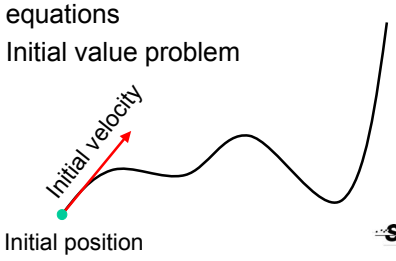

Accelerated Observer

- Numerical integration
- Example: Runge-Kutta
- Trajectory

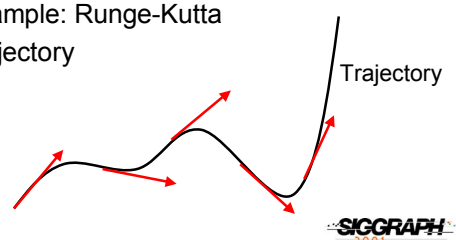

Acceleration & Rendering

- Rendering a single snapshot is not influenced by acceleration of camera
- Use current position and velocity for rendering
- Co-moving frame of reference
- All relativistic rendering techniques can be used

Accelerated Motion

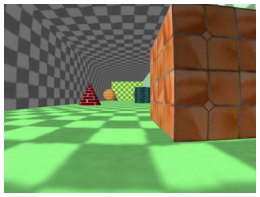
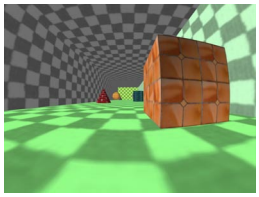

v=0.3c v=0.623c

(Motion towards the end of the box)

Accelerated Motion

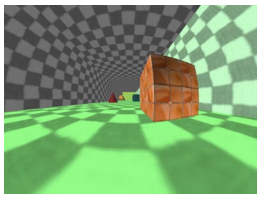
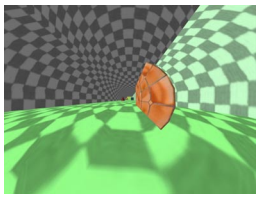

v=0.817c v=0.975c

(Motion towards the end of the box)

Accelerated Motion

- Objects ahead seem to move away when accelerating, although the observer gets closer
- Due to increasing aberration of light
- Objects subtend a smaller solid angle

User Interaction

- Motion of fast vehicle controlled by acceleration
- User can walk within the vehicle
- Tracking of position and velocity
- Relativistic-vehicle-control metaphor

User Interaction

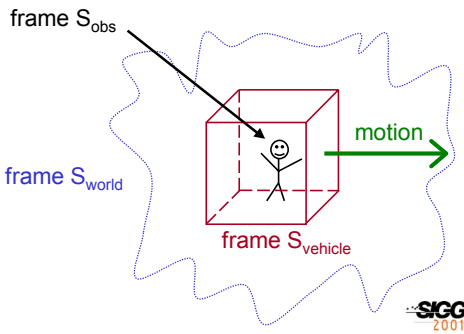

User Interaction

- 3 frames of reference
  - head of the observer
  - vehicle
  - outside world
- Tracking of position and velocity wrt. frame of the vehicle
- Lorentz transformation to “outside world”

Virtual Environment

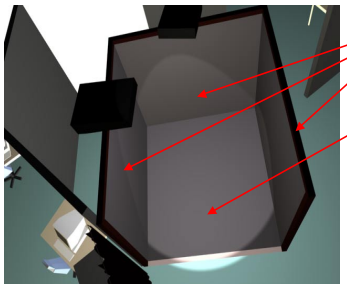

Virtual Environment

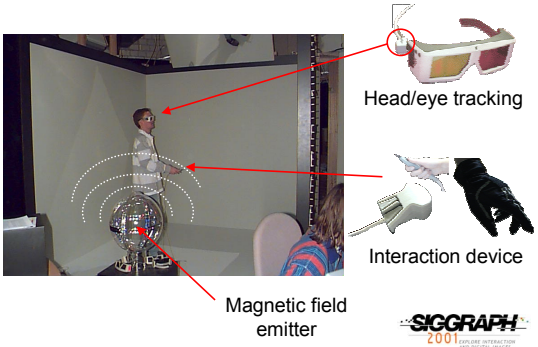

Virtual Environment

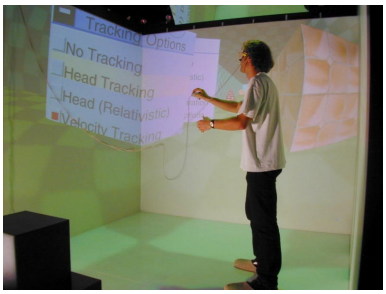

Virtual Environment

- Benefits:
  - Immersion
  - Active and passive locomotion

Part VI:

GRAND CONCLUSION

What Have We Learned?

- **Scene and illumination transformations** under extreme conditions of relativity have much in common with familiar graphics
- **Relativistic objects** must be modeled with world lines
- **Relativistic IBR is possible** because tracing light rays to occlusion edges is invariant under Lorentz transforms

What Have We Learned?

- **Relativistic rendering is based on**
  - Aberration of light or
  - Transformation of events and
  - Doppler effect and
  - Searchlight effect
- **Acceleration** is possible within special relativity
- **Light bends** in interesting ways in the presence of gravity

Applications

- Visualization as a research tool
- Education and public relations
- Entertainment, e.g., science fiction movies

Additional Information on Relativistic Visualization

D. Weiskopf
University of Stuttgart

A. Hanson
Indiana University

Additional Information on the Web

A web site with additional information and resources for this course can be accessed on `http://wwwvis.informatik.uni-stuttgart.de/relativity`.

Literature on Relativistic Visualization

Einstein's original work on the special theory of relativity was published in 1905 [9]. Its title "Zur Elektrodynamik bewegter Körper" ("On the electrodynamics of moving bodies") shows that the focus is on the connection between the description of electromagnetic phenomena (based on Maxwell's equations) and the kinematics of moving objects. Miller's book [22] contains a translation of Einstein's paper into English, along with more background information and historic remarks.

There exist numerous textbooks on special relativity, see, e.g., Møller [24] or Rindler [31]. The books by Misner et al. [23], Weinberg [36], d'Inverno [8], and Wald [35] primarily focus on general relativity, but contain some information on special relativity as well.

Remarkably, the issue of visual appearance and perception in special relativity was ignored for a long time, and consequently numerous misleading statements and interpretations persisted. Apart from a previously disregarded article by Lampa [21] in 1924 on the invisibility of the Lorentz contraction, it was only in 1959 that the first coherent solutions to this problem were described by Penrose [29] and Terrell [34]. (Reference [29] is included in the course notes, pages E-1–E-3; reference [34] is included on pages F-1–F-5). Later, more detailed descriptions of the geometrical appearance of fast moving objects were given by Weisskopf [44], Boas [4], Scott and Viner [33], and Scott and van Driel [32].

The first published work of which we are aware that used advanced graphics techniques to produce shaded images of fast-moving objects was that of Hsiung and Dunn [14] and Hsiung and Thibadeau [15]. (Reference [15] is included in the course notes,

pages G-1–G-8.) They proposed an extension of normal three-dimensional ray tracing for image shading of fast moving objects. This technique accounts for relativistic effects on the apparent geometry as seen by the observer. Hsiung et al. [17] investigated relativistic ray tracing in more detail and included the visualization of the Doppler effect. Exploiting relativistic ray tracing, Hsiung et al. [16] used the viewer-dependent variation of the observed color of objects in the scene for the visualization of relativistic time dilation.

Real-time visualization of relativistic effects exploiting the *time-buffer* method was introduced by Hsiung et al. [18]. (Reference [18] is included in the course notes, pages H-1–H-7). The time-buffer technique resembles and can be mapped onto the normal z-buffer. It allows for relativistic polygon rendering using a scan-line technique suitable for real-time applications, and makes use of contemporary computer graphics hardware to achieve interactive frame rates. Gekelman et al. [12], Chang et al.[6], and Betts [3] study the polygon rendering approach in more detail and present comprehensive treatments.

Weiskopf et al. [42, 43] investigated special relativistic effects on illumination in detail, considering both the Doppler and the searchlight effects. (Reference [42] is included in the course notes, pages I-1–I-15). They showed how ray tracing and polygon rendering can be adapted to correctly incorporate relativistic illumination effects. Weiskopf et al. [42] contains a derivation of the transformation of radiance and irradiance, giving the complete mathematical basis for simulating the searchlight effect.

Texture-based special relativistic rendering was proposed by Weiskopf [37] in order to exploit modern graphics hardware—especially, texturing and pixel fragment operations—for the real-time visualization of relativistic effects on geometry and illumination. Image-based special relativistic rendering was introduced by Weiskopf et al. [41], allowing for the production of photo-realistic images and movies without the need for laborious three-dimensional geometric modeling. (Reference [41] is included in the course notes, pages J-1–J-9).

Another issue in special relativistic visualization is user interaction and navigation. Usually, a user navigates through a virtual world by moving a virtual camera. The velocity or direction of motion of the camera is changed by acceleration. Therefore, acceleration is a prerequisite for an interactive virtual environment for special relativity. It is important to point out that special relativity is perfectly capable of describing the accelerated motion of object, as long as gravitation can be neglected. (Gravitation is described by general relativity.) Rau et al. [30] described how acceleration can be incorporated into special relativistic visualization and presented a simple relativistic flight simulator. Weiskopf [38] extends relativistic interaction techniques to support an immersive virtual environment for special relativity.

A comprehensive introduction to the general theory of relativity can be found, e.g., in the textbooks by Misner et al. [23], Weinberg [36], d'Inverno [8], or Wald [35].

The following articles are concerned with the appearance of objects under the influence of gravitational light deflection. Typically, well-known metrics with closed-form solutions are investigated. The most prominent example is the so-called Schwarzschild solution for a spherically symmetric, static distribution of matter. Nollert et al. [28], Ertl et al. [10], and Nemiroff [25], for example, investigated the appearance of a neutron star or the flight to a black hole. Nollert et al. [27] and Kraus [20] described general relativistic ray tracing in more detail. Gröller[13] gave a generic approach to non-linear ray tracing as a visualization technique. Bryson[5] presented a virtual environment for the visualization of geodesics in general relativity, where examples of the Schwarzschild and Kerr solutions are shown. (The Kerr solution describes the spacetime of a rotating black hole.) Weiskopf [39] showed how general relativistic ray tracing can be used as a visualization tool in gravitational research. (Reference [39] is included in the course notes, pages K-1–K-5).

Some specific examples for general relativistic objects and their corresponding curved spacetimes used in this course are the rigidly rotating disk of dust and the warp metric. Neugebauer and Meinel [26] and Ansorg [2] presented background information on the physics of the rigidly rotating disk of dust. The warp metric was proposed by Alcubierre [1] in 1994; Clark et al. [7] investigated the view from inside the warp spaceship. Ford and Roman [11] presented a comprehensible discussion of the problems of negative energy, “exotic” matter, and causality, which occur for the metric of the warp drive and traversable wormholes. Kobras et al. [19] proposed a method for imaged-based rendering in a general relativistic setting, presenting the visualization of the warp metric as an example.

A comprehensive presentation of techniques for special and general relativistic visualization can be found in Weiskopf [40].

Acknowledgments: Reprints Included in Course Notes

We would like to thank the authors and publishers who gave us permission to include the reprints of the papers below in the course notes.

- Roger Penrose and Cambridge University Press, Cambridge, U.K. for the permission to reprint the article: R. Penrose, “The apparent shape of a relativistically moving sphere”, Proceedings of the Cambridge Philosophical Society, vol. 55, 1959, pages 137–139.

- James Terrell and The American Physical Society (APS) for the permission to reprint the article: J. Terrell, “Invisibility of the Lorentz contraction”, Physical Review, vol. 116, no. 4, 1959, pages 1041–1045.

- Robert H. Thibadeau and ACM for the permission to reprint the article: P.-K. Hsiung, R. H. Thibadeau, “Spacetime visualization of relativistic effects”, Proceedings of the 1990 ACM Annual Conference on Cooperation, pages 236–243.
- Robert H. Thibadeau and ACM for the permission to reprint the article: P.-K. Hsiung, R. H. Thibadeau, M. Wu, “T-buffer: fast visualization of relativistic effects in spacetime”, Computer Graphics, vol. 24, no. 2, 1990, pages 83–88.
- ACM for the permission to reprint the article: D. Weiskopf, U. Kraus, H. Ruder, “Searchlight and Doppler effects in the visualization of special relativity: a corrected derivation of the transformation of radiance”, ACM Transactions on Graphics, vol. 18, no. 3, 1999, pages 278–292.
- IEEE for the permission to reprint the article: D. Weiskopf, D. Kobras, H. Ruder, “Real-world relativity: image-based special relativistic visualization”, Proceedings of the IEEE Visualization 2000 Conference, pages 303–310.
- IEEE for the permission to reprint the article: D. Weiskopf, “Non-linear ray tracing as a visualization tool for gravitational physics”, Proceedings of the IEEE Visualization 2000 Conference, pages 445–448.

References

[1] M. Alcubierre. The warp drive: hyper-fast travel within general relativity. *Classical and Quantum Gravity*, 11:L73–L77, 1994.

[2] M. Ansorg. Timelike geodesic motions within the general relativistic gravitational field of the rigidly rotating disk of dust. *Jounal of Mathematical Physics*, 39(11):5984–6000, 1998.

[3] C. Betts. Fast rendering of relativistic objects. *The Journal of Visualization and Computer Animation*, 9(1):17–31, 1998.

[4] M. L. Boas. Apparent shape of large objects at relativistic speeds. *American Journal of Physics*, 29(5):283–286, May 1961.

[5] S. Bryson. Virtual spacetime: An environment for the visualization of curved spacetimes via geodesic flows. In *Proceedings of Visualization ’92*, pages 291–298, 1992.

[6] M.-C. Chang, F. Lai, and W.-C. Chen. Image shading taking into account relativistic effects. *ACM Transactions on Graphics*, 15(4):265–300, Oct. 1996.

[7] C. Clark, W. A. Hiscock, and S. L. Larson. Null geodesics in the Alcubierre warp-drive: the view from the bridge. *Classical and Quantum Gravity*, 16:3965–3972, 1999.

[8] R. A. d' Inverno. *Introducing Einstein's Relativity*. Clarendon Press, Oxford, 1992.

[9] A. Einstein. Zur Elektrodynamik bewegter Körper. *Annalen der Physik*, 17:891–921, 1905. In German.

[10] T. Ertl, F. Geyer, H. Herold, U. Kraus, R. Niemeier, H.-P. Noller, A. Rebetzky, H. Ruder, and G. Zeller. Visualization in astrophysics. In *Eurographics '89 Proceedings*, pages 149–158, 1989.

[11] L. H. Ford and T. A. Roman. Negative energy, wormholes and warp drive. *Scientific American*, pages 30–37, Jan. 2000.

[12] W. Gekelman, J. Maggs, and L. Xu. Real-time relativity. *Computers in Physics*, 5(4):372–385, July/Aug. 1991.

[13] E. Gröller. Nonlinear ray tracing: Visualizing strange worlds. *The Visual Computer*, 11(5):263–276, 1995.

[14] P.-K. Hsiung and R. H. P. Dunn. Visualizing relativistic effects in spacetime. In *Proceedings of Supercomputing '89 Conference*, pages 597–606, 1989.

[15] P.-K. Hsiung and R. H. Thibadeau. Spacetime visualization of relativistic effects. In *Proceedings of the 1990 ACM Annual Conference on Cooperation*, pages 236–243, Feb. 1990.

[16] P.-K. Hsiung, R. H. Thibadeau, C. B. Cox, and R. H. P. Dunn. Time dilation visualization in relativity. In *Proceedings of the Supercomputing '90 Conference*, pages 835–844, 1990.

[17] P.-K. Hsiung, R. H. Thibadeau, C. B. Cox, R. H. P. Dunn, M. Wu, and P. A. Olbrich. Wide-band relativistic Doppler effect visualization. In *Proceedings of the IEEE Visualization '90 Conference*, pages 83–92, Oct. 1990.

[18] P.-K. Hsiung, R. H. Thibadeau, and M. Wu. T-buffer: Fast visualization of relativistic effects in spacetime. *Computer Graphics*, 24(2):83–88, Mar. 1990.

[19] D. Kobras, D. Weiskopf, and H. Ruder. Image-based rendering and general relativity. In V. Skala, editor, *WSCG 2001 Conference Proceedings*, pages 130–137, Plzen, 2001.

[20] U. Kraus. Light deflection near neutron stars. In H. Riffert, H. Ruder, H.-P. Nollert, and F. W. Hehl, editors, *Relativistic Astrophysics*, pages 66–81. Vieweg, 1998.

[21] A. Lampa. Wie erscheint nach der Relativitätstheorie ein bewegter Stab einem ruhenden Beobachter? *Zeitschrift für Physik*, 27:138–148, 1924. In German.

[22] A. I. Miller. *Albert Einstein's Special Theory of Relativity*. Addison-Wesley, Reading, MA, 1981.

[23] C. W. Misner, K. S. Thorne, and J. A. Wheeler. *Gravitation*. Freeman, New York, 1973.

[24] C. Møller. *The Theory of Relativity*. Clarendon Press, Oxford, second edition, 1972.

[25] R. J. Nemiroff. Visual distortions near a neutron star and black hole. *American Journal of Physics*, 61(7):619–632, July 1993.

[26] G. Neugebauer and R. Meinel. General relativistic gravitational field of a rigidly rotating disk of dust: Solution in terms of ultraelliptic functions. *Physical Review Letters*, 75:3046, 1995.

[27] H.-P. Nollert, U. Kraus, and H. Ruder. Visualization in curved spacetimes. I. Visualization of objects via four-dimensional ray-tracing. In F. W. Hehl, R. A. Puntigam, and H. Ruder, editors, *Relativity and Scientific Computing*, pages 314–329. Springer, 1996.

[28] H.-P. Nollert, H. Ruder, H. Herold, and U. Kraus. The relativistic "looks" of a neutron star. *Astronomy and Astrophysics*, 208:153, 1989.

[29] R. Penrose. The apparent shape of a relativistically moving sphere. *Proceedings of the Cambridge Philosophical Society*, 55:137–139, 1959.

[30] R. T. Rau, D. Weiskopf, and H. Ruder. Special relativity in virtual reality. In H.-C. Hege and K. Polthier, editors, *Mathematical Visualization*, pages 269–279. Springer Verlag, Heidelberg, 1998.

[31] W. Rindler. *Introduction to Special Relativity*. Clarendon Press, Oxford, second edition, 1991.

[32] G. D. Scott and H. J. van Driel. Geometrical appearances at relativistic speeds. *American Journal of Physics*, 38(8):971–977, Aug. 1970.

[33] G. D. Scott and R. R. Viner. The geomentrical appearence of large objects moving at relativistic speeds. *American Journal of Physics*, 33(7):534–536, July 1965.

[34] J. Terrell. Invisibility of the Lorentz contraction. *Physical Review*, 116(4):1041–1045, Nov. 1959.

[35] R. M. Wald. *General Relativity*. University of Chicago Press, 1984.

[36] S. Weinberg. *Gravitation and Cosmology: Principles and Applications of the General Theory of Relativity*. John Wiley & Sons, New York, 1972.

[37] D. Weiskopf. Fast visualization of special relativistic effects on geometry and illumination. In *Proceedings of EG/IEEE TCVG Symposium on Visualization 2000*, pages 219–228, 2000.

[38] D. Weiskopf. An immersive virtual environment for special relativity. In *Proceedings WSCG 2000 Conference*, pages 337–344, 2000.

[39] D. Weiskopf. Non-linear ray tracing as a visualization tool for gravitational physics. In *Proceedings of the IEEE Visualization 2000 Conference*, pages 445–448, 2000.

[40] D. Weiskopf. *Visualization of Four-Dimensional Spacetimes*. Dissertation, University of Tübingen, 2001. http://w210.ub.uni-tuebingen.de/dbt/volltexte/2001/240.

[41] D. Weiskopf, D. Kobras, and H. Ruder. Real-world relativity: Image-based special relativistic visualization. In *Proceedings of the IEEE Visualization 2000 Conference*, pages 303–310, 2000.

[42] D. Weiskopf, U. Kraus, and H. Ruder. Searchlight and Doppler effects in the visualization of special relativity: A corrected derivation of the transformation of radiance. *ACM Transactions on Graphics*, 18(3):278–292, July 1999.

[43] D. Weiskopf, U. Kraus, and H. Ruder. Illumination and acceleration in the visualization of special relativity: A comment on fast rendering of relativistic objects. *The Journal of Visualization and Computer Animation*, 11(4):185–195, 2000.

[44] V. F. Weisskopf. The visual appearance of rapidly moving objects. *Physics Today*, 13(9):24–27, 1960.

THE APPARENT SHAPE OF A RELATIVISTICALLY MOVING SPHERE

By R. PENROSE

Received 29 July 1958

It would be natural to assume that, according to the special theory of relativity, an object moving with a speed comparable with that of light should *appear* to be flattened in the direction of motion on account of its FitzGerald–Lorentz contraction. It will be shown here, however, that this is by no means generally the case. It turns out, in particular, that the appearance of a sphere, no matter how it is moving, is always such as to present a *circular* outline to any observer. Thus an instantaneous photograph* of a rapidly moving sphere has the same outline as that of a stationary sphere.

This result may seem paradoxical at first. For example, it might be thought that for a distant sphere moving perpendicularly to the line joining its centre to the observer, the flattening in its direction of motion would certainly be apparent. As the tangents from the observer to the flattened sphere are all nearly the same length, it might seem that the finite velocity of light is irrelevant here. However, the light which appears to the observer to be coming from the leading part of the sphere leaves the sphere at a later ime, in the observer's frame, than that which appears to come from the trailing part. In fact the light from the trailing part reaches the observer from *behind* the sphere, which it can do since the sphere is continually moving out of its way.) The length of the image of the sphere in the direction of motion is thus greater than might otherwise be expected, so that if it were not for the flattening the sphere would appear to be elongated.

In order to prove the exact result that the sphere always presents a circular outline, it is more convenient to consider the sphere as being at rest and the observer moving, this being allowable according to the special principle of relativity. If the sphere is accelerating, in order that it may reasonably be said to remain a sphere throughout its motion, it must be always instantaneously at rest and spherical in *some* Lorentz frame. The sphere will then satisfy the Born conditions for a rigid body (see Synge (3), p. 36). Now the light received by the observer, O, at an instant of his time, from what appears to him to be the outline of the sphere, comes from the sphere at one instant of *its* time. This shows that the acceleration of the sphere is irrelevant. Furthermore, a stationary observer at O clearly sees something with a circular outline. All this is evident from the symmetry. It is therefore only necessary to consider what transformation of the field of vision must be employed when passing from a stationary to a moving observer at the same point, and to show that this transformation is one which sends apparent circles into apparent circles.

* This is not a 'snapshot' in the sense of Synge ((3), p. 120) in which the sphere would indeed appear flattened. I am concerned, here, with a world-picture rather than a world-map (see Milne (1), p. 107), so that the finite velocity of the light coming from the sphere must be taken into account.

One way of doing this is to use the relativistic aberration formula*

$$\tan \tfrac{1}{2}\theta' = \tan \tfrac{1}{2}\theta \sqrt{\frac{c-v}{c+v}}.$$

A stereographic projection of the unit sphere with centre O, from the point for which $\theta = \pi$, sends circles into circles, and the above formula leads simply to an expansion of the plane of projection by an amount $\sqrt{\{(c-v)/(c+v)\}}$.

Alternatively, the following purely geometrical (space-time) argument, suggested to me by J. L. Synge, may be used. Consider the intersection of the past null cone of the event O with any hyperplane through O containing a time-like vector. The hyperplane represents the history of a plane moving with a constant velocity and the past null cone of O represents the history of a sphere with fixed centre and uniformly decreasing radius. They intersect in a circle which converges on O along a right circular cone. Hence, a stationary observer at the event O sees a circle only. Now this holds equally well in any Lorentz frame and therefore shows that a cone of light which appears as a circle to a stationary observer at O also appears as a circle to any moving observer at O.

There is yet another way of obtaining this result, namely by using properties of two-component spinors. Any past null vector (t, x, y, z) with $t < 0, t^2-x^2-y^2-z^2 = 0$ can be represented as a hermitian matrix which is minus the product of a two-component spinor (a, b) with its conjugate (see Veblen (4)). Thus,

$$\begin{pmatrix} t-z & x+iy \\ x-iy & t+z \end{pmatrix} = -\begin{pmatrix} \bar{a}a & \bar{a}b \\ \bar{b}a & \bar{b}b \end{pmatrix}.$$

A direction along the past light cone is then uniquely associated with the corresponding spinor ray, i.e. with the ratio $\lambda = b/a$. Now the points of the light cone at time $t = -1$ constitute a sphere $\mathscr{S}$, whose equations are

$$x^2+y^2+z^2 = 1; \quad t = -1.$$

The field of vision of a stationary observer at the origin may be conveniently represented by this sphere. But $\mathscr{S}$ may be projected stereographically from the point $(-1, 0, 0, -1)$ into the plane $z = 0, t = -1$, with the point $(-1, x, y, z)$ projecting into $(-1, x/(1+z), y/(1+z), 0)$. This plane may be taken as the Argand plane of the complex number

$$\frac{x}{1+z}+i\frac{y}{1+z} = \frac{x+iy}{z-t} = -\frac{\bar{a}b}{\bar{a}a} = -\lambda.$$

The sphere $\mathscr{S}$ can then be regarded as the Argand sphere of $-\lambda$. But a proper Lorentz transformation of the directions through the origin corresponds to a linear transformation of the spinors (a, b), i.e. to a bilinear transformation of λ. This sends circles into circles on $\mathscr{S}$ as required, so that the result follows.

* This is not the usual formula, which is $\cos\theta = \dfrac{\cos\theta' - v/c}{1-(v/c)\cos\theta'}$ (see Synge (3), p. 147). The two forms are easily shown to be equivalent.

It is perhaps worth remarking here that the fact that any proper homogeneous Lorentz transformation is determined by its effect on any three null directions (see Synge (3), p. 99) is here seen to be equivalent to the corresponding property for complex numbers under bilinear transformations (or points of a projective line under a projectivity).

These considerations can also be applied to non-spherical objects moving with uniform velocity. The appearance of such an object is always a circular transform (i.e. product of inversions) of what it would appear in some orientation when stationary. Thus, straight lines appear circular (or straight). Since a stationary circle may appear elliptical, a moving circle can appear boomerang shaped (inverse of an ellipse). In view of this, it is doubtful whether it would be correct to say that a sphere always appears *spherical* rather than just saying it has a circular outline, since the intersection of two spheres does not necessarily appear circular. Nevertheless, there is no other consistent shape which presents a circular outline when stationary, to any observer.

Finally, it may be remarked that all the above considerations apply equally well to a de Sitter space (Minkowski 4-sphere, see Schrödinger (2)) owing to its symmetry. The foregoing arguments apply almost without change.

REFERENCES

(1) Milne, E. A. *Relativity, gravitation and world-structure* (Oxford, 1935).
(2) Schrödinger, E. *Expanding universes* (Cambridge, 1956).
(3) Synge, J. L. *Relativity: the special theory* (Amsterdam, 1956).
(4) Veblen, O. Geometry of two-component spinors. *Proc. Nat. Acad. Sci., Wash.*, 19 (1933), 100–9.

St John's College
Cambridge

PHYSICAL REVIEW VOLUME 116, NUMBER 4 NOVEMBER 15, 1959

Invisibility of the Lorentz Contraction*

JAMES TERRELL
Los Alamos Scientific Laboratory, University of California, Los Alamos, New Mexico
(Received June 22, 1959)

It is shown that, if the apparent directions of objects are plotted as points on a sphere surrounding the observer, the Lorentz transformation corresponds to a conformal transformation on the surface of this sphere. Thus, for sufficiently small subtended solid angle, an object will appear—optically—the same shape to all observers. A sphere will photograph with precisely the same circular outline whether stationary or in motion with respect to the camera. An object of less symmetry than a sphere, such as a meter stick, will appear, when in rapid motion with respect to an observer, to have undergone rotation, not contraction. The extent of this rotation is given by the aberration angle $(\theta-\theta')$, in which θ is the angle at which the object is seen by the observer and θ' is the angle at which the object would be seen by another observer at the same point stationary with respect to the object. Observers photographing the meter stick simultaneously from the same position will obtain precisely the same picture, except for a change in scale given by the Doppler shift ratio, irrespective of their velocity relative to the meter stick. Even if methods of measuring distance, such as stereoscopic photography, are used, the Lorentz contraction will not be visible, although correction for the finite velocity of light will reveal it to be present.

INTRODUCTION

EVER since Einstein presented his special theory of relativity[1] in 1905 there seems to have been a general belief that the Lorentz contraction should be visible to the eye. Indeed, Lorentz stated[2] in 1922 that the contraction could be photographed. Similar statements appear in other references too numerous to be mentioned, and even Einstein's first paper leaves the impression,[3] perhaps unintentionally, that the contraction due to relativistic motion should be visible. The usual statement is that moving objects "appear contracted," which is somewhat ambiguous. The special theory predicts that the contraction can be observed by a suitable experiment, and the words "observe" and "see" seem to be used interchangeably in this connection.

There is, however, a clear distinction between observing and seeing. An observation of the shape of a fast-moving object involves simultaneous measurement of the position of a number of points on the object. If done by means of light, all the quanta should leave the surface simultaneously, as determined in the observer's system, but will arrive at the observer's position at different times. Similar restrictions would apply to the use of radar as an observational method. In such observations the data received must be corrected for the finite velocity of light, using measured distances to various points of the moving object. In seeing the object, on the other hand, or photographing it, all the light quanta arrive simultaneously at the eye (or shutter), having departed from the object at various earlier times. Clearly this should make a difference between the contracted shape which is in principle observable and the actual visual appearance of a fast-moving object.

CONFORMALITY OF ABERRATION

The basic question of the visibility of the Lorentz contraction may be stated as that of the appearance of a rapidly moving object in an instantaneous photograph. The object, of known shape when at rest, is assumed to have a high uniform speed relative to the camera. The camera is assumed to be at rest in a Galilean (unaccelerated) frame of reference. Of course it would make no difference if the camera were, instead, considered to move at high speed past the stationary object, but the photograph produced must be examined at rest, so it is simpler to consider the camera as stationary. The mechanism of the camera must be such as to give it essentially instantaneous shutter speed and sharp focus over the necessary depth of field.

The questions of whether to use photographic film which lies in a plane or is curved so that all points are at the same distance from the lens (or pinhole), and whether to use a lens corrected to eliminate optical distortions, could be troublesome. To simplify matters, it is assumed that the object subtends a visual solid angle sufficiently small that these matters need not be considered. It is assumed that the camera is pointed directly at the apparent position of the object, so that the light rays strike the film in a perpendicular direction, producing an image in the center of the photographic film. The camera is assumed, also for simplicity,

* This work was supported by the U. S. Atomic Energy Commission.

[1] A. Einstein, Ann. Physik 17, 891 (1905).

[2] H. A. Lorentz, *Lectures on Theoretical Physics* (Macmillan and Company, Ltd., London, 1931; translated from Dutch edition of 1922), Vol. 3, p. 203.

[3] In reference 1 [English translation from *The Principle of Relativity* (Dover Publications, Inc., New York, reprinted from 1923 Methuen edition)] Einstein stated: "A rigid body which, measured in a state of rest, has the form of a sphere, therefore has in a state of motion—viewed [betrachtet] from the stationary system—the form of an ellipsoid of revolution with the axes $R(1-v^2/c^2)^{\frac{1}{2}}$, R, R. Thus, whereas the Y and Z dimensions of the sphere (and therefore of every rigid body of no matter what form) do not appear [nicht erscheinen] modified by the motion, the X dimension appears [erscheint] shortened in the ratio $1:(1-v^2/c^2)^{\frac{1}{2}}$, i.e., the greater the value of v, the greater the shortening. For $v=c$ all moving objects—viewed [betrachtet] from the "stationary" system—shrivel up into plane figures."

not to be rotating to follow the motion of the object, but this is an unessential restriction and would make no difference in the results so long as distortion of the camera due to relativistic angular motion is negligible.

With these assumptions and restrictions defined, the problem of the photographic (or visual) appearance of a rapidly moving object is not a difficult one. The optical image produced by a pinhole lens on a photographic emulsion at constant distance from the aperture is identical with the picture produced by plotting, on a spherical surface centered at the point of observation (eye or camera lens), the apparent visual directions of all points of the object as seen by observer O. For an observer O' having zero velocity relative to the object, this would clearly result in an uncontracted image. If this particular observer is located instantaneously at the same position as that of observer O, with respect to whom the object is not at rest, it is possible to calculate the apparent directions of these same points, as seen by O, from the equation for relativistic aberration.

Spherical polar coordinate angles θ and ϕ, forming an orthogonal coordinate system (θ is the polar angle and ϕ the azimuthal angle), are to be used by observer O in plotting on the spherical surface the apparent instantaneous direction of various points of the moving object. Let the object be moving at constant velocity v, relative to O, in the direction $\theta=0$. Let observer O be receiving light from some particular point of the object which appears to be in the direction (θ,ϕ). Let observer O' be instantaneously at the position of O, using the coordinate system (θ',ϕ'), and moving with velocity v relative to O in the direction $\theta=0=\theta'$. The relation between these two sets of coordinate angles is that of the aberration equation, derived[1] from the Lorentz transformation, and given by

$$\sin\theta=\frac{(1-v^2/c^2)^{\frac{1}{2}}\sin\theta'}{1-(v/c)\cos\theta'}, \tag{1}$$

or

$$\cos\theta=\frac{\cos\theta'-v/c}{1-(v/c)\cos\theta'}. \tag{1'}$$

In these equations c is, of course, the velocity of light. The azimuthal angles are not affected by the Lorentz transformation, so that

$$\phi=\phi'. \tag{2}$$

It may be shown that this transformation of the angles of observation is equivalent to a conformal transformation on the spherical surfaces centered on the observers. This fact and its consequences were apparently first pointed out quite recently.[4]

Consider a small rectangular area of differential extent on the surface centered on observer O, oriented along lines of constant θ and ϕ. The angles subtended by the sides of this rectangle are $d\theta$ and $\sin\theta d\phi$. As seen by observer O' the corresponding angles are $d\theta'$ and $\sin\theta' d\phi'=\sin\theta' d\phi$. Differentiation of Eq. (1) gives the simple relation

$$\frac{d\theta'}{d\theta}\frac{\sin\theta'}{\sin\theta}=\frac{1-(v/c)\cos\theta'}{(1-v^2/c^2)^{\frac{1}{2}}}=\frac{(1-v^2/c^2)^{\frac{1}{2}}}{1+(v/c)\cos\theta}=M. \tag{3}$$

Thus the two rectangles have identical ratios between their length and width. This, with the perpendicularity between sides which is true for both rectangles, is sufficient to establish the conformality of the transformation of angles of observation. The factor M is the magnification, the ratio between subtended angles as seen by observers O' and O, or the ratio of apparent distances of the object from the two observers. It is interesting that M is precisely the Doppler shift factor, becoming $[(1-v/c)/(1+v/c)]^{\frac{1}{2}}$ for $\theta=0=\theta'$.

The property of conformality in this sense, which is intrinsic to relativistic aberration, is sufficient to ensure that observers O and O' will obtain pictures which are identical, except for a magnification factor, over comparable regions of small subtended solid angle. Thus a spherical object will produce a perfectly round image[5] for both observers O and O', in spite of the Lorentz contraction which O may observe by suitable methods. Quite generally, objects will appear the same shape, visually, to all observers, no matter what the relative motion of object and unaccelerated observer may be. Obviously these conclusions also extend to accelerated objects. Although acceleration will in general change the shape of the object, all observers at a given point will agree as to what this shape is, as revealed in their photographs. Even accelerated observers will obtain similar photographs, provided that the cameras are not appreciably distorted by the acceleration. In this way the apparent shape of any object is invariant to the Lorentz transformation, although the "actual" shape, as given by careful measurement, will vary due to the Lorentz contraction.

Thus the Lorentz contraction is effectively invisible. Only when stereoscopic vision or photography is used, combining observations from two different locations, can any distortion of the object due to motion be seen, and even this is not the expected contraction, as will be discussed in a later section.

[4] J. Terrell, Bull. Am. Phys. Soc. Ser. II, 4, 294 (1959), and unpublished paper on *The Clock "Paradox"*, Los Alamos Document LADC-2842 (April 1957).

[5] R. Penrose, Proc. Cambridge Phil. Soc. 55, 137 (1959), has recently proved that a sphere will be seen as having a circular outline by all observers, regardless of the relative velocity of sphere and observer. Penrose gives several proofs, of which the simplest involves the stereographic projection of a sphere centered at the point of observation onto its equatorial plane from the pole $\theta=\pi$. This transformation sends circles into circles, and aberration merely expands the plane of projection by the factor $[(c-v)/(c+v)]^{\frac{1}{2}}$. Penrose's conclusions agree with some given in this paper, although his paper deals almost exclusively with spherical objects. For this special case there is no restriction as to subtended visual angle. For finite subtended angle the surface of a moving sphere would appear somewhat distorted, although its outline would be precisely circular.

APPEARANCE OF MOVING METER STICK

At this point it may be objected that a meter stick in motion past the observer in such a way that it is moving parallel to its length, and is momentarily seen by the observer at its point of closest approach, will surely be seen as contracted. This case, probably the first to come to mind, is illustrated in Fig. 1 for the case $v/c=0.8$. Two meter sticks, S and S', are shown here in such positions as to be seen instantaneously by observer O at 90°. Meter stick S is stationary with respect to observer O; meter stick S' is moving with velocity v in the direction $\theta=0°$; both meter sticks are aligned along the direction $\theta=0°$. At the earlier time when the light which reaches observer O left S', both ends of the front face of the meter stick were at the same distance from O, so that he does indeed see them as they were at simultaneous earlier times, and the length of the meter stick S' appears contracted by comparison with S, which was at the same distance. However, at the still earlier time when light left the back side of the meter stick, stick S' was displaced farther to the left. This results in the visibility of the left-hand end of S', if it is assumed to be a physical stick having three dimensions. Thus the meter stick gives the appearance of having undergone rotation rather than contraction.

Consider how this situation appears to observer O', who is also moving with velocity v, with respect to O, in the direction $\theta=0=\theta'$. To O' both meter sticks will appear to be in the direction $\theta'=\cos^{-1}(v/c)$. Stick S' will appear stationary and turned through the angle $(\theta-\theta')$ with respect to his line of sight. Stick S will appear to be moving at high speed v to the left, but will not appear contracted. Because the right-hand side of S was much farther away from O' at the time light seen by O' left it than was the left-hand side when light left it, the time lags increase the apparent length of S in such a way that its contracted length appears quite normal (in two dimensions, as in the photograph).

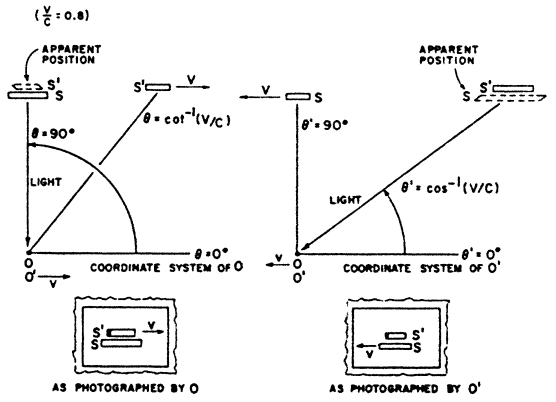

FIG. 1. Two meter sticks, S and S', as seen by observers O and O', who are located momentarily at the same point. In the coordinate system of observer O, O', and S' are moving to the right with velocity v, while S is stationary.

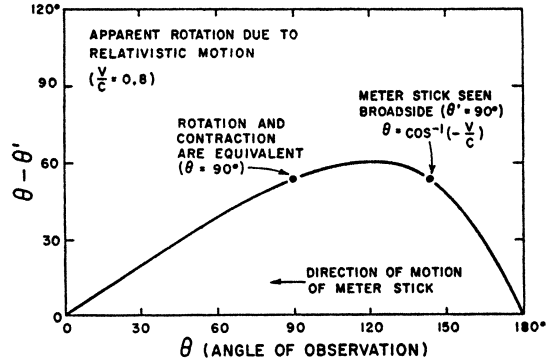

FIG. 2. Apparent rotation from known orientation as seen for relativistic motion of a meter stick with respect to an observer. The meter stick is assumed to be moving in the direction $\theta=0°$ and to be oriented along its direction of motion.

In fact, as has been shown, both observers O and O' see the same things, except for the apparent distance. Thus the photographs taken by O and O', shown in Fig. 1, are identical, or could be made identical by the use of an enlarger. It is probable that observers O and O' will put different interpretations on what they see, but the conformality of aberration ensures that, at least over small solid angles, each will see precisely what the other sees. No Lorentz contractions will be visible, and all objects will appear normal.

APPARENT ROTATION DUE TO RELATIVISTIC MOTION

It is apparent from the discussion above that objects in rapid motion appear visually to have undergone a rotation of extent $(\theta-\theta')$, the aberration angle, from their "true" or known orientations. The angle θ is the angle at which the object appears to be, with the coordinate system chosen so that the object is moving past the observer O (considered stationary) in the direction $\theta=0$. The angle θ' is the apparent direction of the object as perceived by another observer O', located at the same position at the same time, to whom the object appears stationary. The angles θ and θ' are related by the aberration equation, Eq. (1).

The dependence of the apparent rotation on the angle of observation is shown in Fig. 2 for the case $v/c=0.8$. For $\theta=0$ and $\theta=\pi$, the apparent rotation is zero. Two other angles are of special interest. For $\theta=\pi/2$ the rotation is such that $\cos(\theta-\theta')=(1-v^2/c^2)^{\frac{1}{2}}$, and a linear object which was oriented in the direction $\theta=0$, at the earlier time when light left it, will appear contracted by the rotation just to the extent of the Lorentz contraction. This does not constitute a proof of the visibility of the contraction, as this relation does not hold for other orientations, angles of observation, and shapes, and since the appearance of the object is normal at all times. The apparent rotation would, to observer O', be a real rotation. The other angle of interest is that for which $\cos\theta=-v/c$; for this angle $\theta'=\pi/2$, and the

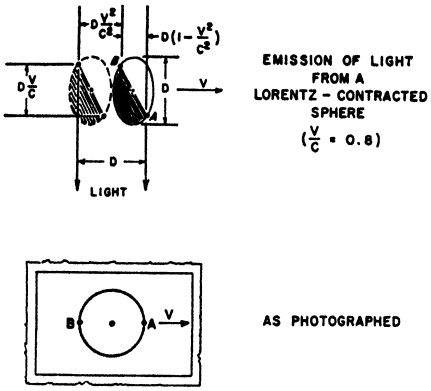

FIG. 3. Mechanism by which a Lorentz-contracted moving sphere produces a round photographic image. The shaded area is the visible portion of the spherical surface, with A and B the farthest visible points along the direction of motion. The dashed ellipse represents the earlier position of the sphere when the light which will arrive at the camera simultaneously with light from A left B.

object, if linear and oriented along $\theta=0$, will then be seen broadside, with no view of the ends.

Thus a meter stick which is traveling, and oriented, in the direction $\theta=0$ will appear to observer O to be rotating about its line of motion in such a way as to appear broadside at $\theta=\cos^{-1}(-v/c)$, and to present a view of its rear end from that time on. For $\theta=\pi/2$ the rotation will foreshorten the length to the same extent as the Lorentz contraction, and for a meter stick traveling nearly at the speed of light little will be seen at this angle of apparent closest approach, or at most angles, except the rear end.

For an object of rotational symmetry, such as a sphere, no possibility of confusing rotation and contraction exists. Thus a sphere will always produce a round photographic image, no matter what its unaccelerated motion. The mechanism by which this occurs is shown in Fig. 3. A Lorentz-contracted sphere is assumed to be moving to the right with velocity v relative to the observer; for the purpose of this figure $v/c=0.8$. The sphere is to be viewed at $\theta=\pi/2$. The uncontracted diameter of the sphere is D, giving a contracted diameter of $D(1-v^2/c^2)^{\frac{1}{2}}$. However, the farthest visible points on the sphere, A and B, as measured along the direction of motion, are not this far apart. This corresponds to the visual effect of apparent rotation. As plotted on the uncontracted sphere, the visible area is tilted from its position for $v=0$ by $(\theta-\theta')$; here $\theta=\pi/2$ so that $\cos(\theta-\theta')=(1-v^2/c^2)^{\frac{1}{2}}$. Thus the distance between the farthest visible points is reduced to $D(1-v^2/c^2)$ as measured along the direction of motion. As measured along the line of sight, perpendicular to the motion, this distance is Dv/c. Thus the light which reaches the observer from B must leave B at a time Dv/c^2 earlier than the light that leaves A in order to arrive simultaneously with the light from A. During this time the sphere moves a distance Dv^2/c^2, so that the distance between A and B appears to be D, as seen or photographed by the observer. Thus the sphere appears uncontracted in the observer's photograph.

Physically, the reason that A is the farthest visible point is that light leaving points beyond A on the spherical surface will be intercepted by the motion of the sphere. Similarly, point B is visible, though on the far side of the sphere, because light emitted from this point will not be stopped by the sphere, which moves out of the path of the light.

STEREOSCOPIC VISION

If stereoscopic vision or photography is to be considered, the situation becomes more complicated. Simultaneous observations of direction of a given object from two observation points constitute a valid means of measuring distance to the object. Thus, with stereoscopic vision, all points will appear to be at the proper distance even with relativistic speeds. However, what is seen at a given time is the situation which existed at an earlier time, and not all parts of the object are seen at the same earlier time. This produces curious visual distortions of the sort shown in Fig. 1 at the apparent positions of S and S', constituting shear and contraction or elongation, depending on the situation. For instance, an object coming directly toward the observer is seen in three dimensions to be elongated along its direction of motion by the ratio $[(1+v/c)/(1-v/c)]^{\frac{1}{2}}=M(180°)$, and incidentally appears farther away, by the same ratio, than if the observer had the same velocity as the object.

At other angles of observation the situation is less simple to describe. In general, if an observer sees two points on a stationary object which are at precisely the same visual angle but at different distances, another observer at the same point but moving in a different reference frame will see the two points as M times farther away and M times farther apart. Here M is given by Eq. (3). In general, this results in apparent shear of the object, as seen with stereoscopic vision. Precisely the same effects would occur with the apparent perspective of the object, even with nonstereoscopic vision, if the object were near enough to make perspective noticeable.

CONCLUSIONS

It has been shown that the Lorentz transformation is conformal in the angles of observation, so that the photograph obtained by an observer depends only on the place and time of taking the picture and is independent of the relative motion of observer and object photographed. This statement must be restricted to small solid angles in the same way that conformal transformations preserve shapes only for differential areas. Thus the visual appearance of an object is invariant (except for Doppler shifts of frequency), not

depending on its (unaccelerated) motion. Effectively, then, the Lorentz contraction is invisible. Any hopes of seeing the contraction in a rapidly moving space vehicle or astronomical body must be discarded.

Although apparent distortion due to rapid motion can be seen by means of steroscopic vision or photography, it is not of the same type as one might expect from the Lorentz contraction.

None of the statements here should be construed as casting any doubt on either the observability or the reality of the Lorentz contraction, as all the results given are derived from the special theory of relativity.

P.-K. Hsiung, R. H. Thibadeau, "Spacetime visualization of relativistic effects", Proceedings of the 1990 ACM annual conference on Cooperation (1990), 236-243, © 1990 ACM, reprinted with kind permission from Robert H. Thibadeau and ACM

Spacetime Visualization of Relativistic Effects

Ping-Kang Hsiung*
Robert H. Thibadeau†
Carnegie Mellon University
Pittsburgh, Pennsylvania 15213

Abstract

We have developed an innovative ray-tracing algorithm to describe *R*elativistic *E*ffects in *S*pace*T*ime ("REST"). Our algorithm, called *REST-frame*, models light rays that have assumed infinite speed in conventional ray-tracing to have a *finite* speed c in spacetime, and uses general Lorentz Transformation, which connects the spacetime description of a single event in two inertial coordinate systems (*frames*) that differ by a constant velocity, to perform the relativistic translation and aberration of light rays.

In this paper, we report the extension of our previous work for visualizing relativistic motion in spacetime to include relativistic Doppler color shift and the simulation of complex kinematic systems in which objects of different relativistic velocities coexist. Our simulations have produced non-intuitive images showing anisotropic deformation (*warping*) of space and intensity concentration/spreading of light sources in spacetime. Images of objects undergoing relativistic Doppler shift are also generated.

By applying state-of-the-art computation technology and simulation techniques to the earlier quests in Physics that were conducted mainly by *thought experiment*, we demonstrate, through our new revelations, that *REST-frame* offers a powerful *experimentation tool* to study and explore some of the most exciting aspects of the natural world; particularly, the rich physical properties associated with the finite speed of light.

Keywords: Apparent effects of Special Relativity. Relativistic Doppler shift. Scientific visualization. Computer simulation. Computer image synthesis. Ray-tracing.

*Department of Electrical and Computer Engineering, Carnegie Mellon University. (412) 268-2524. pkh@cs.cmu.edu
†Imaging Systems Laboratory, The Robotics Institute, Carnegie Mellon University. rht@vi.ri.cmu.edu
This research was partially supported by Imaging Systems Laboratory, The Robotics Institute, Carnegie Mellon University.

1 Introduction

1.1 Motivations

The revival of interest in Special Relativity in the early 1960's was focused on the appearance of relativistic objects under *ad hoc* conditions. Until that time, for nearly fifty-five years since the inception of the special theory, such phenomena had not been fully explored.

Our intent today has been to produce simulation images with visual realism that incorporate the effects of

- object deformation due to relativistic spacetime geometry, and
- complete intra-object and inter-object optical phenomena, such as perspective projection, reflection, refraction and shadow casting.

Flexible selection of simulation parameters including viewpoint, viewing direction, viewing time and relative traveling velocity between objects and the observer is also essential. These requirements are accomplished by the application of an innovative ray-tracing algorithm, which we called *REST-frame*.

In this paper, we extend our previous work for visualizing one dimensional (1D) and three dimensional (3D) relativistic motion in spacetime to include a more general class of problems, in which the observed objects undergo *different* 3D motion relative to the observer. We also model the Doppler color shift due to relativistic motion.

1.2 Background and previous work

Einstein's Special Theory of Relativity (1905) postulated [12][13][9]:

1. Non-existence of preferred reference system (*"The Principle of Relativity"*): the laws of physics must be the same for observers in all inertial reference systems.[1]
2. Constancy of speed of light: c is constant in a vacuum in all inertial frames and is independent of the motion of a light source relative to the observer.

Some consequences of the spacetime model are:

[1] A reference system, or *reference frame*, is *inertial* in spacetime if it is nonaccelerating.

P.-K. Hsiung, R. H. Thibadeau, "Spacetime visualization of relativistic effects", Proceedings of the 1990 ACM annual conference on Cooperation (1990), 236-243, © 1990 ACM, reprinted with kind permission from Robert H. Thibadeau and ACM

- The measured space and time coordinates are dependent upon the reference frame from which the measurement is made.
- The Lorentz Transformation relates measured spacetime coordinates between inertial reference frames.
- Lengths perpendicular to relative motion remain the same measurements for all inertial observers. Lengths parallel to relative motion are measured to have undergone contraction in comparison with their rest lengths.

James Terrell (1959)[14] made an early distinction between the *appearance* or visibility of relativistic effects and the *measurement* of relativistic effects. Following the initial work of Penrose (1959)[10] and Terrell, interest was sparked and a number of related papers were published.[2] The extent of this revival of interest was limited in that scientists lacked the computing power, ray-tracing technique, and visualization outlook.

Ray-tracing synthesizes images using a model that reverses the image formation process in nature [3][2](figure (1)). Rays are traced from pixels on the image plane through a

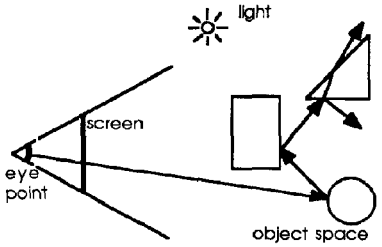

Figure 1: Ray-tracing principle

fixed "eye-point" (or "viewpoint") into the object space that forms the scene. Reflection and refraction rays ("secondary rays") are recursively spawned when rays meet (*"hit"*) objects. Light intensity is computed on the object surface at every ray-object intersection point according to some illumination model[11][17][15][1], and contributes to the final pixel intensity of the synthesized image.

This ray-tracing computation can be modeled as two interacting processes: the *intersection process* and the *shading process* (figure (2))[4]. The former solves for intersection points where rays hit scene object surfaces, while the latter performs shading computation.

In the traditional ray-tracing algorithms, a light ray had always been regarded as if it traveled with infinite speed, and Galilean-Newtonian transformation was used to model relative motion between dynamic systems and the observer. When the scene objects and the observer (or the camera plate) are in relative motion at speeds comparable to light speed, Special Relativity requires the time information to be interwoven with the spatial coordinates in defining the vision formation process. Light speed must be treated as *finite*, and reference frames are to be connected by Lorentz Transformation.

[2]Interested readers can find a more extensive bibliography in [5] about those papers as well as about research in ray-tracing simulation.

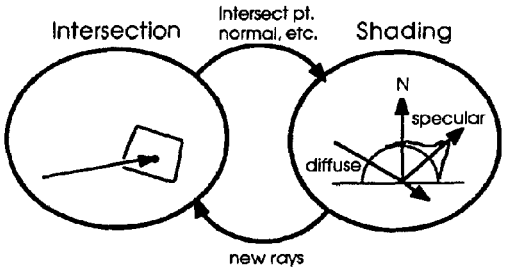

Figure 2: Ray-tracing computation model

In [5], we first treated the subject of visualizing the spacetime world of Special Relativity using the new ray-tracing technique *REST-frame*. Objects were assumed to make 1D motion relative to the observer. The 3D motion extension of our original work has since been completed[6]. A fast spacetime visualization method based on the scanline operation has also been designed and implemented[7].

2 Approach

2.1 *REST-frame* ray-tracing

The *REST-frame* technique synthesizes the visual effects in spacetime by incorporating the finite speed of light in ray-tracing to simulate the Special Relativity physics. Light-rays are traced back to their source events in the *past* in spacetime from the observation point, which is itself an event in spacetime. The three key elements in our approach are:

1. Time modeling in the ray-tracing equations: A ray that passes spacetime event[3] $[x_0, y_0, z_0, t_0]$ and travels in 3D direction $\vec{a}$ in a frame S is modeled as

$$r\vec{a}y_{REST} = (x, y, z) = (x(t_0),\ y(t_0),\ z(t_0)) + c(t_0 - t)\,\vec{a} \quad (t \le t_0) \qquad (1)$$

   Where t is the time the ray (traveling at light speed c) passes the coordinates (x, y, z) in S, starting at $[x_0, y_0, z_0, t_0]_S$.

2. Lorentz Transformation of rays between frames: For inertial Cartesian coordinate system $S'(x', y', z')$ with time t' that travels at a 3D velocity $\vec{V} = (u, v, w)$ relative to system $S(x, y, z)$ and t, if its X', Y' and Z' axes coincide with X, Y and Z, respectively, of S at time $t = t' = 0$, then the spatial and time coordinates[4] $\vec{X}'$ and t' can be derived from $\vec{X}$ and t in S using Lorentz Transformation[9]

$$\vec{X}' = \vec{X} + [\frac{(\gamma - 1)}{\| \vec{V} \|^2}(\vec{X} \cdot \vec{V}) - \gamma t]\vec{V}$$
$$t' = \gamma(t - \frac{\vec{X} \cdot \vec{V}}{c^2}) \qquad (2)$$

[3]We use the symbol (x, y, z) for 3D positional coordinates and $[x, y, z, t]$ for a spacetime event point. When we designate a specific reference frame S, we use $(x, y, z)_S$ and $[x, y, z, t]_S$. Individually, each component is written with a subscript S (e.g. t_S). We also use $[x_0, y_0, z_0, t_0]_S$ as a shorthand for spacetime event $[x(t_0), y(t_0), z(t_0), t_0]_S$, and $(x_0, y_0, z_0)_S$ for spatial point $(x(t_0), y(t_0), z(t_0))_S$.

[4]$\vec{X}' = (x', y', z')_{S'}$ and $\vec{X} = (x, y, z)_S$.

P.-K. Hsiung, R. H. Thibadeau, "Spacetime visualization of relativistic effects", Proceedings of the 1990 ACM annual conference on Cooperation (1990), 236-243, © 1990 ACM, reprinted with kind permission from Robert H. Thibadeau and ACM

in which $\| \vec{V} \|^2 = u^2+v^2+w^2$, and $\gamma = 1/\sqrt{1 - \frac{\|\vec{V}\|^2}{c^2}}$. Vector $\vec{V}$ is sometimes replaced by vector $\vec{\beta} = (\beta_x, \beta_y, \beta_z) = (u/c, v/c, w/c)$.

For the ray in eq. (1), the S' representation of ray origin can be obtained by applying eq. (2) to the S frame origin $[x_0, y_0, z_0, t_0]_S$. This transformation has the effect that a ray *appears* to have its origin translated when moving from S to S'.

The ray direction $\vec{a}$ in S and $\vec{a'}$ in S' satisfy the following relativistic aberration equation:[5]

$$\vec{a'} = \frac{\vec{a} + [\frac{(\gamma-1)}{\|\vec{V}\|^2}(\vec{a} \cdot \vec{V}) + \gamma]\vec{V}}{\gamma(1 + \vec{a} \cdot \vec{V})} \quad (3)$$

3. Ray-object intersection in spacetime: For all objects that are in motion at a same speed relative to the image formation frame S, we can find a frame S' such that the objects are *stationary* in S',[6] and S' shares the three Cartesian coordinate axes with S at their common origin event [0, 0, 0, 0].

   We transform screen rays defined ("fired") in S to their S' representations, and perform intersection test with the stationary objects in S'. Shade calculation and secondary rays spawning are also conducted conveniently in S'.

2.2 Multiple frame intersection

In order to extend the ray-object intersection method explained in section 2.1 to systems of objects with multiple velocities, it is necessary to consider multiple inertial frames S'_1, S'_2, ..., S'_n. Any object or group of objects which travels at a unique

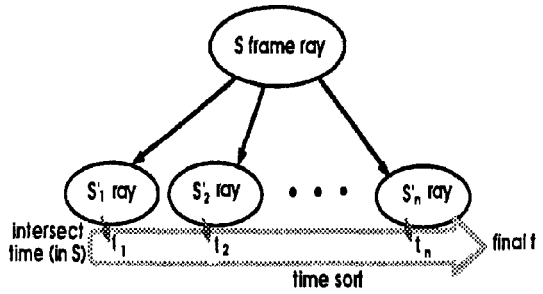

Figure 3: Multiple frame intersection and time sort

velocity with respect to observer frame S may be placed in its own proper frame S'_i. Our object space has thus been divided into a series of coexistent inertial frames. We then fire rays into all of the coexistent frames (figure 3). A given ray may result in one of three cases:

1. The ray misses all objects in all frames. The background color is returned, as is done for a "ray miss" in the conventional ray-tracing.
2. The ray hits one object at one spacetime event. The appropriate shade for that event is returned, again as was done previously.
3. The ray hits objects in more than one frames. This requires the hit events to be sorted in order of time in frame S, so that the most *recent* event is found; it is this event which is displayed.

The sort used in the third case is analogous to the *visibility sort* performed in conventional ray-tracing. In the latter, there is one single frame S'=S; any given hit event supersedes those that occurred before it in time.

We note that this multiple frame intersection method may be performed recursively, as is required for the computation of reflection and/or transmission of light in ray tracing. Each secondary ray, originated from a hit event in some S'_i, however, must be translated into the frames S'_1, S'_2, ..., S'_n for the reflected or transmitted event to be detected amongst the various inertial frames.

2.3 Relativistic Doppler effect

A light source in relativistic motion is *observed* to have a frequency shift according to the following formula:

$$f = \frac{1}{\gamma(1 + \vec{e} \cdot \vec{V})} f_o \quad (4)$$

The symbols used in equation (4) are

f_o : *frequency of light in its proper frame S'.*
f : *frequency of light observed in S.*
$\vec{e}$: *observed direction of light in S.*
$\vec{V}$: *Velocity of S' relative to S.*

The $\frac{1}{\gamma(1+\vec{e}\cdot\vec{V})}$ part is sometimes called the *Doppler shift factor.*

We implement the Doppler frequency shift effect by conducting the conventional ray-tracing shading in S' frame, and transforming the final color returned to each pixel[7] by its screen ray using eq. (4).

3 Implementation and experiments

3.1 Implementation

We have implemented this *REST-frame* ray-tracing approach based on the bounding volume intersection acceleration technique[8][5]. The scene objects are defined in an input file. Also included in the file are the viewpoint, view time, view angle and view direction parameters. For the multiple velocity simulations, we partition the objects by their frames, and specify their respective frame velocity independently. The light sources are assumed to be isotropic and stationary in the objects frame. We performed our experiments on an Apollo DN-10000 system with 2 CPU boards and 32M byte of physical memory. Most of our simulations took less than 5 minutes to produce 512 by 512 images, although for some complex scenes, the simulations exceeded 2 hours.

[5] See [12][9] for derivation.

[6] Such an S' is called the *proper frame* or *rest frame* for the objects.

[7] in observer frame S.

3.2 Experimental results

3.2.1 Headlamp effect

In the first set of experiments, we place a 2 x 2 array of light sources at a fixed distance in front of a diffusive plane. The plane and the light sources are in S' and move towards/away from the viewpoint in the viewing direction, which is perpendicular to the plane. Our results are shown in figures (4), (5), (6), (7), (8).

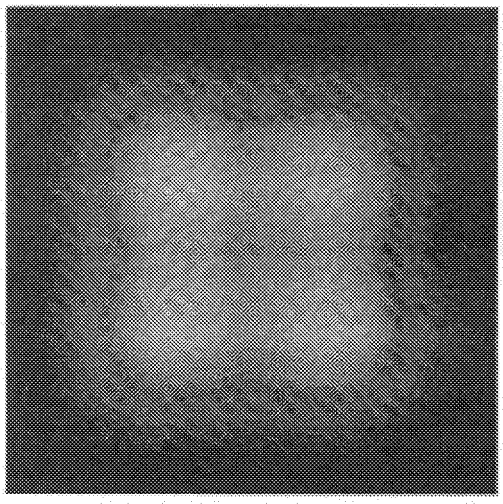

Figure 4: Light sources viewed at stationary (©1989 Hsiung)

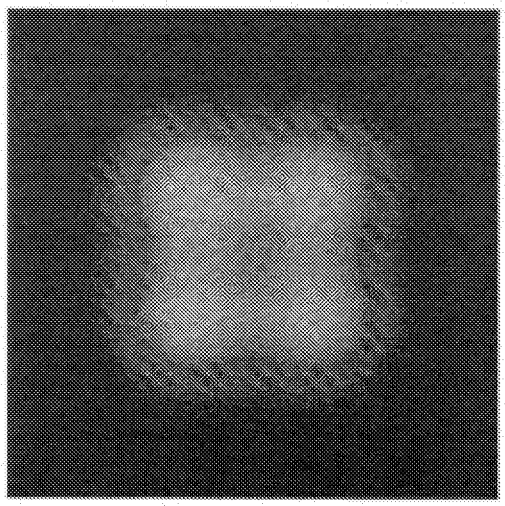

Figure 5: Light sources moving towards observer at 0.5c (©1989 Hsiung)

The imaging times in all figures are the same: the time when event [0, 0, 0, 0] arrives at the imaging plate. Therefore, the concentrating and flooding of light sources patterns revealed in these pictures are purely caused by the anisotropic warping of spacetime inherent in relativistic imaging, rather than by changing viewing configurations. This variation of light intensity distribution in space is termed *headlamp effect* in [16].[8]

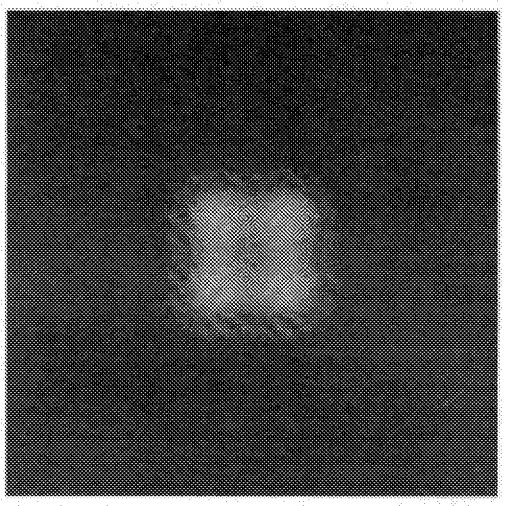

Figure 6: Light sources moving towards observer at 0.9c (©1989 Hsiung)

3.2.2 Multiple frame intersection

The second set of experiments has the scene configuration of an 11 x 11 array of bars, each aligned with the Z axis, spreading evenly on the X-Y plane in S'. The viewer is located at a fixed distance away on the positive Z axis in S, and looks towards the X-Y plane. Figure (9) shows the stationary image.

In figure (10), the bars travel in row formation in the X direction. The travel speeds of the bar rows increase from 0.0c at the bottom row to 0.9c at second to top row, in increment of 0.1c; the top row travels at 0.99c.

Figure (11) shows bar rows traveling in parallel to the +Z direction towards the observer. The middle row is moving at 0.95c, the rows next to it at 0.9c, and 0.7c, 0.5c, 0.3c, 0.0c subsequently. The lens-like effect[5] shows up with varying extent in rows due to the variation in traveling speed.

3.2.3 Relativistic Doppler effect

Our third set of experiments consists of a tile array that travels at various velocities in simulations. In each simulation, the Doppler shift factor in eq. (4) is computed at every pixel on the image plate. These numbers, rather than the absolute pixel color values, are then stored as the simulation output. To produce a final image, the output pixels are scaled and mapped to grayscale level of 0-255 in postprocessing. The scaling/mapping serves as a normalization process to increase the displayable dynamic range based on 256 grayscale levels; the resulting images thus show a *relative* measure of the Doppler shift.

Our results are shown in figures (12), (13), (14), and (15).

[8] We noticed that in *"Star-Trek IV"*, this effect was not done correctly.

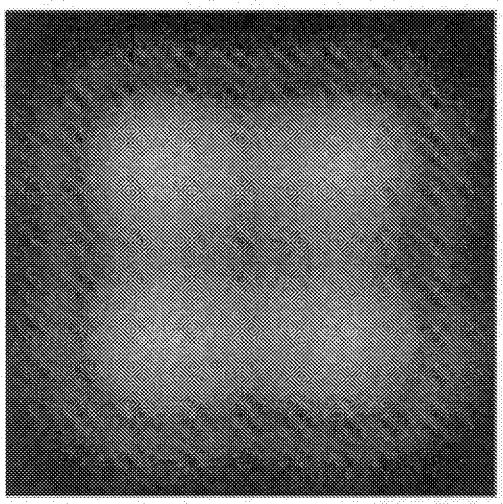

Figure 7: Light sources moving *away from* observer at 0.5c (©1989 Hsiung)

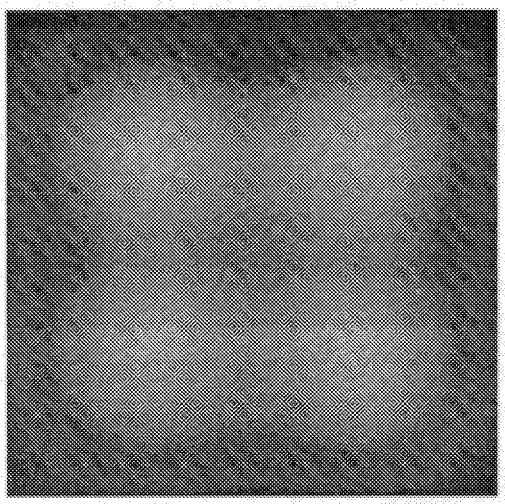

Figure 8: Light sources moving *away from* observer at 0.9c (©1989 Hsiung)

Figures (13) and (15) are, respectively, figures (12) and (14) quantized to 15 levels. We make the following remarks about these images:

- The brighter pixels represent higher Doppler shift levels, and the darker pixels the lower levels. The background portion of the images is from the void space, and is pseudo-colored to enhance the images.

  In the 0.8c sideways motion simulation, the range of the factors is (0.538, 0.703) – a red-shift over the entire image. A 0.9c sideways motion under the same viewing condition (images not shown) gives range of (0.398, 0.50), which is a narrower shift range. In the simulation of 0.9c objects motion towards the observer, the shift factor range is (3.407, 4.359).

- Figure (13) clearly shows the the concentric iso-Doppler-factor rings arisen from the symmetric spacetime geometry resulted from the relativistic motion. The central ring contains pixels of the highest shift factors.

- Figure (15) shows the interesting vertical stripes of iso-factor pixels. Each stripe covers pixels that have similar $(\vec{s} \cdot \vec{V})$ values.

4 Discussion

4.1 Possible extensions

We are making extensions of our current implementation in the following directions:

- A more complete light source model that incorporates moving light sources and self luminous bodies. Our current light sources are static in space and time.[9]

- A generalization to the current (constant and linear) motion model. Specifically, the modeling of acceleration and angular motion. In the first case, events at different pasts have different linear velocities. In the second case, points on a rotating object surface experiences different linear velocities relative to the viewer.

- Texture mapping — an element necessary to show, for instance, the surface feature distortion on a fast moving planet.

4.2 Color shift

In this paper, we have chosen to show the relative (normalized) scalar values of the Doppler shift factor, instead of the absolute RGB color images of the Doppler effect. To perform the latter approach, these following issues are involved:

- The surface properties of the objects need to be represented in the language of power spectral density, instead of the commonly used RGB or XYZ values.

- Dynamic range re-normalization: The Doppler shift in the more interesting motion conditions tends to be so severe (ref. section 3.2.3) that

  - part or all of the *defined* object spectrum will become invisible. A re-normalization of the intensity as well as repair of color components is needed to make vision possible.

  - The resulting dynamic range of the spectrum is always wider than the original. This means in the visible spectral range, the energy is less than the original energy. In most cases, the resulting images will be too dim to view. Intensity compensation of a different type than the one above is necessary to restore the visibility of the images.

[9] In either S or the S'.

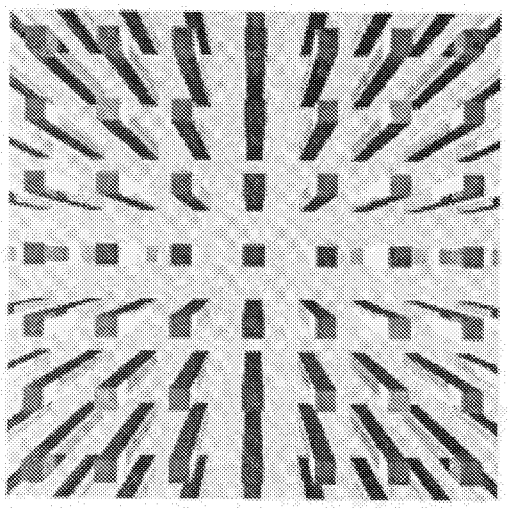

Figure 9: Array of bars viewed at $\beta = 0.0$ (©1989 Hsiung, Dunn & Loofbourrow)

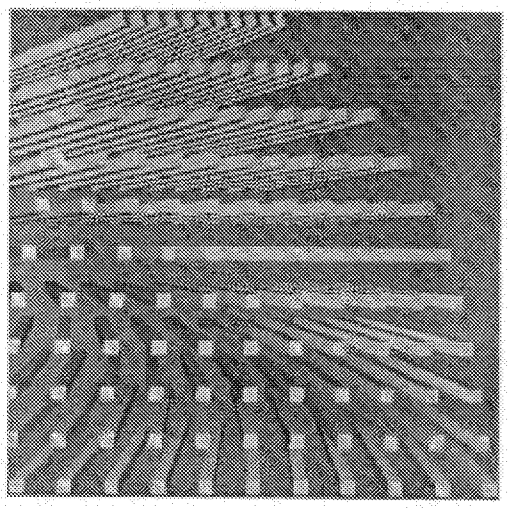

Figure 10: Bar rows with incremental sideways speeds from bottom to top (©1989 Hsiung & Loofbourrow)

We have completed our initial investigation and software implementation to simulate (power spectral based) relativistic Doppler shift. Our work in this area will be reported in a future paper.

5 Conclusion and future work

The *REST-frame* algorithm is a construct used for the study of nature. It is a new analytical tool which moves beyond the root mathematical language of modern physics by means of an interactive exploratory visualization methodology. The *REST-frame* algorithm allows us to create an environment for empirical simulation. This methodology is a preliminary step towards expanding the conceptual building-blocks with which we perceive the world as well as towards increasing the visionary capacity of the mind.

We submit that this visualization tool and the associated techniques could have far-reaching impact on future research in such diverse fields as the following: cosmology, nuclear science, space science and exploration, cognitive science and perceptual studies, computer micro-architecture and networks. Further work may involve the simulation of visual effects in accelerated frames of reference and in animation studies of macroscopic and microscopic domains.

Acknowledgments

We would like to thank Nathan Loofbourrow and Michael Wu for their assistance. Thanks are also due to Robert H. P. Dunn for his profound ideas about this research. We are grateful to Kathryn Porsche for her insightful suggestions that contributed to this presentation.

References

[1] R. Cook and K. Torrance. A reflectance model for computer graphics. *ACM Trans. Graphics*, 1(1):7–24, Jan 1982.

[2] Andrew Glassner. *An Introduction to Ray-Tracing*. Academic Press Limited, 1989.

[3] R. Goldstein and R. Nagel. 3-D visual simulation. *Simulation*, 25, 1971.

[4] Ping-Kang Hsiung. Data structures for ray-tracing. *Thesis Proposal, Carnegie Mellon University*, Feb. 1989.

[5] Ping-Kang Hsiung and Robert H. P. Dunn. Visualizing relativistic effects in spacetime. In *Proceedings of the Supercomputing '89 Conference*, Nov. 13-17, 1989.

[6] Ping-Kang Hsiung and Robert H. Thibadeau. Spacetime visualization of 3D relativistic motion. *Unpublished document*, Oct., 1989.

[7] Ping-Kang Hsiung, Robert H. Thibadeau, and Michael Wu. T-buffer: fast visualization of relativistic effects in spacetime. In *1990 Symposium on Interactive 3D Graphics (to appear)*, March 18-21, 1990.

[8] T.L. Kay and J.T. Kajiya. Ray tracing complex scenes. *Computer Graphics (SIGGRAPH)*, 269–278, Aug. 1986.

[9] C. Møller. *The Theory of Relativity*. Oxford University Press, 1960.

[10] R. Penrose. The apparent shape of a relativistically moving sphere. *Proceedings of the Cambridge Philosophical Society*, 55:137–9, July 29 1958.

[11] Bui Phong. Illumination for computer generated pictures. *CACM*, 18(6):311, June 1975.

[12] Robert Resnick. *Introduction to Special Relativity*. Rensselaer Polytechnic Institute, 1968.

[13] E. Taylor and J. Wheeler. *Spacetime Physics*. M.I.T. / Princeton, 1966.

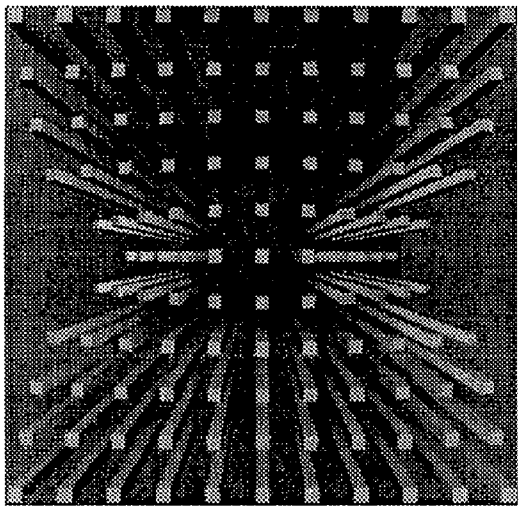

Figure 11: Bar rows with varying speeds towards observer; see text (©1989 Hsiung & Loofbourrow)

[14] J. Terrell. Invisibility of the Lorentz contraction. *Physical Review*, 116(4):1041, 1959.

[15] K. E. Torrance and E. M. Sparrow. Theory for off-specular reflection from rougheded surfaces. *Journal of the Optical Society of America*, 1105, 1967.

[16] V.F. Weisskopf. The visual appearance of rapidly moving bodies (section). *Physics Today*, 13(9):24, 1960.

[17] T. Whitted. An improved illumination model for shaded display. *CACM*, 343–349, June 1980.

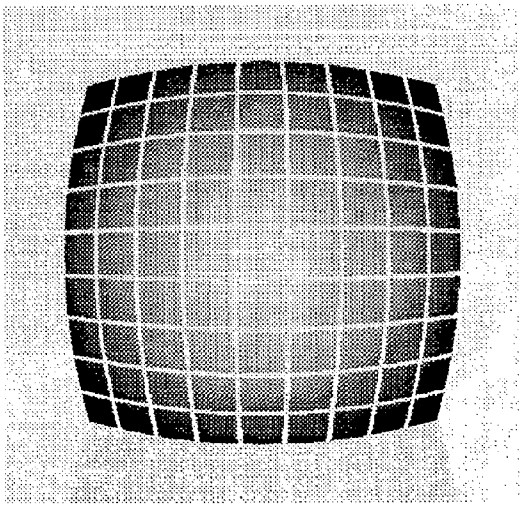

Figure 12: Doppler shift: objects traveling towards observer at 0.9c (©1989 Hsiung)

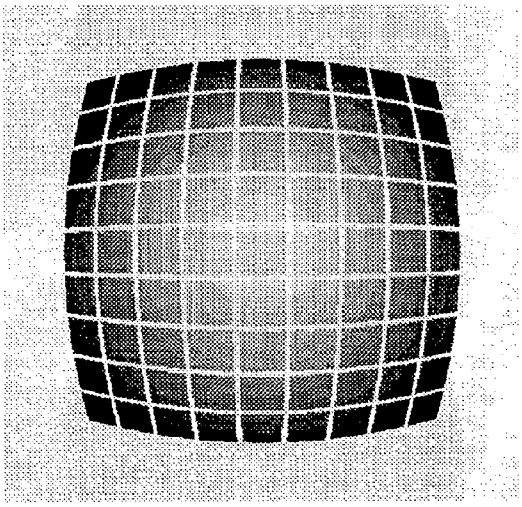

Figure 13: Doppler shift (quantized): objects traveling towards observer at 0.9c (©1989 Hsiung)

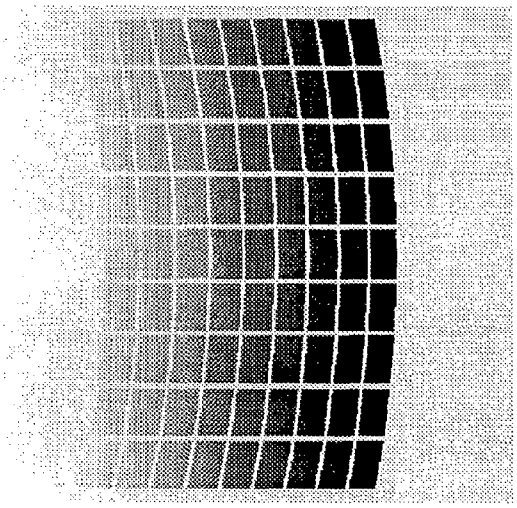

Figure 14: Doppler shift: transverse objects traveling at 0.8c (©1989 Hsiung)

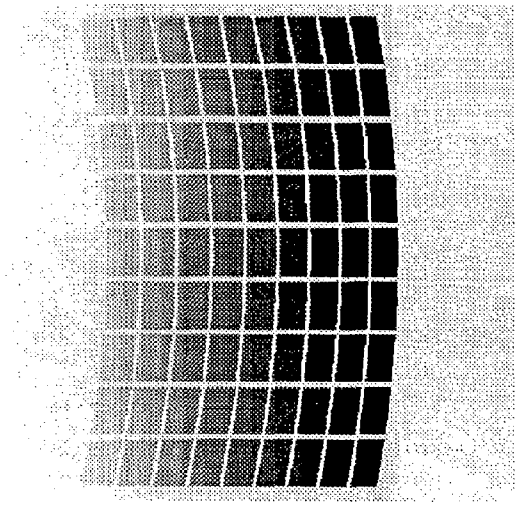

Figure 15: Doppler shift (quantized): transverse objects traveling at 0.8c (©1989 Hsiung)

P.-K. Hsiung, R. H. Thibadeau, M. Wu, "T-buffer: fast visualization of relativistic effects in spacetime", Computer Graphics 24 (2), March 1990, 83-88, © 1990 ACM, reprinted with kind permission from Robert H. Thibadeau and ACM

T-Buffer: Fast Visualization of Relativistic Effects in Spacetime

Ping-Kang Hsiung*
Robert H. Thibadeau†
Michael Wu‡
Carnegie Mellon University
Pittsburgh, Pennsylvania 15213

Abstract

We have developed an innovative ray-tracing simulation algorithm to describe *R*elativistic *E*ffects in *S*pace*T*ime ("REST"). Our algorithm, called *REST-frame*, models light rays that have assumed infinite speed in conventional ray-tracing to have a *finite* speed in spacetime, and uses the non-Newtonian Lorentz Transformation to relate measurements of a single event in different inertial coordinate systems (*inertial frames*). Our earlier work [5][6][7] explored the power of *REST-frame* as an *experimentation tool* to study the rich visual properties in natural world modeled by Special Relativity. Non-intuitive images of the anisotropic deformation ("warping") of space, the intensity concentration/spreading of light sources in spacetime, and the relativistic Doppler shift were visualized from our simulations.

REST-frame simulations are computationally expensive. Several hours of CPU time may be needed to generate one intricate image on a relatively powerful DECStation 3100. This high simulation cost of *REST-frame* precludes its application in interactive, real-time graphics environments.

In this paper, we report a scanline based *REST-frame* rendering method that provides a faster alternative to the original ray-tracing based *REST-frame* implementation. This new method operates in the spirit of the classical Z-buffer in computer graphics[2] and the inter-inertial frames point-mapping method investigated in physics in the early 1960's[14][12], and determines the visibility of points in spacetime by their spatial *and* temporal visibility. Specifically, all spacetime event points that are *potentially* visible from the viewpoint at the imaging time are geometrically projected in three dimensional (3D) space to the image plane pixel buffer. Multiple points with a same pixel affiliation are sorted by their *time distance* from the imaging time, and the most recent spacetime point is displayed.

This method, which we call *"Time-Buffer"* or *"T-Buffer"*, offers a significant speed improvement over the original *REST-frame* in software, and permits a dedicated Z-buffer-type hardware implementation that promises interactive, real-time relativistic effects in simulations on a contemporary graphic workstation.

Motion blur in real world images caused by the non-infinitesimal exposure time of image-taking can be simulated by *"Stochastic T-Buffer"*, which perturbs the *time component* of the scan-converted spacetime events that are potentially visible. The classical A-Buffer technique[1] that models translucency also can be adapted easily in T-Buffer. The limitation of T-Buffer is its inability to model specular reflection and refraction in optics,[1] which our original *REST-frame* implementation simulates completely.

*Department of Electrical and Computer Engineering, Carnegie Mellon University. (412) 268-2524. pkh@vap.vi.ri.cmu.edu

†Imaging Systems Laboratory, The Robotics Institute, Carnegie Mellon University. rht@vi.ri.cmu.edu

‡Department of Electrical and Computer Engineering, Carnegie Mellon University. mw2u@andrew.cmu.edu

This research was partially supported by the Inland/Fisher-Guide Division of General Motors Corporation and the Imaging Systems Laboratory, The Robotics Institute, Carnegie Mellon University.

1 Introduction

In the conventional rendering algorithms, light had always been regarded as if it traveled with infinite speed, and Galilean-Newtonian transformation was used to model relative motion between dynamic systems and the observer. When the scene objects and the observer (or the camera plate) are in relative motion at speeds comparable to light speed, Special Relativity requires the time information to be interwoven with the spatial coordinates in defining the vision formation process. Light speed must be treated as *finite*, and inertial reference frames[2] ("frames" in short) are to be connected by the Lorentz Transformation.

In [5], we first treated the subject of visualizing the spacetime world of Special Relativity with the application of an innovative ray-tracing technique *REST-frame*. Objects were assumed to make one dimensional (1D) motion relative to the observer. The simulation of 3D relativistic motion was later completed[6]. Extension to simulate kinematic systems containing objects of different relativistic velocities was reported in [7], which also included our initial investigation of the relativistic Doppler shift

[1] although it does render diffusive reflection and shadow casting correctly.

[2] A reference system, or *reference frame*, is *inertial* if it is nonaccelerating.

P.-K. Hsiung, R. H. Thibadeau, M. Wu, "T-buffer: fast visualization of relativistic effects in spacetime", Computer Graphics 24 (2), March 1990, 83-88, © 1990 ACM, reprinted with kind permission from Robert H. Thibadeau and ACM

effects.

Our original *REST-frame* implementation took a ray-tracing based simulation approach.[3] It gave good turn-around times for simple scenes, but became expensive in computation for more complex scenes. In a 3D lattice scene that contained 432 diffusive cylinders, 1731 reflective spheres and 12 light sources, some simulations took over two hours on a DECStation 3100 workstation to generate non-antialiased images of 512 by 512 in resolution, or a rendering rate of roughly 450 rays per second. Whereas *REST-frame* simulations reveal intricate images of complete and accurate optical phenomena of reflection, refraction and shadow casting under relativistic condition, their cost in time precludes most real-time, interactive graphics applications to benefit from it; a faster, perhaps less complete, visualization method may be more desirable in the latter environments. In this paper, we report one such method — T-Buffer, and discuss its speed advantage and some other features.

2 Approach

In order to model the physics of high speed motion, the *REST-frame* technique synthesizes the visual effects in spacetime by incorporating the true physics of Special Relativity and finite light-speed in its simulations. Specificially, it includes the two postulates of Special Relativity[11][13][9]:

1. Non-existence of preferred reference system (*"The Principle of Relativity"*): the laws of physics must be the same for observers in all inertial reference systems.
2. Constancy of speed of light: c is constant in a vacuum in all inertial frames and is independent of the motion of a light source relative to the observer.

According to these postulates, the *measured* space and time coordinates are dependent upon the reference frame from which the measurement is conducted; and the Lorentz Transformation equations relate measured spacetime coordinates between inertial reference frames.

2.1 Principle

A block diagram of our T-Buffer implementation of *REST-frame* is presented in figure (1). We assume the image plane to be stationary in a frame S, and the objects to move *in unison* with respect to S at a velocity $\vec{V} = (u, v, w)$. Of the infinite frames in which the objects are stationary, we can find one frame S' that has its axes X', Y' and Z' coincide with the S frame axes X, Y and Z, respectively, at time $t = t' = 0$. We call S the imaging frame or the camera frame, and S' the object frame. The measurements of every spacetime event[4] e in S and S' can be connected through the Lorentz Transformation[9]:

$$\vec{X'} = \vec{X} + [\frac{(\gamma - 1)}{\| \vec{V} \|^2}(\vec{X} \cdot \vec{V}) - \gamma t]\vec{V}$$

$$t' = \gamma(t - \frac{\vec{X} \cdot \vec{V}}{c^2}) \quad (1)$$

in which $\| \vec{V} \|^2 = u^2 + v^2 + w^2$, and $\gamma = 1/\sqrt{1 - \frac{\|\vec{V}\|^2}{c^2}}$. Vector $\vec{V}$ is sometimes replaced by vector $\vec{\beta} = (\beta_x, \beta_y, \beta_z) = (u/c, v/c, w/c)$. The Inverse Lorentz Transformation is

$$\vec{X} = \vec{X'} + [\frac{(\gamma - 1)}{\| \vec{V'} \|^2}(\vec{X'} \cdot \vec{V'}) - \gamma t']\vec{V'}$$

$$t = \gamma(t' - \frac{\vec{X'} \cdot \vec{V'}}{c^2}) \quad (2)$$

In which vector $\vec{V'} = -\vec{V}$. As a shorthand, we will write eq. (1) as $e'_{S'} = Le_S$ and eq. (2) as $e_S = L^{-1}e'_{S'}$. L and L^{-1} are the Lorentz Transformation operator and its inverse, respectively, and e_S and $e'_{S'}$ stand for the spacetime descriptions of an event in S and S', respectively.

Let us denote the viewpoint (the camera position) as $(x_{from}, y_{from}, z_{from})$ and the imaging time as t_{from} in S. Together, they form the *imaging event* e_{from_S}. If we perform the Lorentz Transformation to the imaging event, we get its S' description $e'_{from_{S'}}$:

$$e'_{from_{S'}} = [x'_{from}, y'_{from}, z'_{from}, t'_{from}]_{S'} = L\, e_{from_S} \quad (3)$$

According to the second postulate of Special Relativity ("constancy of light-speed"), all events $e'_{v_{S'}} = [x', y', z', t']_{S'}$ that are potentially visible from the imaging event $e'_{from_{S'}}$ in *temporal* sense must satisfy

$$\| e'_{v_{S'}} e'_{from_{S'}} \|_{3D} = c|t' - t'_{from_{S'}}| \quad (4)$$

That is, all potentially visible events $e'_{v_{S'}}$ satisfy the time constraint

$$t' = t_{from_{S'}} - \frac{1}{c}\sqrt{(x' - x'_{from})^2 + (y' - y'_{from})^2 + (z' - z'_{from})^2} \quad (5)$$

For each spatial point (x', y', z') in S', equation (5) dictates the time at which event $e_{v_{S'}} = [x', y', z', t']$ must have occurred in S' in order for it to reach the camera plate (at light speed c) at time t_{from_S}. For every point on the object surfaces,[5] this equation gives the specific emission time in S' of the photons from the (steadily illuminated or illuminating) surface point that precisely make it to the viewpoint[6] at the imaging time.

For the final geometric visibility test, every such potentially visible event $e'_{v_{S'}}$ is transformed into the camera frame S by applying eq. (2) to it:

$$e_{v_S} = [x, y, z, t]_S = L^{-1}\, e'_{v_{S'}} = L^{-1}\, [x', y', z', t']_{S'} \quad (6)$$

In S, the spatial coordinates of e_{vS} is perspectively projected to the image plane and its associated "Time-Buffer" that registers a time for each pixel. The value t of e_{v_S} is then compared against the Time-Buffer time of the pixel onto which e_{v_S} is spatially projected, and *a larger t replaces the smaller t* in the Time-Buffer. The replacement rule is based on the observation that t represents the time in the past that a potentially visible event occurred, and a 3D point in a more recent past (a larger t) obscures all points in the more remote past (the smaller t's), if the point is opaque.[7]

[3] Ours is a ray-tracer that uses the hierarchical bounding box[8][4] method to accelerate ray-object intersection test.

[4] We use the symbol (x, y, z) for 3D positional coordinates and $[x, y, z, t]$ for a spacetime event point. When we designate a specific reference frame S, we use $(x, y, z)_S$ and $[x, y, z, t]_S$. Individually, each component is written with a subscript S (e.g. t_S). We also use $\vec{X'} = (x', y', z')_{S'}$ and $\vec{X} = (x, y, z)_S$.

[5] Note that object points are stationary in S'.

[6] which is measured as in motion in S'.

[7] This replacement rule is the opposite of that of the conventional Z-buffer, but is consistent with the geometric interpretation of the latter.

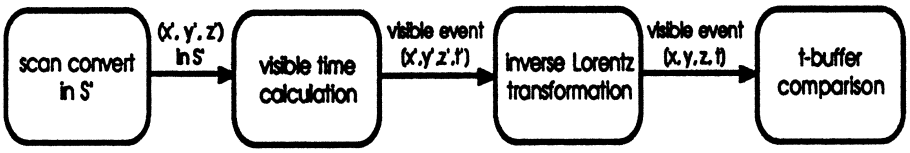

Figure 1: T-Buffer algorithm block diagram

2.2 Algorithm

In summary, the T-Buffer algorithm works as follows (refer to figure (1)):

1. Initialization:
   (a) Initialize the Time-Buffer array to -HUGE_VAL.
   (b) Use eq. (3) to determine the imaging event in S', $[x'_{from}, y'_{from}, z'_{from}, t'_{from}]_{S'}$.
2. T-Buffer visibility test:
   (a) For each object in S', scan-convert its surface to obtain spatial points $(x', y', z')_{S'}$.
   (b) From eq. (5), calculate the visible time t' associated with each point $(x', y', z')_{S'}$. This gives the *potentially visible* event $[x', y', z', t']_{S'}$ in spacetime corresponding to $(x', y', z')_{S'}$.
   (c) Transform each event $[x', y', z', t']_{S'}$ to its S coordinates $[x, y, z, t]$ using eq. (6).
   (d) Use the time t in $[x, y, z, t]$ to do Time-Buffer comparison/replacement. When a replacement occurs, the ID of the scanned object is also stored in the corresponding image pixel memory.
3. Image rendering: For each image pixel, retrieve the object ID and render the pixel according to the cosine law of diffusive reflection.

2.3 Extensions

2.3.1 Shadow

Shadow casting can be easily added to T-Buffer by applying shadow-buffering technique[10]. The light sources in each *REST-frame* simulation can be stationary in either the camera frame S or the object frame S'. These two possible configurations result in different relative speeds for the "mirror light sources" — the imaginary light sources reflected off object surfaces — to the imaging event. Note that in either case, the speed of light is non-additive, and the correct treatment is naturally accounted for in our algorithm.

2.3.2 Motion Blur

Motion blur can be simulated by Stochastic T-Buffer that adds perturbation to the time component of every scan converted event $[x', y', z', t']_{S'}$ (figure (2)). The foundation for time perturbation is the inclusion in the Lorentz Transformation (and its inverse) of the relative motion between objects and image plane. Consequently, a time perturbation in S' is correctly transformed into a spatial displacement in the imaging frame S.

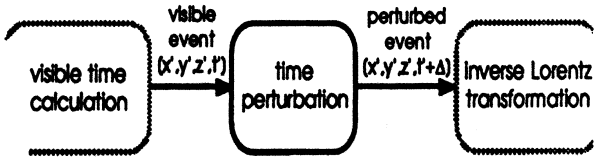

Figure 2: Motion blur modification of T-Buffer

3 Experiments

In this section, we show images generated by our software T-Buffer implementation, and evaluate the T-Buffer performance.

3.1 T-Buffer images

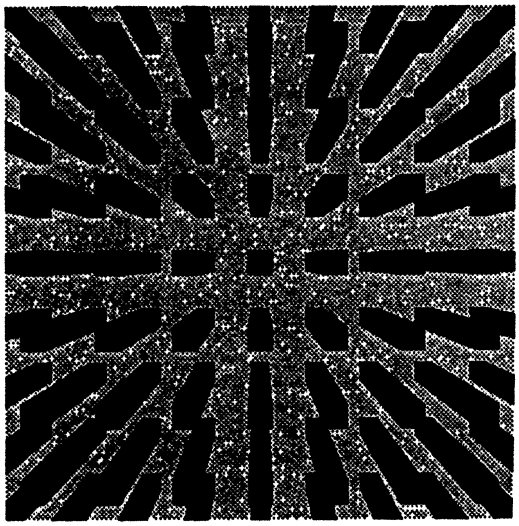

Figure 3: Array of bars at stationary ($\vec{\beta} = (0, 0, 0)$)

Figures (3), (4), (5), (6), and (7) are images generated by T-Buffer. For comparison of image quality, we show in Figure (8) an image produced by our previous ray-tracing based implementation under the same viewing condition as in Figure (7). The reflective highlight apparent in Figure (8) is not reproduced by T-Buffer in (7), although this difference is not essential.

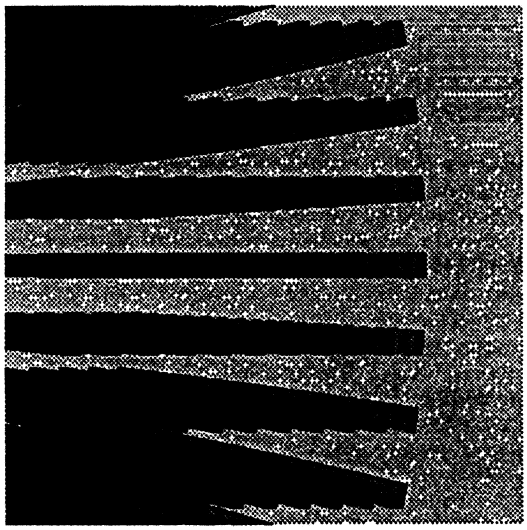

Figure 4: Array of bars at $\vec{\beta} = (0.9, 0, 0)$

	teapot (0.0c)	teapot (0.9c)	bars (0.9c)
Polygons	9121	9121	678
Scan time	1.366 S	1.950 S	10.883 S
T-Buffer time	7.184 S	12.533 S	146.05 S
Shading time	3.883 S	4.450 S	6.433 S
Polygons/sec	733.6	481.8	4.15
Memory usage	17M Byte	17M Byte	16M Byte

Table 1: Basic characterization (with shadow)

3.2 Performance evaluation

Table 1 shows the basic performance characteristics of T-Buffer on an Apollo DN-10000 system with 32M Bytes of memory. Both "teapot" and "bars" in our simulations had 4 light sources. Shadow casting was not included in the simulations. The T-Buffer time in the table refers to the T-Buffer comparison/replacement time. Note the extremely low efficiency in the "bars" column. The bars scene refers to the bar array shown in Figure (3), (4) and (5), which has a high percentage of polygons that are invisible or close to orthogonal to the final image plane, and thus has many wasted scan-conversion and T-Buffer operations.

To compare T-Buffer with our ray-tracing based *REST-frame* implementation, we ran both programs on a same set of simulation tasks. Some representative timing data are summarized in Table 2 and 3 (We rate the ray-tracing version based on polygon/second to compare with T-Buffer). Each timing datum in Table 2 is the sum of its corresponding scan time, T-Buffer time and shading time. In favorable cases, the speed improvement

	teapot (0.0c)	teapot (0.9c)	bars (0.9c)
No shadow	12.43 S	18.93 S	163.37 S
Poly/sec	733.6	481.8	4.15
Shadowed	35.72 S	56.17 S	334.8 S
Poly/sec	255.4	162.4	2.03

Table 2: Performance comparison (T-Buffer)

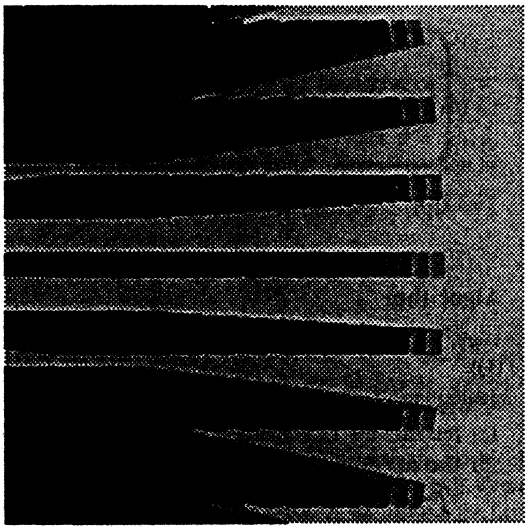

Figure 5: Bar array at $\vec{\beta} = (0.9, 0, 0)$, with 0.05 second shutter time

	teapot (0.0c)	teapot (0.9c)	bars (0.9c)
No shadow	78.00 S	85.00 S	200.0 S
Poly/sec	116.94	107.31	3.39
Shadowed	218.3 S	258.0 S	769.3 S
Poly/sec	41.78	35.35	0.88

Table 3: Performance comparison (Ray-traced)

of the software T-Buffer over our ray-tracing based *REST-frame* is 6-7 times.

4 Discussion and future work

4.1 Execution efficiency

Our preliminary T-Buffer implementation can be further optimized for better time and memory efficiencies. Two possible improvements are to perform scan-conversion in screen (pixel) space, rather than in object space in our current coding, and to employ orthographic projection, instead of perspective projection, to screen space.

4.2 Hardware acceleration

Hardware acceleration of T-Buffer can easily be realized. With some minor design modifications, an existing hardware Z-buffer circuitry can be converted into a T-Buffer engine. The changes involve adding the t' calculation circuit that computes eq. (5) (the second step in fig. (1)), and inverting the comparison/replacement rule for buffered values.

4.3 Multiple velocity system

To extend the T-Buffer method to simulate systems of objects with multiple velocities, it is necessary to consider multiple inertial frames S'_1, S'_2, ..., S'_n. Any object or group of objects which travels at a unique velocity with respect to imaging frame

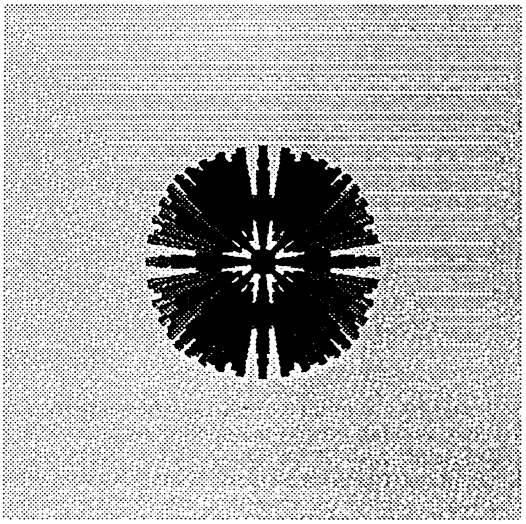

Figure 6: Bar array traveling towards viewer at 0.99c

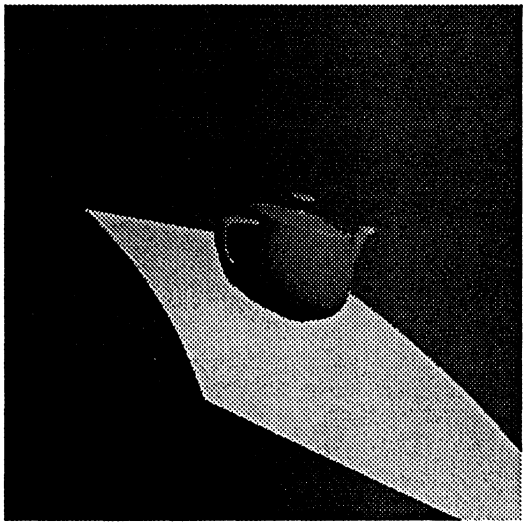

Figure 7: Teapot at $\vec{\beta} = (0.9, 0, 0)$

S may be placed in its own proper frame S'_i, and be related to S by a unique Lorentz Transformation L_i. The object space is thus divided into a series of co-existent inertial frames. All objects in every frame are scan-converted, and the events transformed to S to perform the final T-Buffer operation.

4.4 Features and limitation

The classical A-Buffer technique[1] that models translucency also can be adapted in T-Buffer. The limitation of T-Buffer is its inability to model specular reflection and refraction in optics.

4.5 Future work

We plan to test T-Buffer on a hardware graphics accelerator that we are constructing. At the heart of this accelerator is the new Intel processor *i860*[3]. We plan to explore the fast floating point processing facilities as well as the Z-buffer hardware support on this processor.

5 Conclusion

The *REST-frame* simulation technique fills in a void in past research, and provides one opportunity for exploring the historical fascination with visualizing Special Relativity effects that exist in physics as well as in many segments of our popular cultures.

Our previous ray-tracing based *REST-frame* implementation generated very high quality images that incorporated fine optical effects of reflection, refraction and shadow casting, but took long times to complete. In some time-critical applications, e.g. flight simulation, computer animation and video games, absolute realism and optical precision that this earlier *REST-frame* implementation offers is not essential. Rather, the emphasis is the speed of simulations — preferably at real-time.

The T-Buffer technique this paper presents provides a desirable solution to such applications by optimizing image synthesis speed at the expense of lower optical complexity in the resulting images. The advantage of T-Buffer over our previous implementation is twofold:

1. The software T-Buffer implementation runs over six times faster than the earlier *REST-frame* in favorable cases.
2. Furthermore, it can be mapped onto the well-developed Z-buffer based *rendering pipeline* that resides in most of the contemporary graphics workstations.

The availability of this latter hardware option makes the ultimate *real-time* simulation and animation of relativistic effects technologically feasible.

6 Acknowledgments

We would like to thank Robert H. P. Dunn and John Zsarnay for their generous assistance to our work. We also thank Kathryn Porsche for her insightful suggestions that contributed to this presentation. Finally, we are grateful for the valuable comments provided by our reviewers.

References

[1] L. Carpenter. The A-buffer, an antialiased hidden surface method. *Computer Graphics (SIGGRAPH)*, 103–108, 1984.

[2] E. Catmull. Computer display of curved surfaces. In *Proc. IEEE Conf. Computer Graphics Pattern Recognition Data Struct.*, page 11, May 1975.

[3] Intel Corp. *i860 64-Bit Microprocessor Programmer's Reference Manual*. Intel Corp., 1989.

[4] Andrew Glassner. *An Introduction to Ray-Tracing*. Academic Press Limited, 1989.

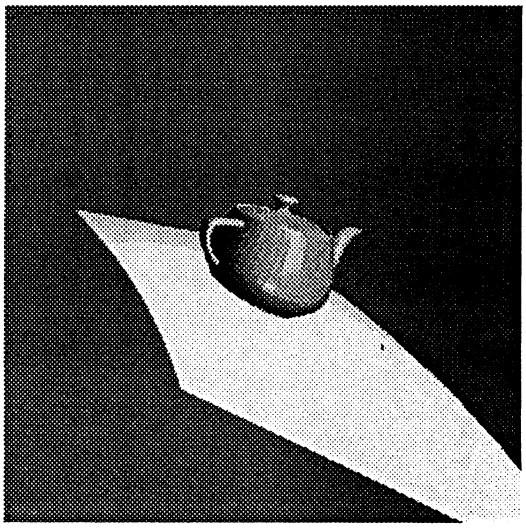

Figure 8: Teapot at $\vec{\beta} = (0.9, 0, 0)$ (Ray-tracing based simulation)

[5] Ping-Kang Hsiung and Robert H. P. Dunn. Visualizing relativistic effects in spacetime. In *Proceedings of the Supercomputing '89 Conference*, Nov. 13-17, 1989.

[6] Ping-Kang Hsiung and Robert H. Thibadeau. Spacetime visualization of 3D relativistic motion. *Unpublished document*, Oct., 1989.

[7] Ping-Kang Hsiung and Robert H. Thibadeau. Spacetime visualization of relativistic effects. In *ACM 1990 Computer Science Conference (to appear)*, Feb. 20-22, 1990.

[8] T.L. Kay and J.T. Kajiya. Ray tracing complex scenes. *Computer Graphics (SIGGRAPH)*, 269–278, Aug. 1986.

[9] C. Møller. *The Theory of Relativity*. Oxford University Press, 1960.

[10] N. Magnenat-Thalmann and D. Thalmann. *Image synthesis: theory and practice*. Springer-Verlag, 1987.

[11] Robert Resnick. *Introduction to Special Relativity*. Rensselaer Polytechnic Institute, 1968.

[12] G. D. Scott and M. R. Viner. The geometrical appearance of large objects moving at relativitic speeds. *American Journal of Physics*, 18(2):109–144, Jan 1965.

[13] E. Taylor and J. Wheeler. *Spacetime Physics*. M.I.T. / Princeton, 1966.

[14] Sten Yngström. Observation of moving light-sources and objects. *Arkiv för Fysik*, 367, 1962.

Color images for this paper can be found in the color plate section.

P.-K. Hsiung, R. H. Thibadeau, M. Wu, “T-buffer: fast visualization of relativistic effects in spacetime”, Computer Graphics 24 (2), March 1990, 83-88, © 1990 ACM, reprinted with kind permission from Robert H. Thibadeau and ACM

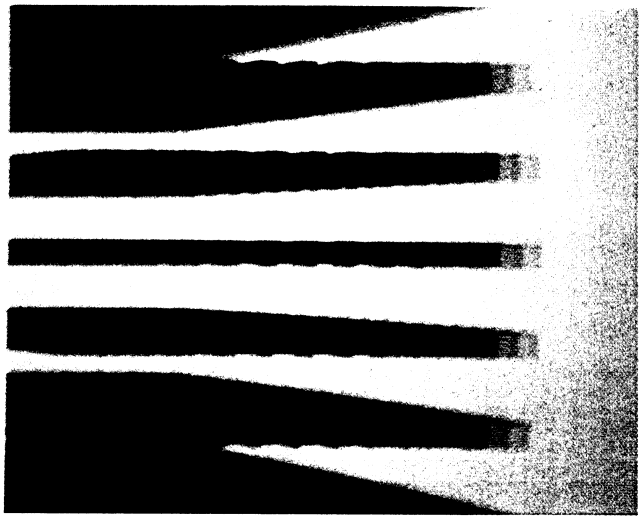

Plate 1: Bar array at $\vec{\beta}= (0.9, 0, 0)$, with 0.05 second shutter time

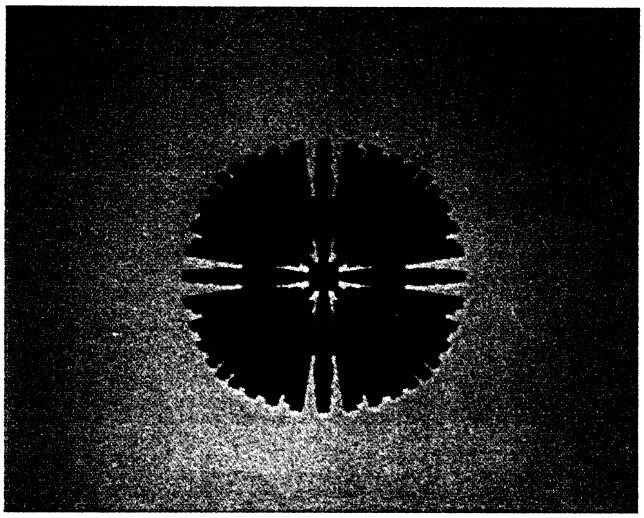

Plate 2: Bar array traveling towards viewer at 0.99c

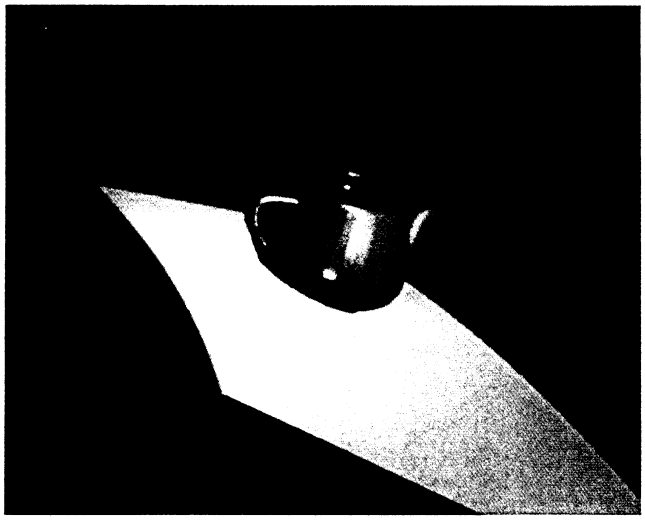

Plate 3: Teapot at $\vec{\beta}= (0.9, 0, 0)$ (Ray-tracing based simulation)

IIsiung, Thibadeau and Wu, “T-Buffer: Fast Visualization of Relativistic Effects in Spacetime”.

Searchlight and Doppler Effects in the Visualization of Special Relativity: A Corrected Derivation of the Transformation of Radiance

DANIEL WEISKOPF, UTE KRAUS, and HANNS RUDER
University of Tübingen

We demonstrate that a photo-realistic image of a rapidly moving object is dominated by the searchlight and Doppler effects. Using a photon-counting technique, we derive expressions for the relativistic transformation of radiance. We show how to incorporate the Doppler and searchlight effects in the two common techniques of special relativistic visualization, namely ray tracing and polygon rendering. Most authors consider geometrical appearance only and neglect relativistic effects on the lighting model. Chang et al. [1996] present an incorrect derivation of the searchlight effect, which we compare to our results. Some examples are given to show the results of image synthesis with relativistic effects taken into account.

Categories and Subject Descriptors: I.3.7 [**Computer Graphics**]: Three-Dimensional Graphics and Realism—*Color, shading, shadowing, and texture*; J.2 [**Computer Applications**]: Physical Sciences and Engineering—*Physics*

General Terms: Algorithms, Theory

Additional Key Words and Phrases: Aberration of light, Doppler effect, illumination, Lorentz transformation, searchlight effect, special relativity

1. INTRODUCTION

Einstein’s Theory of Special Relativity is widely regarded as a difficult and almost incomprehensible theory. One important reason for this is that the properties of space, time, and light in relativistic physics are totally different from those in classical, Newtonian physics. In many respects they

This work was supported by the Deutsche Forschungsgemeinschaft (DFG), and is part of the project D4 within the Sonderforschungsbereich 382
Authors’ address: Theoretical Astrophysics, University of Tübingen, Auf der Morgenstelle 10, Tübingen, D-72076, Germany

ACM Transactions on Graphics, Vol. 18, No. 3, July 1999, Pages 278–292.

are contrary to human experience and everyday perception, which is based on low velocities.

Mankind is limited to very low velocities compared to the speed of light. For example, the speed of light is a million times faster than the speed of an airplane and 40,000 times faster than the speed at which the space shuttle orbits the earth. Even in the long term, there is no hope of achieving velocities comparable to the speed of light. Computer simulations are the only means of visually exploring the realm of special relativity, and thus can help the intuition of physicists.

The visual appearance of rapidly moving objects shows intriguing effects of special relativity. Apart from a previously disregarded article by Lampa [1924] about the invisibility of the Lorentz contraction, the first solutions to this problem were given by Penrose [1959] and Terrell [1959]. Various aspects were discussed by Weisskopf [1960]; Boas [1961]; Scott and Viner [1965]; Scott and van Driel [1970]; and Kraus [2000].

Hsiung and Dunn [1989] were the first to use advanced visualization techniques for image shading of fast moving objects. They propose an extension of normal three-dimensional ray tracing. Hsiung and Thibadeau [1990] and Hsiung et al. [1990a] add the visualization of the Doppler effect. Hsiung et al. [1990b] and Gekelman et al. [1991] describe a polygon rendering approach based on the apparent shapes of objects as seen by a relativistic observer. Polygon rendering was also used as a basis for a virtual environment for special relativity [Rau et al. 1998; Weiskopf 1999].

Most authors concentrate their efforts on geometrical appearance and, apart from the Doppler effect, neglect relativistic effects on the lighting model. Chang et al. [1996], however, present a complete description of image shading which takes relativistic effects into account. We agree with most parts of their article, but would like to correct their derivation of the relativistic transformation of radiance. We show how the correct transformation of radiance fits in their shading process. The combination of Chang et al.’s work and this article gives a comprehensive presentation of special relativistic rendering.

We demonstrate that a photo-realistic image is dominated by the searchlight and Doppler effects, which are greatly underestimated when we view the examples given by Chang et al. The Doppler effect causes a shift in wavelength of the incoming light, which results in a change of color. The searchlight effect increases the apparent brightness of the objects ahead when the observer approaches these objects at high velocity. The Doppler effect, the relativistic aberration of light, and time dilation, among others, contribute to the searchlight effect.

2. DERIVATION OF THE TRANSFORMATIONS

2.1 The Transformation of Radiance

The following derivation of the searchlight effect is based on a photon-counting technique. A similar approach can be found in articles by Peebles and Wilkinson [1968]; McKinley [1979; 1980]; and Kraus [2000].

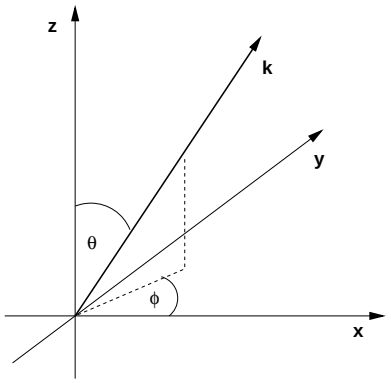

Fig. 1. A photon with wave vector $\vec{k}$.

Consider two inertial frames of reference S and S', with S' moving with velocity v along the z axis of S. Suppose the observer O is at rest relative to S and the observer O' is moving with speed v along the z axis of S. The usual Lorentz transformation along the z axis connects frames S and S'.

In reference frame S, consider a photon with circular frequency ω, wavelength λ, energy E, and wave vector $\vec{k} = (\omega \sin\theta \cos\phi,\ \omega \sin\theta \sin\phi,\ \omega \cos\theta)/c$ with spherical coordinates θ and ϕ, as shown in Figure 1.

In frame S', the circular frequency is ω', the wavelength is λ', the energy is E', and the wave vector is $\vec{k'} = (\omega' \sin\theta' \cos\phi',\ \omega' \sin\theta' \sin\phi',\ \omega' \cos\theta')/c$. The expressions for the Doppler effect and the aberration connect these two representations, cf., McKinley [1979] and Møller [1972]:

$$\lambda' = \lambda D \tag{1}$$

$$\omega' = \omega / D \tag{2}$$

$$E' = E / D \tag{3}$$

$$\cos\theta' = \frac{\cos\theta - \beta}{1 - \beta\cos\theta} \tag{4}$$

$$\phi' = \phi \tag{5}$$

$$D = \frac{1}{\gamma(1 - \beta\cos\theta)} \tag{6}$$

where D is the Doppler factor, $\gamma = 1/\sqrt{1 - \beta^2}$, $\beta = v/c$, and c is the speed of light.

Radiance is the radiant power per unit of foreshortened area emitted into a unit solid angle. A detector at rest in S measures the energy-dependent radiance

$$L_E(\theta, \phi) = \frac{d\Phi}{dE\, dA_\perp\, d\Omega}$$

where Φ is the radiant power or radiant flux, E is the energy, $d\Omega$ is the solid angle, and $dA_\perp$ is the area dA of the detector projected along the radiation direction (θ, ϕ). The radiant flux Φ is the radiant energy per unit time. Accordingly, the wavelength-dependent radiance is

$$L_\lambda(\theta, \phi) = \frac{d\Phi}{d\lambda\, dA_\perp\, d\Omega} \tag{7}$$

with the wavelength λ.

In reference frame S, consider a group of photons, dN in number, with energies between E and $E + dE$ and propagation directions in the element of solid angle $d\Omega$ around (θ, ϕ). Here, the energy-dependent radiance is

$$L_E(\theta, \phi) = \frac{dN\, E}{dE\, dA_\perp\, d\Omega\, dt}$$

or

$$dN = \frac{L_E(\theta, \phi)}{E} dE\, dA_\perp d\Omega\, dt$$

We choose the area dA to be perpendicular to the z axis, so that

$$dA_\perp = dA \cos\theta$$

The z component of the velocity of the photons is $c\cos\theta$. The photons passing dA between time t_0 and time $t_0 + dt$ are contained in the shaded volume dV in Figure 2:

$$dV = dA\, dt\, c \cos\theta$$

Consider another area $d\tilde{A}$ with the same size and orientation as dA. Still in reference frame S, suppose $d\tilde{A}$ is moving with velocity v along the z axis. The photons passing $d\tilde{A}$ between t_0 and $t_0 + dt$ are contained in the shaded volume in Figure 3:

$$d\tilde{V} = dA\, dt(c \cos\theta - v) = \frac{\cos\theta - \beta}{\cos\theta} dV$$

The ratio of the number of photons passing $d\tilde{A}$ in the time interval dt and the number of photons passing dA is the same as the ratio of the volume $d\tilde{V}$ and the volume dV:

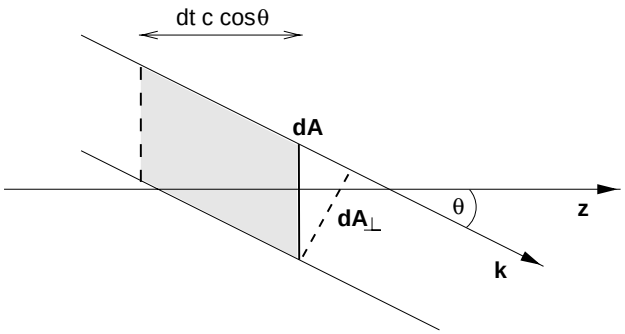

Fig. 2. Photons with propagation direction along the wave vector $\vec{k}$. The area of the detector is denoted dA and is perpendicular to the z axis; $dA_\perp$ is the projection of dA along the radiation direction. The shaded volume dV contains the photons passing dA between time t_0 and time $t_0 + dt$.

$$d\tilde{N} = \frac{L_E(\theta, \phi)}{E}\, dE\, d\Omega\, dt\, \cos\theta\, d\tilde{A}\, \frac{\cos\theta - \beta}{\cos\theta} \tag{8}$$

Now consider the same situation in reference frame S'. The area $d\tilde{A}$ is at rest in S'. The time interval is

$$dt' = dt/\gamma \tag{9}$$

The number of photons counted does not depend on the frame of reference, i.e.,

$$d\tilde{N} = d\tilde{N}' = \frac{L'_{E'}(\theta', \phi')}{E'} dE' d\Omega' dt' \cos\theta' d\tilde{A}' \tag{10}$$

From Eqs. (8) and (10), we obtain

$$\frac{L_E(\theta, \phi)}{L'_{E'}(\theta', \phi')} = \frac{E}{E'} \frac{dE'}{dE} \frac{d\Omega'}{d\Omega} \frac{dt'}{dt} \frac{\cos\theta'}{\cos\theta - \beta} \frac{d\tilde{A}'}{d\tilde{A}} \tag{11}$$

Since the area $d\tilde{A}$ is perpendicular to the separating velocity, it is not changed by Lorentz transformations:

$$d\tilde{A}' = d\tilde{A} \tag{12}$$

With Eqs. (4) and (5), the transformed solid angle is

$$\frac{d\Omega'}{d\Omega} = \frac{\sin\theta'}{\sin\theta} \frac{d\theta'}{d\theta} = \frac{d(\cos\theta')}{d(\cos\theta)} = \frac{1}{\gamma^2(1 - \beta\cos\theta)^2} = D^2 \tag{13}$$

Using Eqs. (3), (4), (9), (12), (13), and (11), we obtain

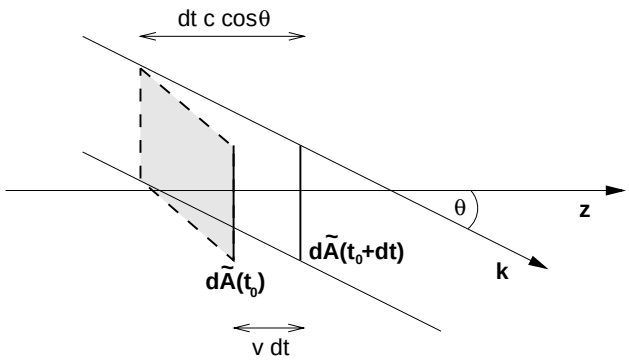

Fig. 3. Photons with propagation direction along the wave vector $\vec{k}$. The area $d\tilde{A}$ moves with velocity v along the z axis. The shaded volume $d\tilde{V}$ contains the photons passing $d\tilde{A}$ between t_0 and $t_0 + dt$.

$$\frac{L_E(\theta, \phi)}{L'_{E'}(\theta', \phi')} = D^3 = \frac{E^3}{E'^3}$$

With the relation between energy and wavelength,

$$\lambda = \frac{hc}{E}, \; d\lambda = -\frac{hc}{E^2}\, dE$$

and with

$$L_\lambda(\theta, \phi)|d\lambda| = L_E(\theta, \phi)|dE|$$

we get

$$L_\lambda(\theta, \phi) = L_E(\theta, \phi)\frac{E^2}{hc}$$

Ultimately, then, the transformation expression for the wavelength-dependent radiance is

$$\frac{L_\lambda(\theta, \phi)}{L'_{\lambda'}(\theta', \phi')} = D^5 \tag{14}$$

The transformation law for the following integrated quantity is easily obtained from this equation. With the use of Eq. (1), the transformed radiance is

$$L(\theta, \phi) = \int_0^\infty L_\lambda(\theta, \phi) d\lambda = D^4 \int_0^\infty L'_{\lambda'}(\theta', \phi')\, d\lambda' = D^4 L'(\theta', \phi') \tag{15}$$

2.2 Incident Irradiance from a Point Light Source

The measure for radiant power leaving a point light source in an element of solid angle $d\Omega$ and in a wavelength interval is called the wavelength-dependent intensity I_λ:

$$I_\lambda = \frac{d\Phi}{d\Omega\, d\lambda} \tag{16}$$

The wavelength-dependent irradiance E^i_λ is the radiant power per unit area in a wavelength interval:

$$E^i_\lambda = \frac{d\Phi}{dA\, d\lambda} \tag{17}$$

For a surface patch on the object, the wavelength-dependent irradiance $E^{i'}_{\lambda'}$ coming from a moving point light source is

$$E^{i'}_{\lambda'} = \frac{1}{D^5} \frac{\cos \alpha'}{r'^2} I_\lambda \tag{18}$$

with the angle α' between the normal vector to the surface and the direction of the incident photons and with the apparent distance r' of the light source from the surface patch. These quantities are measured in the reference frame of the object, whereas the wavelength-dependent intensity I_λ is measured in the reference frame of the light source. Accordingly, the integrated, wavelength-independent irradiance is

$$E^{i'} = \frac{1}{D^4} \frac{\cos \alpha'}{r'^2} I \tag{19}$$

The derivation of these equations is presented in the Appendix. Observe that for an isotropic point source in one frame of reference, we get an anisotropic source in the other frame of reference due to the implicit angle dependency in the Doppler factor D.

3. COMPARISON WITH DERIVATION BY CHANG ET AL.

Chang et al. [1996] present a complete treatment of relativistic image shading, which contains apparent geometry, the searchlight and Doppler effects, and a detailed description of the shading process. However, their derivation of the transformation properties of radiance is based on mistaken interpretations of the Theory of Special Relativity and leads to a tremendous divergence from our correct results, presented above.

Chang et al. derive their expressions based on the assumption that the same amount of radiant power is emitted from a surface patch on the object and the corresponding surface patch on the apparent surface. Hence, they

compute the relation between the area of the surface patch on the object and the area of the corresponding surface patch on the apparent surface, as well as the relation between the respective normal vectors. They treat the apparent surface as an object at rest with respect to the observer.

Their derivation is not correct for the following reasons:

Radiant power depends on time intervals and on the energy of photons, both of which are subject to Lorentz transformations. These transformations are missing in Chang et al.’s work.

The observer is moving with respect to the surface patch of the object. Approaching the object, the observer’s detector sweeps up photons so that the rate at which radiant energy is received is increased by the observer’s motion. This increase is absent for radiation from the apparent surface, which is stationary in the observer’s rest frame. Chang et al. ignore this effect as well.

In Chang et al.’s Eq. (36), the transformation of a solid angle is not correct. The mistake is in their calculation of the partial derivatives $\partial\Theta'/\partial\Theta$, $\partial\Theta'/\partial\Phi$, $\partial\Phi'/\partial\Theta$, and $\partial\Phi'/\partial\Phi$ with the use of their Eq. (31) for the transformation of the direction of the light ray. Equation (31) is valid for the special case of polar angle $\Theta = \pi/2$ only, and cannot be used to calculate partial derivatives.

Both wavelength and wavelength intervals are subject to Lorentz transformations. When calculating the radiance per wavelength interval in their Eq. (39) from Eq. (38), Chang et al. apply the Lorentz transformation to the wavelength, but not to the wavelength interval.

In their Eq. (38), they ultimately end up with a factor of D in the transformation of radiance, and also in in their Eq. (39) in the transformation of wavelength-dependent radiance, which differs from the correct result by a factor of D^3 and D^4, respectively. Similarly, the calculation of irradiance in their Eq. (46) and of wavelength-dependent irradiance in their Eq. (47) differs from the correct result by the same factor of D^3 and D^4, respectively.

4. THE SHADING PROCESS

The searchlight and Doppler effects can be readily incorporated in the two common techniques of special relativistic visualization, i.e., ray tracing and polygon rendering.

Relativistic ray tracing as described by Hsiung and Dunn [1989] is an extension of normal 3D-ray tracing. The ray starting at the eye point and intersecting the viewing plane is transformed according to special relativity, i.e., the direction of light is turned due to relativistic aberration. At this point the transformed properties of light can be included by calculating the transformed radiance as well as the transformed wavelength.

In this framework it is not sufficient to consider only three tristimulus values, such as RGB, but the wavelength-dependent energy distribution of light has to be taken into account. The spectral energy distribution has to be known over an extensive range so that the Doppler-shifted energy

distribution can be calculated for wavelengths in the visible range. For final image synthesis, the tristimulus values can easily be obtained from the wavelength-dependent radiance that gets to the eye point.

Relativistic polygon rendering is based on the apparent shapes of objects with respect to the observer. The shading process is described by Chang et al. in full detail. In this process, the expressions for irradiance in step (2)(d)(iv) and for the transformation of radiance in step (2)(f) have merely to be replaced by our Eqs. (18) and (14), respectively. The Doppler factor in Eq. (18) depends on the direction of the photons that reach the object and on the relative velocity of the frame of the point light source and the frame of the object, whereas the Doppler factor in Eq. (14) depends on the direction of the photons that reach the observer and on the relative velocity of the frame of the object and of the frame of the observer.

5. EXAMPLES

The appearance of a scene similar to Chang et al.’s STREET in Figures 4 to 7 shows the tremendous effects of the transformation of radiance on image synthesis. These pictures show the apparent geometry and the radiance transformation, but neglect color changes due to the Doppler effect. Since the spectral energy distribution of the light reflected by the objects in the STREET is unknown, we only show gray-scale images that take the total energy of the whole spectral energy distribution into account. In this case, Eq. (15) is applied. If we used a speed as high as Chang et al.’s, $0.99c$, we would not be able to display the high intensities in Figure 7 properly. So we choose a velocity of $0.8c$. These images were generated by using the ray-tracing method described above. The relativistic extensions are implemented into *RayViS* [Gröne 1996], a normal 3D-ray-tracing program.

Figures 8 and 9 show the appearance of the sun moving at a speed of $0.5c$ to illustrate color changes due to relativistic lighting. We used the polygon-rendering technique described above to produce these images. A detailed presentation of the rendering software can be found in our previous work [Rau et al. 1998; Weiskopf 1999].

6. CONCLUSION

We have demonstrated that, aside from the apparent geometry, the searchlight and Doppler effects play dominant roles in special relativistic visualization. Ray tracing and polygon rendering, two standard techniques in computer graphics, can easily be modified and extended to take into account the searchlight and Doppler effects.

The transformation of radiance could serve as an important element in even more sophisticated shading algorithms in order to generate photorealistic and physically correct images of fast moving objects. For example, radiosity could be extended to visualize relativistic flights through stationary scenes.

Fig. 4. Original appearance of the street.

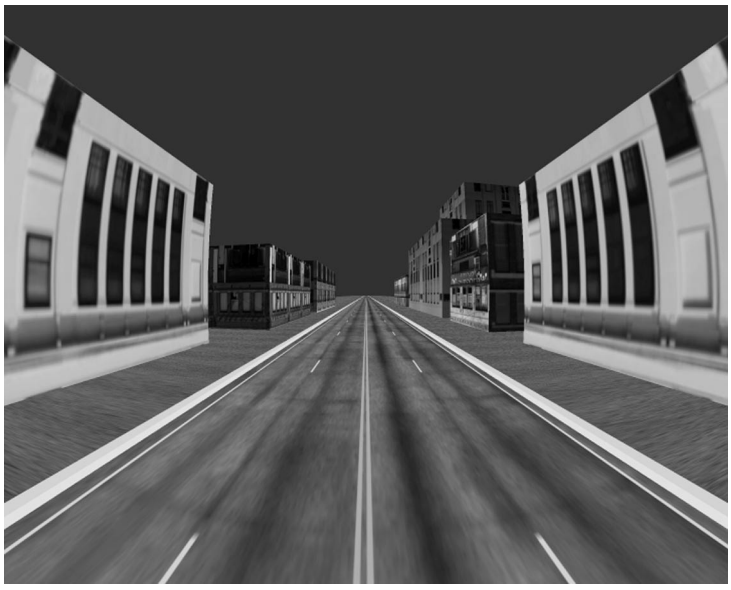

Fig. 5. Appearance of the street with respect to a moving observer. The viewer is rushing into the street with a speed of $0.8c$. The light sources are at rest in the street's coordinate system. The searchlight and Doppler effects are ignored.

Fig. 6. Visualization of the searchlight effect based on the incorrect derivation by Chang et al. The viewer is rushing into the street with a speed of $0.8c$. The light sources are at rest in the street's coordinate system.

Fig. 7. Visualization of the searchlight effect based on the correct Eq. (15) for the transformation of radiance. The difference from Figure 6 is significant. The viewer is rushing into the street with a speed of $0.8c$. The light sources are at rest in the street's coordinate system.

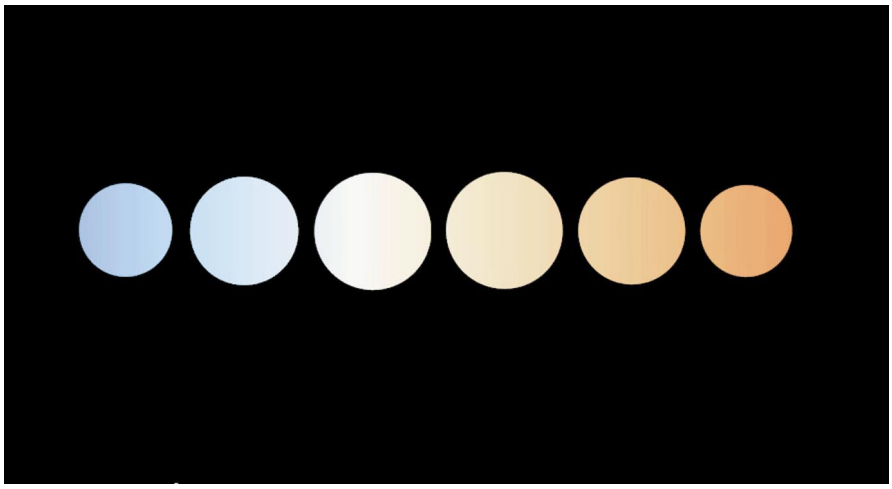

Fig. 8. Visualization of the Doppler effect only: the Doppler-shifted spectral energy distribution is shown with no further transformations. The sun passes by with a speed of $0.5c$. The sun is the only light source and emits blackbody radiation with a temperature of 5762 Kelvin.

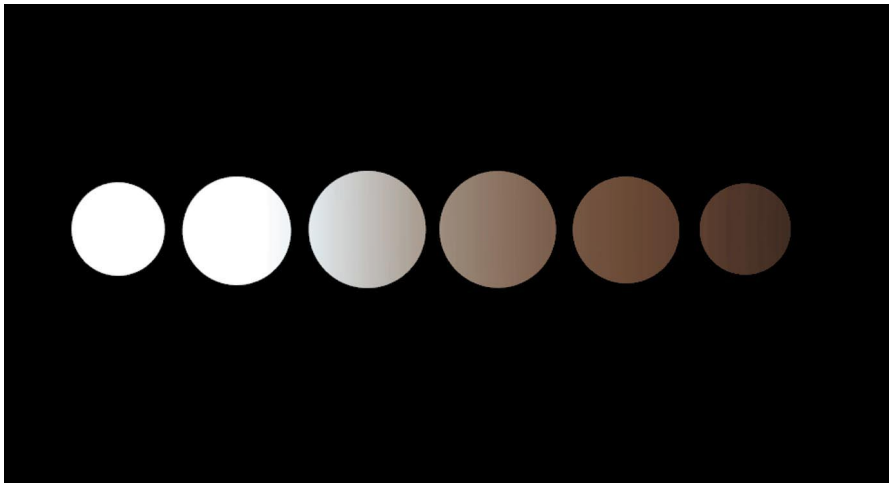

Fig. 9. Visualization of the searchlight and Doppler effects based on Eq. (14). The sun passes by with a speed of $0.5c$. The sun is the only light source and emits blackbody radiation with a temperature of 5762 Kelvin.

APPENDIX

A. INCIDENT IRRADIANCE

The derivation of Eqs. (18) and (19) is presented in this Appendix.

First, consider a finite light source which is at rest in frame S. With Eq. (7), the radiant flux emitted by the light source can be obtained in terms of the wavelength-dependent radiance:

$$d\Phi = L_\lambda \, dA_\lambda^{light} d\Omega^{obj} \, d\lambda \tag{20}$$

where $dA_{\perp}^{light}$ is the area of the projected surface patch of the light source and $d\Omega^{obj}$ is the solid angle of the illuminated surface patch of the object as seen from the position of the light source.

Now consider the same situation in frame S' in which the object is at rest. The radiant flux on the surface patch of the object is

$$d\Phi' = L'_{\lambda'}\, dA_{\perp}^{obj'} d\Omega^{light'}\, d\lambda' \tag{21}$$

with the projected area $dA_{\perp}^{obj'}$ on the object and the solid angle $d\Omega^{light'}$ of the surface patch of the light source as seen from the position of the object. Using Eqs. (14) and (21), we obtain

$$d\Phi' = \frac{1}{D^5} L_{\lambda}\, dA_{\perp}^{obj'} d\Omega^{light'} d\lambda'$$

With the definition in Eq. (17), the incident irradiance emitted from the small solid angle $d\Omega^{light'}$ onto the surface patch of the object is

$$dE_{\lambda'}^{i'} = \frac{d\Phi'}{dA^{obj'} d\lambda'} = \frac{L_{\lambda}}{D^5} \frac{dA_{\perp}^{obj'}}{dA^{obj'}} d\Omega^{light'} \tag{22}$$

The area $dA^{obj'}$ of the surface patch is related to the projected area $dA_{\perp}^{obj'}$ by

$$dA_{\perp}^{obj'} = dA^{obj'} \cos\alpha' \tag{23}$$

with the angle α' between the surface normal and the incident light.

With Eq. (13), the solid angle $d\Omega^{light'}$ is transformed into the frame S of the light source. Furthermore, $d\Omega^{light'}$ is expressed in terms of the projected area on the light source and of the distance between the light source and the surface patch, as shown in Figure 10:

$$d\Omega^{light'} = D^2\, d\Omega^{light} = D^2 \frac{dA_{\perp}^{light}}{r^2} = dA_{\perp}^{light} \left(\frac{D}{r}\right)^2 \tag{24}$$

The light-like connection of the emission event at the light source and the absorption event at the object has the same direction as the wave vector that describes the photons. Therefore, the distance r is transformed in the same way as the circular frequency ω (see Eq. (2)). By following this reasoning or by explicit Lorentz transformation of the separating vector between the emission event and the absorption event, we get

$$r' = r/D \tag{25}$$

Using Eqs. (22), (23), (24), and (25), we obtain the incident wavelength-dependent irradiance originating from a small area of the light source:

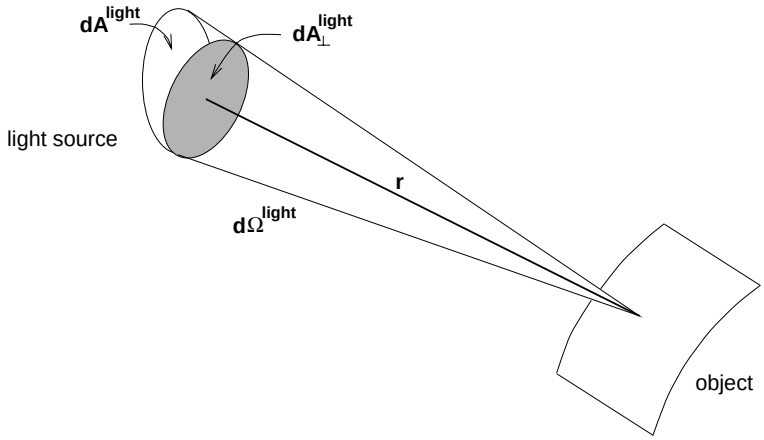

Fig. 10. Geometry of the surface patch of the light source in its rest frame S. The solid angle is given by $d\Omega^{light} = dA_{\perp}^{light}/r^2$. The distance between the light source at emission time and the surface patch of the object at absorption time is denoted r.

$$dE_{\lambda'}^{i'} = \frac{1}{D^5}\frac{\cos\alpha'}{r'^2}L_\lambda \, dA_{\perp}^{light}$$

By integrating over the area of the whole light source, we get the wavelength-dependent irradiance produced by this finite light source:

$$E_{\lambda'}^{i'} = \int \frac{1}{D^5}\frac{\cos\alpha'}{r'^2}L_\lambda \, dA_{\perp}^{light} \tag{26}$$

Now consider a very small, yet finite, light source, described by its wavelength-dependent intensity I_λ. With Eqs. (16) and (20), the wavelength-dependent radiance and the wavelength-dependent intensity from the area $dA_{\perp}^{light}$ are related by

$$dI_\lambda = L_\lambda \, dA_{\perp}^{light} \tag{27}$$

With Eq. (26) and after integrating over the area of the small light source, we find the wavelength-dependent irradiance on the object

$$E_{\lambda'}^{i'} = \int \frac{1}{D^5}\frac{\cos\alpha'}{r'^2}L_\lambda \, dA_{\perp}^{light} = \frac{1}{D^5}\frac{\cos\alpha'}{r'^2}\int L_\lambda \, dA_{\perp}^{light} = \frac{1}{D^5}\frac{\cos\alpha'}{r'^2}I_\lambda$$

This equation even holds for the limit of an infinitesimal light source. Hence we obtain the wavelength-dependent irradiance due to a point light source:

$$E_{\lambda'}^{i'} = \frac{1}{D^5}\frac{\cos\alpha'}{r'^2}I_\lambda$$

Accordingly, the irradiance is

$$E^{i'} = \frac{1}{D^4} \frac{\cos\alpha'}{r'^2} I$$

where I is the intensity of the light source.

REFERENCES

BOAS, M. L. 1961. Apparent shape of large objects at relativistic speeds. *Am. J. Physics 29*, 5 (May), 283–286.

CHANG, M.-C., LAI, F., AND CHEN, W.-C. 1996. Image shading taking into account relativistic effects. *ACM Trans. Graph. 15*, 4 (Oct.), 265–300.

GEKELMAN, W., MAGGS, J., AND XU, L. 1991. Real-time relativity. *Comput. Phys. 5*, 4 (July/Aug.), 372–385.

GRÖNE, A. 1996. Entwurf eines objektorientierten Visualisierungssystems auf der Basis von Raytracing. Ph.D. Dissertation. University of Tübingen, Tübingen, Germany.

HSIUNG, P.-K. AND DUNN, R. H. P. 1989. Visualizing relativistic effects in spacetime. In *Proceedings of the 1989 Conference on Supercomputing* (Reno, NV, Nov. 13–17, 1989), F. R. Bailey, Ed. ACM Press, New York, NY, 597–606.

HSIUNG, P.-K. AND THIBADEAU, R. H. 1990. Spacetime visualization of relativistic effects. In *Proceedings of the 1990 ACM 18th Annual Conference on Computer Science* (CSC ’90, Washington, D.C., Feb. 20–22, 1990), A. Sood, Ed. ACM Press, New York, NY, 236–243.

HSIUNG, P.-K., THIBADEAU, R. H., COX, C. B., DUNN, R. H. P., WU, M., AND OLBRICH, P. A. 1990a. Wide-band relativistic Doppler effect visualization. In *Proceedings of the Conference on Visualization ’90* (Oct. 1990), 83–92.

HSIUNG, P.-K., THIBADEAU, R. H., AND WU, M. 1990b. T-buffer: Fast visualization of relativistic effects in space-time. *SIGGRAPH Comput. Graph. 24*, 2 (Mar. 1990), 83–88.

KRAUS, U. 2000. Brightness and colour of rapidly moving objects: The visual appearance of a large sphere revisited. *Am. J. Physics 68*, 1 (Jan.), 56–60.

LAMPA, A. 1924. Wie erscheint nach der Relativitätstheorie ein bewegter Stab einem ruhenden Beobachter?. *Z. Physik 27*, 138–148.

MCKINLEY, J. M. 1979. Relativistic transformations of light power. *Am. J. Physics 47*, 7 (July), 602–605.

MCKINLEY, J. M. 1980. Relativistic transformation of solid angle. *Am. J. Physics 48*, 8 (Aug.), 612–614.

MØLLER, C. 1972. *The Theory of Relativity*. 2nd ed. Clarendon Press, New York, NY.

PEEBLES, P. J. E. AND WILKINSON, D. T. 1968. Comment on the anisotropy of the primeval fireball. *Phys. Rev. 174*, 5 (Oct.), 2168.

PENROSE, R. 1959. The apparent shape of a relativistically moving sphere. *Proc. Cambridge Philos. Soc. 55*, 137–139.

RAU, R. T., WEISKOPF, D., AND RUDER, H. 1998. Special relativity in virtual reality. In *Mathematical Visualization*, H.-C. Hege and K. Polthier, Eds. Springer-Verlag, Heidelberg, Germany, 269–279.

SCOTT, G. D. AND VAN DRIEL, H. J. 1970. Geometrical appearances at relativistic speeds. *Am. J. Physics 38*, 8 (Aug.), 971–977.

SCOTT, G. D. AND VINER, R. R. 1965. The geometrical appearence of large objects moving at relativistic speeds. *Am. J. Physics 33*, 7 (July), 534–536.

TERRELL, J. 1959. Invisibility of the Lorentz contraction. *Phys. Rev. 116*, 4 (Nov.), 1041–1045.

WEISKOPF, D. 1999. An immersive virtual environment for special relativity. Report Nr. 108, SFB 382. University of Tübingen, Tübingen, Germany. http://www.uni-tuebingen.de/uni/opx/reports/weiskopf_108.ps.gz.

WEISSKOPF, V. F. 1960. The visual appearance of rapidly moving objects. *Physics Today 13*, 9, 24–27.

Received: April 1998; revised: April 1999; accepted: April 1999

D. Weiskopf, D. Kobras, H. Ruder, “Real-world relativity: image-based special relativistic visualization”,
IEEE Visualization 2000, 303–310, © 2000 IEEE, reprinted with kind permission from IEEE

Real-World Relativity: Image-Based Special Relativistic Visualization

Daniel Weiskopf, Daniel Kobras, and Hanns Ruder *

Institute for Astronomy and Astrophysics †
University of Tübingen

Abstract

This paper describes a novel rendering technique for special relativistic visualization. It is an image-based method which allows to render high speed flights through real-world scenes filmed by a standard camera. The relativistic effects on image generation are determined by the relativistic aberration of light, the Doppler effect, and the searchlight effect. These account for changes of apparent geometry, color, and brightness of the objects. It is shown how the relativistic effects can be taken into account by a modification of the plenoptic function. Therefore, all known image-based non-relativistic rendering methods can easily be extended to incorporate relativistic rendering. Our implementation allows interactive viewing of relativistic panoramas and the production of movies which show super-fast travel. Examples in the form of snapshots and film sequences are included.

CR Categories: I.3.3 [Computer Graphics]: Picture/Image Generation—Viewing algorithms I.3.7 [Computer Graphics]: Three-Dimensional Graphics and Realism—Color, shading, shadowing, and texture I.3.8 [Computer Graphics]: Applications—Special relativity J.2 [Physical Sciences and Engineering]: Physics—Theoretical astrophysics

Keywords: image-based rendering, plenoptic function, scientific visualization, special relativity

1 Introduction

Special relativity is widely regarded as a difficult and hardly comprehensible theory, mainly because the properties of space, time, and light in relativistic physics are totally different from those in classical, Newtonian physics. In many respects, they are contrary to human experience and everyday perception, which is based on low velocities.

In the real world, mankind is limited to very slow velocities compared to the speed of light. For example, the speed of light is a million times faster than the speed of an airplane and 40,000 times faster than the speed at which the Space Shuttle orbits the earth. Even in the long term, there is no hope of achieving velocities comparable to the speed of light. Therefore, visualization is the only means of directly exploring the realm of special relativity and may help to stimulate intuition and motivation of people interested in the theory.

There exist well-known rendering techniques for special relativity. However, these methods use a standard geometry-based representation of three-dimensional scenes and hence require time-consuming geometrical modeling and costly rendering. The crucial shortcoming of the geometry-based methods is missing photo-realism. In discussions with editors and producers from TV industry, the demand for relativistic flights through real-world scenes was strongly expressed. Accordingly, special relativistic visualization has not been widely used in professional TV and film productions for edutainment and education yet, although there exist numerous TV documentations about Einstein and his special theory of relativity.

In this paper, we propose a novel image-based approach to special relativistic rendering. This approach overcomes problems of geometry-based rendering and has the following important advantages: No three-dimensional geometric modeling is needed, rendering costs are negligible, and photo-realism is easily achieved.

The basic idea of the image-based approach to relativistic visualization is presented in Sect. 3. We show how all relativistic effects on image generation can be covered by a modification of the plenoptic function[1]. Therefore, the full three-dimensional information about the scene is not required for relativistic rendering. In this framework, only one additional step is appended to the normal non-relativistic rendering pipeline, which is otherwise left unchanged. Hence, the relativistic transformation can easily be incorporated in all known image-based rendering methods.

We present two implementations of image-based relativistic rendering. The first implementation is an interactive panorama viewer which creates snapshots of a panorama with the camera moving at arbitrary speed. The second implementation is a batch job-oriented tool for the production of relativistic movies playing in real-world scenes. It stitches and blends series of views taken by different cameras in order to generate a sequence of images for a relativistic flight.

2 Previous and Related Work

Remarkably, the issue of visual perception in special relativity was ignored for a long time, or wrong interpretations were given. Apart from a previously disregarded article by Lampa[17] in 1924 about the invisibility of the Lorentz contraction, it was only in 1959 that

* {weiskopf,kobras,ruder}@tat.physik.uni-tuebingen.de
† Institute for Astronomy and Astrophysics, Section Theoretical Astrophysics, University of Tübingen, Auf der Morgenstelle 10, D-72076 Tübingen, Germany

the first solutions to this problem were described by Penrose[23] and Terrell[32]. Later, more detailed descriptions of the geometrical appearance of fast moving objects were given by Weisskopf[35], Boas[2], Scott and Viner[29], and Scott and van Driel[28].

Hsiung and Dunn[13] were the first to use advanced visualization techniques for image shading of fast moving objects. They proposed an extension of normal three-dimensional ray tracing. This technique accounts for relativistic effects on the apparent geometry as seen by the observer. Hsiung et al.[14] investigated relativistic ray tracing in more detail and included the visualization of the Doppler effect.

Hsiung et al.[15] introduced the time-buffer for fast visualization of relativistic effects. The time-buffer technique resembles the normal z-buffer and can be mapped onto it. The time-buffer technique allows for relativistic polygon rendering, a scan-line method. It is based on the apparent shapes of objects as seen by a relativistic observer. Gekelman et al.[9] and Chang et al.[3] investigated the polygon rendering approach in detail and gave a comprehensive presentation.

Weiskopf[33] introduced texture-based relativistic rendering for visualizing the apparent geometry of fast moving objects. This approach performs the relativistic transformation on the image plane by texture mapping.

A lot of research has been conducted on the field of non-relativistic image-based rendering. *QuickTime VR*[4] is a well-known method for image-based rendering, which uses panorama pictures. More advanced techniques include plenoptic modeling[20], light fields[18], the lumigraph[12], view morphing[30], and hybrid geometry and image-based rendering[6].

3 Basic Idea

One basic feature of special relativity is the absence of a single universal frame of reference and of a universal time. Any inertial frame is equally valid to describe the physical world.

Often an egocentric point of view is adopted to derive the properties of relativistic rendering, i.e., the camera is at rest and the objects are moving. In this paper, we rather take an exocentric point of view. Here, the objects are considered to be at rest and the observer—the camera—is moving at high speed. In the appendix, the equivalence of both points of view is shown explicitly.

The essence of all image-based rendering methods is the evaluation of the plenoptic function[1]. The full plenoptic function $P(x, y, z, t, \theta, \phi, \lambda)$ is the radiance of the light depending on the direction (θ, ϕ) in spherical coordinates, the spatial position (x, y, z), the time t, and the wavelength λ. The definition of wavelength-dependent radiance can be found, e.g., in [11, Chapt. 13]. Polarization is usually neglected.

We restrict ourselves to a static world, in which all objects and light sources are at rest relative to each other and relative to the objects' frame denoted S_{obj}. In S_{obj}, the plenoptic function can be determined by standard image-based rendering algorithms, since the finite speed of light can be neglected in this static situation.

First, consider the generation of a snapshot taken by a camera at rest in S_{obj}. The spatial position of the camera is (x, y, z) and the time is t. All the information needed for this snapshot is contained in the reduced three-parameter plenoptic function $\tilde{P}(\theta, \phi, \lambda)$, which is evaluated at the respective position and time.

Then, let us bring special relativity back into the game. Consider another observer that is moving relative to the objects. His or her rest frame is denoted S_{observer}. This observer is taking a snapshot at the same position and time as the first observer that is at rest in S_{obj}. What is the plenoptic function for this moving observer and how is it connected to the plenoptic function for the observer at rest?

In general, physical properties can be transformed from one frame of reference to another by the so-called Lorentz transformation. Here, all relevant physical properties are contained in the plenoptic function. Therefore, only the Lorentz transformation of the plenoptic function has to be known. This transformation is discussed in the next section.

Once the plenoptic function $\tilde{P}(\theta, \phi, \lambda)$ with respect to S_{obj} is transformed to $\tilde{P}'(\theta', \phi', \lambda')$ with respect to S_{observer}, the normal rendering process can generate the image seen by the fast moving camera because $\tilde{P}'(\theta', \phi', \lambda')$ is the plenoptic function at rest relative to this camera. (The primed quantities are with respect to S_{observer}.) In this way, all relativistic effects are isolated in the form of the Lorentz transformation of the plenoptic function. The locality property of this transformation allows us to generate relativistic images without knowledge of the depth, or three-dimensional, information about the surrounding scene. Due to the relativity principle the transformation of the plenoptic function can account for both a fast camera and rapidly moving objects.

4 Lorentz Transformation

In this section, the Lorentz transformation of the plenoptic function is described. Relevant for this transformation are the relativistic aberration of light, the Doppler effect, and the searchlight effect. For a detailed presentation of special relativity we refer to [21, 22, 27].

The relativistic aberration of light causes a rotation of the direction of light when one is changing from one inertial frame of reference to another. The aberration of light is sufficient to completely describe the apparent geometry seen by a fast moving camera. Figure 1 illustrates the aberration of light.

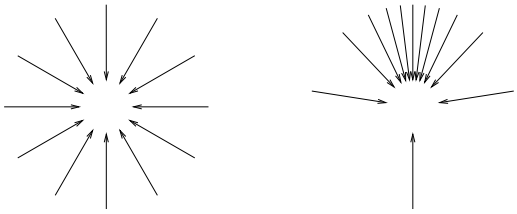

Figure 1: Relativistic aberration of light. The left image shows some of the light rays registered by an observer at rest. The right image shows the same light rays with the observer moving upwards at 90 percent of the speed of light.

The Doppler effect accounts for the transformation of wavelength from one inertial frame of reference to another and causes a change in color.

The searchlight effect is based on the transformation of wavelength-dependent radiance from one inertial frame of reference to another. The transformation of radiance increases the brightness of objects ahead when the observer is approaching these objects at high velocity.

Let us consider two inertial frames of reference, S and S', with S' moving with velocity v along the z axis of S. The usual Lorentz transformation along the z axis connects frames S and S'.

In reference frame S, consider a light ray with the direction (θ, ϕ) and the wavelength λ. In frame S', the light ray is described by the direction (θ', ϕ') and the wavelength λ'. These two representations are connected by the expressions for the relativistic aberration of light, cf. [22],

$$\cos\theta' = \frac{\cos\theta - \beta}{1 - \beta\cos\theta}, \quad (1)$$

$$\phi' = \phi, \quad (2)$$

and for the Doppler effect,

$$\lambda' = D\,\lambda. \tag{3}$$

The Doppler factor D is defined as

$$D = \frac{1}{\gamma(1-\beta\cos\theta)} = \gamma(1+\beta\cos\theta'), \tag{4}$$

where $\gamma = 1/\sqrt{1-\beta^2}$, $\beta = v/c$, and c is the speed of light.

Wavelength-dependent radiance L_λ is transformed from one frame of reference to another according to

$$L'_\lambda(\lambda', \theta', \phi') = D^{-5} L_\lambda(\lambda, \theta, \phi). \tag{5}$$

A derivation of this relation can be found in [34]. Please note that the subscript λ is only attached to indicate wavelength dependency of radiance; it is not a parameter. The proper wavelength parameter is included as a function parameter.

The relativistic aberration of light, the Doppler effect, and the searchlight effect can be combined to form the transformation of the plenoptic function from S to S':

$$\begin{aligned} \tilde{P}'(\theta', \phi', \lambda') &= D^{-5}\tilde{P}(\theta, \phi, \lambda) \\ &= D^{-5}\tilde{P}\left(\arccos\frac{\cos\theta'+\beta}{1+\beta\cos\theta'}, \phi', \frac{\lambda'}{D}\right) \end{aligned} \tag{6}$$

By inverting Eqs. (1)–(3), the parameters θ, ϕ, and λ are substituted by terms containing θ', ϕ', and λ'.

Usually, the direction of motion is not identical to the z axis. Therefore, additional rotations of the coordinate system have to be considered before and after the aberration transformation. These rotations are identical to the standard rotations in three-dimensional Euclidean space. By including these rotations, we obtain the complete Lorentz transformation of the plenoptic function.

With the notation from the previous section, frame S coincides with S_{obj} and frame S' with S_{observer}. Please note that the transformed plenoptic function depends only on the original plenoptic function, the observer's velocity and direction of motion, and the orientations of the two reference frames.

All the information registered by the observer's camera is carried from the surrounding environment to the observer's position via light rays—there is no direct interaction between the camera and the outside objects. The process of image generation is localized at the observer's position, where the actual interaction between the incoming photons and the detector (camera) takes place. In geometric optics, direction, wavelength, radiance, and polarization completely determine the incoming light. The relativistic transformation of the first three quantities is exactly and uniquely described by the aberration, and the Doppler and searchlight effects. Polarization is neglected because it is not registered by standard cameras.

The plenoptic function combines the information about direction, wavelength, and radiance. Accordingly, the Lorentz transformation of the plenoptic function is just the combination of the aberration, and the Doppler and searchlight effects. Bearing the locality of light detection in mind, it can be seen that the transformed plenoptic function provides all the information that is registered by the moving camera. Therefore, the method of this paper generates images which are in total compliance with the physics of special relativity.

5 Relativistic Rendering

Image-based relativistic rendering extends the standard non-relativistic techniques by a transformation of the plenoptic function according to the previous section. This extension is located at the end of the rendering pipeline, just before the final image is generated. All other parts of the rendering pipeline are unaffected.

In the following, some variations of relativistic rendering are described. In particular, we address the issue of missing data, since the wavelength dependency of the plenoptic function cannot be measured by standard cameras. In most cases, data for image-based rendering is acquired by cameras which are sensitive to only three RGB colors and not to the full power spectrum of the incoming light.

5.1 Completely Relativistic Rendering

If the wavelength-dependent plenoptic function $\tilde{P}(\theta, \phi, \lambda)$ is provided in the non-relativistic situation, the transformed plenoptic function $\tilde{P}'(\theta', \phi', \lambda')$ can be computed according to Sect. 4. It is important that $\tilde{P}(\theta, \phi, \lambda)$ is known for an extended range of wavelengths, so that $\tilde{P}'(\theta', \phi', \lambda')$ can be evaluated for wavelengths in the visible range after Doppler-shifting.

Each pixel on the image plane has corresponding spherical coordinates (θ', ϕ'), which are transformed to (θ, ϕ) in the objects' frame. Therefore, each pixel is associated with the wavelength-dependent radiance,

$$L'_\lambda(\lambda') = \tilde{P}'(\theta', \phi', \lambda').$$

For the final display on the screen, three tristimulus values such as RGB have to be calculated from this wavelength-dependent radiance. The RGB values (c_R, c_G, c_B) can be obtained by

$$c_i = \int L'_\lambda(\lambda')\bar{f}_i(\lambda')\,d\lambda', \qquad i = R, G, B,$$

where $\bar{f}_i$ are the respective color-matching functions for RGB, cf. [38].

5.2 Apparent Geometry

The relativistic effects on the apparent geometry can be visualized by using only a partial transformation of the plenoptic function. Here, solely the effects of the aberration of light are taken into account and the searchlight and Doppler effects are neglected, i.e., only the direction (θ, ϕ) of the incoming light is transformed and all other effects are ignored.

This visualization technique is useful when the full spectral information of the plenoptic function is not available, since this information is not needed for the visualization of apparent geometry. Nevertheless, even this restricted relativistic rendering provides some insight into the special theory of relativity and creates impressive visual effects, as shown in Sect. 7.

5.3 Reconstruction of the Power Spectrum

In most cases, data for image-based rendering does not comprise the full power spectrum, but only three RGB values. The power spectrum has to be reconstructed from RGB values in order to include the relativistic effects on geometry and illumination. Unfortunately, this reconstruction is not unique because infinitely many spectra map to one RGB triplet. This phenomenon is called metamerism, cf. [38].

However, a possible spectrum can always be determined and metamerism gives a lot of freedom of doing so. A straightforward approach models the three RGB values by the line spectrum consisting of the corresponding primaries[10]. Sun et al.[31] propose the representation by Gaussian functions with adapted width. Another approach uses Fourier functions[10].

We find the dominant wavelength model[7] useful because it provides a smooth change of color and brightness for a wide range of Doppler factors. The corresponding spectral power distribution consists of a spike at the dominant wavelength and of a uniform distribution, i.e., white light. The luminance and excitation purity determine the levels of the two parts of the spectrum. The parameters for the dominant wavelength model can be computed from RGB values according to [7]. The relativistic situation requires only one slight extension of the original model. Here, the uniform part of the spectrum is not restricted to the range of visible wavelengths, but comprises a larger interval. In this way, the spectrum is still present after Doppler-shifting.

With the reconstructed wavelength-dependent plenoptic function, the algorithm from Sect. 5.1 can generate the fully relativistic image.

5.4 Rendering of a Film Sequence

So far, the generation of just a single snapshot has been described. But how can a film sequence with a fast camera be produced?

In principle, it works the same way as in the non-relativistic situation. The path of the camera is discretized into a finite set of positions. For every element of this set the plenoptic function is evaluated. Therefore, the plenoptic function has to be known at these positions. Then, the relativistic transformation is computed and the corresponding image is generated. Finally, a list of snapshots which represent the film sequence is obtained.

For the film to be physically sound, not only the generation of each single snapshot has to be correct, but also the path of the camera itself. As long as the camera is moving uniformly—at constant speed and with a constant direction of motion—the camera is trivially placed at equidistant positions. However, even an accelerated camera can be described by special relativity. In [26] it is shown how the trajectory of an accelerating observer can be computed. Therefore, the positions and velocities of the camera for each snapshot can be calculated, and image-based relativistic rendering can be performed. This method is valid because the generation of a single image is only determined by the position and velocity of the viewer and by the standard camera parameters, but not by the “history” of the trajectory or the acceleration of the observer.

Our everyday experience is based on length scales in the range of meters, time scales in the range of seconds, and velocity scales in the range of meters per second, i.e., the velocities we are used to are approximately eight orders of magnitude smaller than the speed of light. Length l, time t, and velocity v are related by $v = dl/dt$. Therefore, one has to change the length, time, or velocity scales in order to notice relativistic effects. For example, the time scales could be reduced to the orders of 10^{-8} seconds. We can think of playing a respective recording at super slow-motion, so that we are able to watch processes which involve time spans of only 10^{-8} seconds. Another option is to artificially reduce the speed of light in vacuum, for example, to walking speed. An instructive illustration of reduced speed of light can be found in Mr Tompkins’ world by Gamow[8][1]. In the third approach, length scales are increased to the range of light seconds.

The change of scales is the reason why we can only support static scenes. The real-world camera image is recorded using the true values for the length, time, and velocity scales. In particular, the true speed of light is effectively infinite in all practical situations. The relativistic simulation of a dynamic scene would use images which are instantaneously transported from the object to the camera, instead of the correct, retarded images which take into account the reduced speed of light.

[1] Please note that the illustrations in Mr Tompkins do not show visual perception within special relativity, but only the measurements of Lorentz-contracted lengths.

5.5 Magnification and Anti-Aliasing

The aberration of light does not conserve the element of solid angle. In fact, the infinitesimal solid angle is transformed according to

$$\begin{aligned} \frac{d\Omega'}{d\Omega} &= \frac{\sin\theta'}{\sin\theta}\frac{d\theta'}{d\theta}\frac{d\phi'}{d\phi} = \frac{d(\cos\theta')}{d(\cos\theta)}\frac{d\phi'}{d\phi} \\ &= \frac{d(\cos\theta')}{d(\cos\theta)} = D^2, \end{aligned} \tag{7}$$

with the use of Eqs. (1), (2), and (4).

Therefore, the transformation of the plenoptic function causes a magnification opposite to the direction of motion, whereas objects ahead are scaled down. The demand for a higher resolution towards the back has to be taken into account when the original data for the plenoptic function is acquired. In the rendering process, the sampled data is accessed by bilinear interpolation.

The image contraction for the front view might cause aliasing effects, especially for extremely high velocities. These effects can be reduced by standard supersampling and postfiltering on the image plane.

Since the sampled plenoptic function can be stored in the form of a two-dimensional texture for the coordinates θ and ϕ, antialiasing can alternatively be based on texture filtering techniques. Texture mapping can be considered as the process of calculating the projection of a screen pixel onto the texture image—which is called *footprint*—and computing an average value which best approximates the correct pixel color. There exist a couple of filtering methods, the most prominent of which is MIPmapping[36]. This standard technique supports only a quadratic footprint. Hence, it is not very well suited for our application. The mapping by the aberration equation can generate prolate, anisotropic, and distorted footprints because it substantially changes the angle θ, whereas it leaves the angle ϕ invariant.

Therefore, techniques which support more complex footprints are required. Summed-area tables[5] (SAT), for example, allow prolate rectangular footprints. We have adopted the idea of rectangular axes-aligned footprints for the relativistic situation. In contrast to SAT, we leave out the computation of prefiltered data tables, since each texture is used only once in the rendering process. Filtering provides fair image-quality, even for velocities as high as $\beta = 0.99$ and for images with high spatial frequencies. Respective examples are shown in Sect. 7. The main advantage of a rectangular footprint over more complex footprints is faster computation and rendering.

Fast footprint MIPmapping[16] is based on quadrilateral footprints and makes use of precomputed MIPmaps and weighting tables. Quadrilateral footprints are an improved approximation compared to rectangular axes-aligned footprints. They support anisotropic, rotated, and distorted footprints. Despite the associated complexity, fast footprint MIPmapping should be able to achieve good rendering performance. Its relativistic adaption will be implemented in future work.

6 Implementation

We have implemented the relativistic panorama viewer *Imagine* (IMAge-based special relativistic rendering enGINE), which can read panoramas in the *LivePicture* format[19]. This format is similar to *QuickTime VR*, but uses a spherical projection instead of a cylindrical projection. Therefore, a complete 4π sterad view is supported.

The interactive viewer is written in C++ and is based on standard OpenGL 1.1[37] and *QGLViewer*[24]. The virtual camera is surrounded by a sphere onto which the panorama texture is mapped.

Figure 2: Digital video camera mounted on fork arm.

Texture mapping hardware is used to achieve high rendering performance. The relativistic effects on the apparent geometry are implemented by transforming the texture coordinates according to the relativistic aberration of light. The non-interactive part of the viewer uses software rendering to implement completely relativistic visualization by reconstructing the spectrum according to Sect. 5.3. Texture filtering as described in the previous section is not implemented yet.

Another implementation is *Off-Terdingen*, which is an off-screen, batch job-oriented relativistic movie renderer. It is able to produce movies of relativistic flights through real-world scenes. It is a C++-based software renderer which stitches and blends series of views taken by different cameras in order to generate a sequence of images for a relativistic flight. The parameters and orientations of the cameras are supplied manually. *Off-Terdingen* provides anti-aliasing by means of texture filtering, as described in Sect. 5.5. Additionally, standard supersampling on the image plane can be applied. The data of the original images is accessed by bilinear interpolation.

Adequate data acquisition for the non-relativistic panorama is an issue, since relativistic image-based rendering demands for higher quality of the initial data than standard panorama techniques. First, the resolution of original images has to suffice the magnification by the aberration formula, Eq. (7), when the observer looks into the backward direction. Secondly, a complete 4π sterad panorama should be recorded. Most commercially available panorama systems, however, are based on cylindrical projection, e.g., *QuickTime VR*.

Therefore, we built a camera system which can automatically film a 4π sterad field of view. A standard digital video camera is mounted on a fork arm which was originally designed for a telescope. Figure 2 shows the fork arm with camera. The fork arm is controlled by a mobile computer. Due to the specific geometry of the fork arm the camera can be placed in a way that avoids parallax artifacts when the camera is turned in different directions. The camera system is DV-based. Images are transferred to the mobile computer via IEEE 1394 (Firewire) link. The calibrated image data is stitched by *Off-Terdingen* to render spherical panoramas or relativistic views.

Figure 3: Non-relativistic view.

Figure 4: Relativistic visualization of apparent geometry with $\beta = 0.99$.

7 Results

Figures 3–5 and Color Plates 10–12 provide examples of image-based relativistic rendering. These images were produced by *Off-Terdingen*.

Figures 3–5 show a long corridor. Figure 3 provides the non-relativistic view of the scene. Figure 4 illustrates the effects on apparent geometry when the viewer is rushing into the scene with $\beta = 0.99$. A dominant effect is the increased apparent field of view—the objects seem to move away. Furthermore, straight lines which are perpendicular to the direction of motion become distorted to hyperbolae.

Figure 5 shows completely relativistic rendering with $\beta = 0.3$. Here, the power spectrum is reconstructed by using the dominant wavelength model. Changes in brightness due to the searchlight effect are noticeable. Color changes due to the Doppler effect are present, but cannot be reproduced on the gray-scale image. The searchlight effect heavily brightens the image, so the overall intensity has to be reduced to one half of that in Figs. 3 and 4 in order to avoid extreme clamping of the final gray-scale values.

The pictures on the first page and in Color Plate 10 show the apparent geometry for a snapshot of Yosemite Valley at $\beta = 0.95$. They exhibit the same effects as in Fig. 4, for example the distortion of straight lines to hyperbolae.

Color Plate 11 compares non-relativistic view, apparent geometry, and completely relativistic visualization, analogous to Figs. 3–5. In Color Plate 11(c), the color shift due to the Doppler effect is reproduced and a noticeable blueshift is shown.

Color Plate 12 compares filtering and supersampling techniques. This example shows the visualization of apparent geometry at $\beta = 0.99$. Image 12(a) is rendered without filtering and super-

Figure 5: Completely relativistic rendering with $\beta = 0.3$. The overall intensity is reduced to one half of that in Figs. 3 and 4 in order to avoid extreme clamping of the final gray-scale values.

sampling. Aliasing effects are noticeable, especially on the ceiling. Image 12(b) illustrates filtering with rectangular footprint, as described in Sect. 5.5. Aliasing artifacts are attenuated by texture filtering. In image 12(c), filtering and 2×2 supersampling are combined, yielding a better image quality than mere filtering. This indicates that more sophisticated footprints might improve filtering quality.

The accompanying video presents further examples of relativistic visualization. Here, only the relativistic effects on apparent geometry are taken into account.

The first part of the video shows a relativistic trip across a bridge. This movie was produced with the use of *Off-Terdingen* as well. The recordings of three cameras were stitched together to form the final movie. The film was shown on TV as part of a broadcast on Einstein and special relativity[25]. The first sequence shows the non-relativistic situation. The second sequence presents the relativistic case. The observer accelerates from non-relativistic speed to a maximal velocity of $\beta = 0.9$. In the third sequence, the relativistic and the non-relativistic views are compared. The second part of the video illustrates the interactive relativistic panorama viewer *Imagine*. It was recorded from computer screen during a simulation on an SGI Onyx2 with InfiniteReality graphics board.

8 Conclusion and Future Work

In this paper an image-based approach to special relativistic rendering has been introduced. This approach closes the gap between the well-known non-relativistic image-based techniques and relativistic visualization. We have shown how all relativistic effects on image generation can be covered by a transformation of the plenoptic function. Therefore, only slight modifications of existing rendering methods are required to incorporate the physically correct rendering of super-fast objects.

Photo-realistic images of rapidly moving real-world objects can be generated with great ease. Therefore, image-based special relativistic rendering is a powerful tool to generate movies and snapshots for both edutainment and educational purposes. We have specifically addressed aliasing problems caused by relativistic rendering. We have described supersampling and texture filtering methods to overcome these problems and render high-quality images.

In future work, we will improve the techniques for data acquisition. In particular, we will build a robot-based camera system which can automatically record a sequence of panoramas in order to generate a relativistic film with a large field of view. Resolution and sampling rate will be adapted to the different scalings due to aberration in order to achieve high-quality final pictures. The stitching software will be extended to automatically correct color and brightness variations and small misalignments of the original images. Furthermore, advanced texture filtering techniques will be investigated and implemented.

Acknowledgments

This work was supported by the Deutsche Forschungsgemeinschaft (DFG) and is part of the project D4 within the Sonderforschungsbereich 382. We thank WDR and the Quarks&Co team for their cooperation and the permission to use their material in the accompanying video.

References

[1] E. H. Adelson and J. R. Bergen. The plenoptic function and the elements of early vision. In M. Landy and J. A. Movshon, editors, *Computational Models of Visual Processing*, pages 3–20, Cambridge, 1991. MIT Press.

[2] M. L. Boas. Apparent shape of large objects at relativistic speeds. *American Journal of Physics*, 29(5):283–286, May 1961.

[3] M.-C. Chang, F. Lai, and W.-C. Chen. Image shading taking into account relativistic effects. *ACM Transactions on Graphics*, 15(4):265–300, Oct. 1996.

[4] S. E. Chen. QuickTime VR – An image-based approach to virtual environment navigation. In *SIGGRAPH 95 Conference Proceedings*, pages 29–38, Aug. 1995.

[5] F. C. Crow. Summed-area tables for texture mapping. In *SIGGRAPH 84 Conference Proceedings*, pages 207–212, July 1984.

[6] P. E. Debevec, C. J. Taylor, and J. Malik. Modeling and rendering architecture from photographs: A hybrid geometry and image-based approach. In *SIGGRAPH 96 Conference Proceedings*, pages 11–20, Aug. 1996.

[7] J. D. Foley, A. van Dam, S. K. Feiner, and J. F. Hughes. *Computer Graphics: Principles and Practice*. Addison-Wesley, Reading, Massachusetts, 1990.

[8] G. Gamow. *Mr Tompkins in Paperback*. University Press, Cambridge, 1993.

[9] W. Gekelman, J. Maggs, and L. Xu. Real-time relativity. *Computers in Physics*, 5(4):372–385, July/Aug. 1991.

[10] A. S. Glassner. How to derive a spectrum from an RGB triplet. *IEEE Computer Graphics and Applications*, 9(4):95–99, July 1989.

[11] A. S. Glassner. *Principles of Digital Image Synthesis*. Morgan Kaufmann, San Francisco, 1995.

[12] S. J. Gortler, R. Grzeszczuk, and R. S. M. F. Cohen. The lumigraph. In *SIGGRAPH 96 Conference Proceedings*, pages 43–54, Aug. 1996.

[13] P.-K. Hsiung and R. H. P. Dunn. Visualizing relativistic effects in spacetime. In *Proceedings of Supercomputing ’89 Conference*, pages 597–606, 1989.

[14] P.-K. Hsiung, R. H. Thibadeau, C. B. Cox, R. H. P. Dunn, M. Wu, and P. A. Olbrich. Wide-band relativistic doppler effect visualization. In *Proceedings of the Visualization 90 Conference*, pages 83–92, Oct. 1990.

[15] P.-K. Hsiung, R. H. Thibadeau, and M. Wu. T-buffer: Fast visualization of relativistic effects in spacetime. *Computer Graphics*, 24(2):83–88, Mar. 1990.

[16] T. Hüttner and W. Straßer. Fast footprint MIPmapping. In *Proceedings of the Eurographics/SIGGRAPH workshop on graphics hardware 1999*, pages 35–44, 1999.

[17] A. Lampa. Wie erscheint nach der Relativitätstheorie ein bewegter Stab einem ruhenden Beobachter? *Zeitschrift für Physik*, 27:138–148, 1924. In German.

[18] M. Levoy and P. Hanrahan. Light field rendering. In *SIGGRAPH 96 Conference Proceedings*, pages 31–42, Aug. 1996.

[19] *Live Picture*. Web site: http://www.livepicture.com.

[20] L. McMillan and G. Bishop. Plenoptic modeling: An image-based rendering system. In *SIGGRAPH 95 Conference Proceedings*, pages 39–46, Aug. 1995.

[21] C. W. Misner, K. S. Thorne, and J. A. Wheeler. *Gravitation*. Freeman, New York, 1973.

[22] C. Møller. *The Theory of Relativity*. Clarendon Press, Oxford, second edition, 1972.

[23] R. Penrose. The apparent shape of a relativistically moving sphere. *Proceedings of the Cambridge Philosophical Society*, 55:137–139, 1959.

[24] *QGLViewer*. Web site: http://www.qglviewer.de.

[25] Quarks & Co. Die Relativitätstheorie—Einfach erklärt. Broadcast on 12 November 1999 by German TV station WDR.

[26] R. T. Rau, D. Weiskopf, and H. Ruder. Special relativity in virtual reality. In H.-C. Hege and K. Polthier, editors, *Mathematical Visualization*, pages 269–279. Springer Verlag, Heidelberg, 1998.

[27] W. Rindler. *Introduction to Special Relativity*. Clarendon Press, Oxford, second edition, 1991.

[28] G. D. Scott and H. J. van Driel. Geometrical appearances at relativistic speeds. *American Journal of Physics*, 38(8):971–977, Aug. 1970.

[29] G. D. Scott and R. R. Viner. The geomentrical appearence of large objects moving at relativistic speeds. *American Journal of Physics*, 33(7):534–536, July 1965.

[30] S. M. Seitz and C. R. Dyer. View morphing. In *SIGGRAPH 96 Conference Proceedings*, pages 21–30, Aug. 1996.

[31] Y. Sun, F. D. Fracchia, T. W. Calvert, and M. S. Drew. Deriving spectra from colors and rendering light interference. *IEEE Computer Graphics and Applications*, 19(4):61–67, July/Aug. 1999.

[32] J. Terrell. Invisibility of the Lorentz contraction. *Physical Review*, 116(4):1041–1045, Nov. 1959.

[33] D. Weiskopf. A texture mapping approach for the visualization of special relativity. In *IEEE Visualization 1999 Late Breaking Hot Topics Proceedings*, pages 41–44, 1999.

[34] D. Weiskopf, U. Kraus, and H. Ruder. Searchlight and doppler effects in the visualization of special relativity: A corrected derivation of the transformation of radiance. *ACM Transactions on Graphics*, 18(3):278–292, July 1999.

[35] V. F. Weisskopf. The visual appearance of rapidly moving objects. *Physics Today*, 13(9):24–27, 1960.

[36] L. Williams. Pyramidal parametrics. In *SIGGRAPH 83 Conference Proceedings*, pages 1–11, July 1983.

[37] M. Woo, J. Neider, T. Davis, and OpenGL Architecture Review Board. *OpenGL programming guide: the official guide to learning OpenGL, version 1.1*. Addison-Wesley, Reading, MA, USA, 1997.

[38] G. Wyszecki and W. S. Stiles. *Color Science*. John Wiley & Sons, New York, 2 edition, 1982.

A Equivalence of Exocentric and Egocentric View

One basic feature of special relativity is the absence of a single universal frame of reference and of a universal time. Any inertial frame is equally valid to describe the physical world. Therefore, an egocentric point of view (the camera is at rest and the objects are moving) and an exocentric point of view (the objects are at rest and the camera is moving) are totally equivalent.

Nevertheless, we would like to explicitly show how both points of view can be matched. Only the issues related to the geometrical appearance are discussed. The Doppler and searchlight effects are neglected because they are usually presented in a way equivalent to the exocentric point of view and thus need no further presentation.

A.1 Lorentz Transformation

Events in spacetime are described by four-vectors. A four-vector x^μ consists of one temporal and three spatial coordinates,

$$x^\mu = (x^0, x^1, x^2, x^3) = (ct, x, y, z),$$

where c is the speed of light and $\mu \in \{0, 1, 2, 3\}$.

For an observer moving with velocity $v = \beta c$ along the positive z axis, the four-vector for the same event can be calculated according to the respective Lorentz transformation. The transformed four-vector is

$$x^{\mu\prime} = (\gamma(ct - \beta z), x, y, \gamma(z - \beta ct)), \tag{8}$$

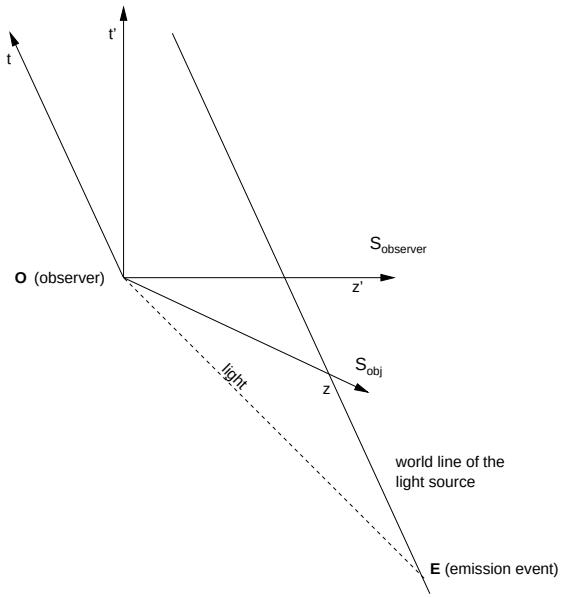

Figure 6: Minkowski diagram for egocentric view.

with $\gamma = 1/\sqrt{1 - \beta^2}$. The inverse Lorentz transformation originates from the Lorentz transformation by substituting β by $-\beta$.

The following considerations are based on relations between the observer's rest frame S_{observer} and the objects' rest frame S_{obj}. Without loss of generality let the origins of the two frame coincide at the event of image production and the observer be moving with β along the positive z axis of S_{obj}. Then, the two frames of reference are related to each other by the above Lorentz transformation. The primed terms are with respect to S_{observer}, the unprimed terms are with respect to S_{obj}.

A.2 Direction of Incoming Light

First, it will be shown that the direction of the incoming light is identical for both points of view. The light emitted by a single point-light source is considered. Figures 6 and 7 show the respective Minkowski diagrams. A Minkowski diagram is a spacetime diagram without the spatial coordinates x and y.

In S_{obj}, the event of light emission is

$$x_E^\mu = (-\sqrt{x_E^2 + y_E^2 + z_E^2}, x_E, y_E, z_E),$$

if the light source is located at the spatial position (x_E, y_E, z_E). The component x_E^0 reflects the time of flight from the emission event to the absorption event at the camera. Alternatively, the emission event can be expressed in spherical coordinates,

$$x_E^\mu = (-r_E, r_E \cos\phi_E \sin\theta_E, r_E \sin\phi_E \sin\theta_E, r_E \cos\theta_E), \tag{9}$$

with $r_E = \sqrt{x_E^2 + y_E^2 + z_E^2}$.

In S_{observer}, the emission event is obtained by the Lorentz transformation,

$$x_E^{\mu\prime} = (-\gamma(r_E + \beta z_E), x_E, y_E, \gamma(z_E + \beta r_E)).$$

The comparison to the analog of Eq. (9) in the observer's frame of reference yields the transformed angles:

$$\cos\theta' = \frac{\cos\theta - \beta}{1 - \beta\cos\theta}, \tag{10}$$

$$\phi' = \phi. \tag{11}$$

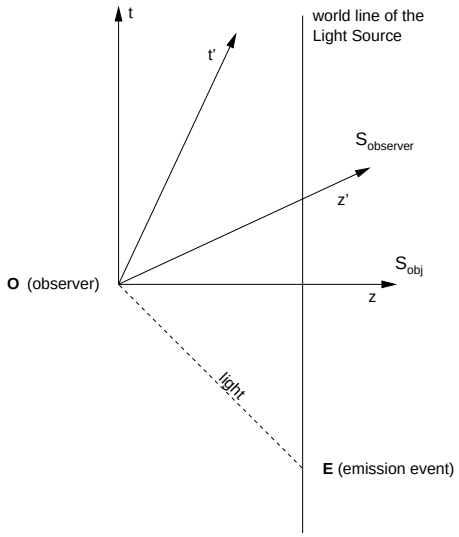

Figure 7: Minkowski diagram for exocentric view.

Therefore, the direction of the incoming light is identical for the egocentric and the exocentric point of view which is based on the aberration equations (1) and (2).

A.3 Visibility

The next concern is the issue of visibility. If one object is hidden by another object in one frame of reference, is it as well hidden in all other frames? Are we allowed to compute visibility in S_{obj} and then use the result in S_{observer}?

Light travels along straight lines in four-dimensional spacetime with respect to every frame. Therefore, the order of emission events along a light ray is independent of the chosen frame of reference and so is the visibility property.

The explicit calculation is as follows. Let us consider two emission events E_1 and E_2. In S_{obj}, let E_2 be hidden by E_1. The respective coordinates are related by

$$x^{\mu}_{E_2} = a\, x^{\mu}_{E_1}, \tag{12}$$

with a constant $a > 1$. With the use of the Lorentz transformation (8), the coordinates of the emission events in S_{observer} follow:

$$x^{\mu}_{E_2}{}' = a\, x^{\mu}_{E_1}{}'.$$

Combined with the fact that the aberration formulae (10) and (11) are invertible, the invariance of visibility under Lorentz transformations is proven. Since the inverse Lorentz transformation is just a Lorentz transformation with opposite direction of motion, the invariance of invisibility is valid for the transformation from S_{observer} to S_{obj} as well.

After all these abstract calculations, how can it be explained that we are able to look “around” relativistic objects and see their back? Figures 8 and 9 clarify the situation for the example of a moving cube. In the egocentric view, Fig. 8, the camera is at rest and the cube is moving with $v = 0.7c$ to the left. The cube is Lorentz-contracted along the direction of motion. Here, the back of the cube becomes visible because the cube outruns the light rays emitted from its back. In the exocentric view, Fig. 9, the cube is at rest and the camera is moving with $v = 0.7c$ to the right. Here, the back of the cube becomes visible because the observer is behind the cube when she or he is registering the incoming light. The rightmost image in Fig. 9 also illustrates the direction of the light ray based on aberration in order to allow a direct comparison to the egocentric view.

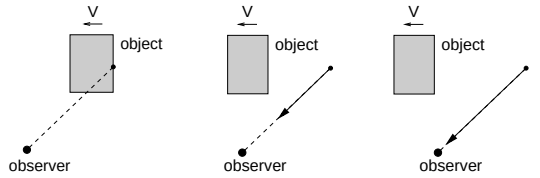

Figure 8: Egocentric view, three snapshots for $\beta = 0.7$.

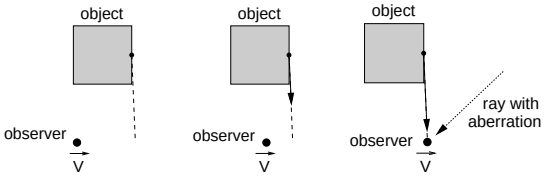

Figure 9: Exocentric view, three snapshots for $\beta = 0.7$.

A.4 Apparent Rotation

The apparent rotation of fast moving objects is closely related to the explanation in the previous section. In the egocentric view, an object seems to be rotated because light emitted from the normally invisible back of the object is outrun by the object and can thus reach the observer. In the exocentric view, the observer is already behind the object and can thus see its back. However, from the observer’s point of view the object seems to still be ahead because of the aberration of the incoming light. Seeing the back side of an object is interpreted as an apparent rotation of the object.

A.5 Summary

We have shown that the egocentric and exocentric view are equivalent with respect to the apparent geometry in special relativistic rendering. The main difficulty in matching both views is to transform all physical components of the system, in particular the position of the observer and the objects.

Usually, the egocentric view is regarded more natural and hence is a widely used model of explanation. In fact, we deem the exocentric view to be more appropriate for the following reasons. First, the exocentric view allows for the transformation of all relevant information about the light field in one operation, as described in Sect. 4. Secondly, an accelerated motion of the observer can be incorporated in the exocentric view without any modification, cf. [26]. Thirdly, the exocentric view better reflects the physical reality. There is no direct interaction between the observer and remote objects. All the information about the surrounding environment is carried to the observer via photons. The generation of a snapshot is based on a local interaction between the photons and the detector (camera). Therefore, it is closer to physics to transform the photons which have reached the observer than to transform emission events far away from the camera.

Figure 10: Flight through Yosemite Valley with $\beta = 0.95$.

(a) (b) (c)

Figure 11: Image (a) shows the non-relativistic view, image (b) the apparent geometry for $\beta = 0.9$, and image (c) completely relativistic rendering with $\beta = 0.2$. The overall intensity in (c) is reduced to 10 percent of that in (a) and (b) to avoid extreme clamping of the final RGB values.

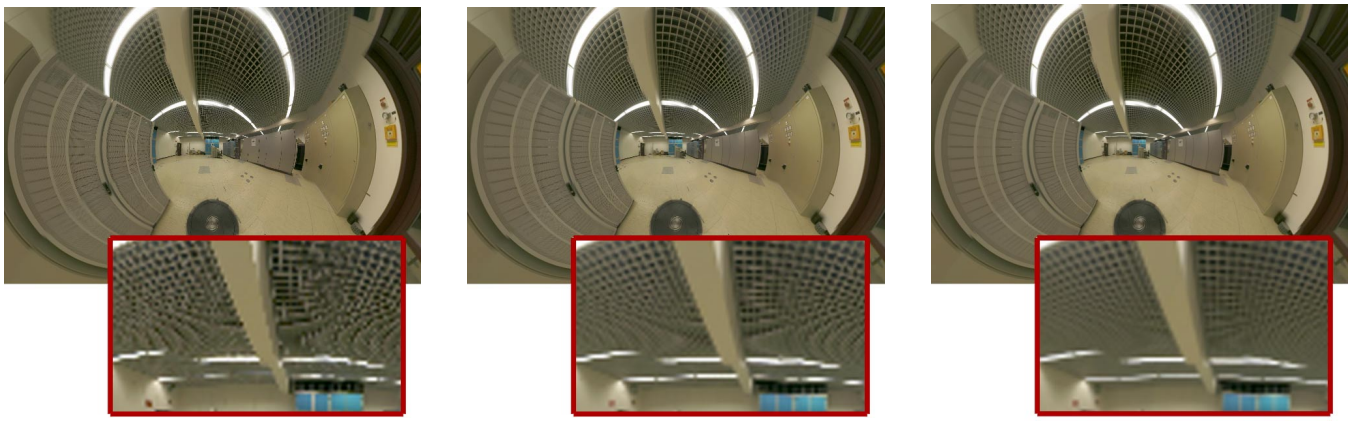

(a) (b) (c)

Figure 12: Comparison of filtering and supersampling techniques for the visualization of apparent geometry at $\beta = 0.99$. Image (a) is rendered without filtering and supersampling, image (b) illustrates filtering with rectangular footprint, and image (c) documents the combination of filtering and 2×2 supersampling.

D. Weiskopf, “Four-dimensional non-linear ray tracing as a visualization tool in gravitational physics”,
IEEE Visualization 2000, 445–448, © 2000 IEEE, reprinted with kind permission from IEEE

Four-Dimensional Non-Linear Ray Tracing as a Visualization Tool for Gravitational Physics

Daniel Weiskopf*

Institute for Astronomy and Astrophysics†
University of Tübingen

Abstract

In this paper, general relativistic ray tracing is presented as a tool for gravitational physics. It is shown how standard three-dimensional ray tracing can be extended to allow for general relativistic visualization. This visualization technique provides images as seen by an observer under the influence of a gravitational field and allows to probe spacetime by null geodesics. Moreover, a technique is proposed for visualizing the caustic surfaces generated by a gravitational lens. The suitability of general relativistic ray tracing is demonstrated by means of two examples, namely the visualization of the rigidly rotating disk of dust and the warp drive metric.

CR Categories: I.3.8 [Computer Graphics]: Applications—General relativity J.2 [Physical Sciences and Engineering]: Physics—Theoretical astrophysics

Keywords: differential geometry, four-dimensional spacetimes, general relativity, ray tracing, scientific visualization

1 Introduction

Within Einstein’s general theory of relativity, gravitation is described geometrically in the form of a four-dimensional curved spacetime which is formulated by the mathematical theory of differential geometry. Light rays are deflected by gravitational sources because of the curvature of spacetime. The bending of light rays can be taken into account by non-linear ray tracing. In this way, images as seen by an observer—a camera—under the influence of a gravitational field can be generated.

The intent of this paper is to show how general relativistic ray tracing can be the basis for various visualization techniques in gravitational physics. First, ray tracing provides an intuitive approach to numerical or analytical results of gravitational physics, which is especially useful for presentations to colleagues or a wider public. Secondly, it allows a systematic investigation of light rays and the underlying geometry of spacetime. Thirdly, fractal structures for light rays can be identified. Fourthly, the properties of a gravitational lens can be explored, especially its caustic structure. The aptitude of these visualization techniques is demonstrated by means of two examples—the rigidly rotating disk of dust and the warp drive metric.

2 Previous and Related Work

In the physics and computer graphics literature, there are some articles concerned with the appearance of objects under the influence of gravitational light deflection. Usually, only well-known metrics are investigated, which are provided in closed form. The first example is the so-called Schwarzschild solution for a spherically symmetric, static distribution of matter. In [16, 7, 14], for example, the appearance of a neutron star or the flight to a black hole are investigated. Gröller[9] gives a generic approach to non-linear ray tracing as a visualization technique. Bryson[4] presents a virtual environment for the visualization of geodesics in general relativity, where examples of the Schwarzschild and Kerr solutions are shown. (The Kerr solution describes the spacetime of a rotating black hole.)

3 Background

In this section, only a very brief overview of the mathematical background of general relativity can be given. For a detailed presentation we refer, e.g., to [13, 19].

A basic concept of differential geometry is the infinitesimal distance ds,

$$ds^2 = \sum_{\mu,\nu=0}^{3} g_{\mu\nu}(\mathbf{x})\, dx^\mu dx^\nu,$$

where $g_{\mu\nu}(\mathbf{x})$ is an entry in a $4 * 4$ matrix—the metric tensor at the point $\mathbf{x}$ in spacetime—and dx^μ is an infinitesimal distance in the μ direction of the coordinate system.

Paths of objects under the influence of gravitation are identical to so-called geodesics. Geodesics are the “straightest” lines in curved spacetime and have extreme lengths. Geodesics are solutions to a set of ordinary second-order differential equations, the geodesic equations,

$$\frac{d^2x^\mu(\lambda)}{d\lambda^2} + \sum_{\nu,\rho=0}^{3} \Gamma^\mu_{\nu\rho}(\mathbf{x}) \frac{dx^\nu(\lambda)}{d\lambda} \frac{dx^\rho(\lambda)}{d\lambda} = 0, \qquad (1)$$

where λ is an affine parameter for the geodesic line. The Christoffel symbols $\Gamma^\mu_{\nu\rho}$ are determined by the metric according to

$$\Gamma^\mu_{\nu\rho}(\mathbf{x}) = \frac{1}{2} \sum_{\alpha=0}^{3} g^{\mu\alpha}(\mathbf{x}) \left(\frac{dg_{\alpha\nu}(\mathbf{x})}{dx^\rho} + \frac{dg_{\alpha\rho}(\mathbf{x})}{dx^\nu} - \frac{dg_{\nu\rho}(\mathbf{x})}{dx^\alpha} \right),$$

with $g^{\mu\alpha}(\mathbf{x})$ being the inverse of $g_{\mu\alpha}(\mathbf{x})$.

This paper is focused on a special type of geodesics which are denoted lightlike or null geodesics. The null geodesics are of great importance because they determine the causal structure of spacetime, i.e., they separate regions which cannot have any causal influence on a given point in spacetime. Light rays are identical to these null geodesics. They obey the null condition

$$g_{\mu\nu}(\mathbf{x}) \frac{dx^\mu(\lambda)}{d\lambda} \frac{dx^\nu(\lambda)}{d\lambda} = 0. \qquad (2)$$

In the ray tracing program, the initial position in spacetime and the initial spatial direction of the light ray are determined by the position, orientation, and field of view of the observer’s camera and by the coordinates of the corresponding pixel on the image plane.

*weiskopf@tat.physik.uni-tuebingen.de

†Institute for Astronomy and Astrophysics, Section Theoretical Astrophysics, University of Tübingen, Auf der Morgenstelle 10, D-72076 Tübingen, Germany

The time component of the initial direction is fixed by the null condition (2). Therefore, the geodesic equations (1) yield an initial value problem for ordinary differential equations. There exist well-known numerical methods for solving this problem, cf., e.g., [17].

A common problem in general relativity is that many terms depend on the chosen coordinate system and do not have a direct physical or geometric interpretation; for example, this is true for the spatial and temporal coordinates or the metric itself. A major advantage of ray tracing is its independence of the coordinate system. The final images are results of a *gedankenexperiment*: What would an observer see, what would a camera measure? Hence, the images have an immediate physical meaning and are coordinate-free.

This paper is focused on visualizing the geometric structure of light rays in a gravitational field. Therefore, only visual distortions due to gravitational light bending are considered. Changes of color due to the Doppler effect and gravitational redshift, as well as changes of the intensity of the incoming light are neglected.

4 General Relativistic Ray Tracing

The implementation of general relativistic ray tracing is based on *RayViS*[10], which is an object-oriented and easily extensible ray tracing program written in C++. In *RayViS*, all relevant parts of the visualization system are derived from abstract basis classes which allow the extension of the original functionality by subclassing.

Figure 1 shows the basic structure of the program. The image plane is sampled by the `Sample Manager` which uses the `Projector` to generate a `Ray` corresponding to the pixel under consideration. The `Ray` communicates with the `Scene` in order to find intersections with scene objects, calculate secondary rays and shadow rays, and determine illumination. Finally, the resulting color is stored in the image by the `Sample Manager`.

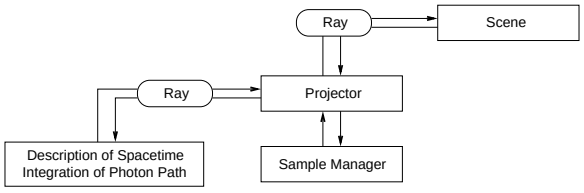

Figure 1: Structure of the ray tracing system.

Relativistic rendering requires two major extensions of the standard three-dimensional Euclidean ray tracing system.

First, the standard ray class which represents a straight light ray in three dimensions is replaced by a class which represents a bent light ray in four dimensions. This bent ray is approximated by a polygonal line whose points possess one temporal and three spatial coordinates.

Secondly, the standard ray projector which generates a light ray corresponding to a pixel on the image plane has to be modified. The new projector provides the interface to the physics of spacetime and communicates with the solver for the geodesic equations (1). This system of ordinary differential equations can be solved by numerical integration. The standard technique in our implementation is the Runge-Kutta method of fourth order[17]. Here, any physical configuration can be examined by replacing the module which supplies the information about the metric and the Christoffel symbols. The advantage of this modular and object-oriented concept is a freedom of choice of the simulated system, combined with a complete, sophisticated rendering environment and only minimal extra implementation costs.

In standard three-dimensional ray tracing, rendering time is significantly determined by the computation of intersections between rays and objects. This is not true for general relativistic ray tracing because here the generation of bent light rays by solving the geodesic equations plays an even more dominant role. Usually, general relativistic ray tracing is a couple of magnitudes slower than non-relativistic ray tracing. Therefore, parallelization is an urgent need for general relativistic ray tracing. Fortunately, the computation of the null geodesics and the ray–object intersections for one pixel is independent of those for the other pixels. Hence, parallelization is performed on a per-pixel basis and utilizes a domain decomposition on the image plane. The granularity can be as fine as a single pixel in order to achieve good load balancing. The implementation makes use of MPI[12] and thus is platform-independent. It scales well, even up to a several hundred nodes on a massive-parallel architecture such as the CRAY T3E.

5 Gravitational Lensing and Caustics

Gravitational fields bend light rays and can thus play the role of a lens—a gravitational lens. Gravitational lensing was early predicted by Einstein himself. In fact, the light deflection measured during the total eclipse of the sun in 1919 was the first experimental evidence for general relativity. Today gravitational lenses are a hot topic in astronomy and are extensively used in observations in various ways. A comprehensive presentation of gravitational lensing can be found in [18].

The main difference between optical lenses and gravitational lenses is that the deflection caused by a typical, spherical convex, optical lens increases with the distance of the ray from the optical axis, whereas the deflection caused by a gravitational lens decreases with the impact parameter. A standard optical lens has a focal point onto which rays parallel to the optical axis are focused. In contrast, a gravitational lens has no focal point. However, the qualitative behavior of a gravitational lens can be described by its caustic surfaces. A gravitational lens might bend light rays in a way that the light emitted by the same source can follow different trajectories to reach the observer, i.e., the light source is projected onto multiple points on the observer’s image plane. A caustic surface separates regions where the image multiplicity changes.

Standard gravitational lensing theory uses a couple of approximations which are valid for most astrophysical objects. For example, only small angles of deflection are allowed, the mass distribution is assumed to be nearly stationary, and the mass of the lens and the image source are considered to be projected onto planes—the lens plane and the source plane, respectively. Based on these approximations, the observed data is normally analyzed to reconstruct the properties of the source or the lens, e.g., its mass distribution.

In this paper, a different approach is pursued. First, image synthesis is used instead of analysis. We aim at visualizing a known gravitational field to gain further insight in its characteristics. Secondly, the approximations from above are dropped and the geodesic equations are completely solved. In this way, one can deal with phenomena related to strong gravitational fields, large angles of deflection, and extended and rotating gravitating objects.

We have studied two means of visualizing gravitational lenses. The first technique directly utilizes general relativistic ray tracing. Here, objects are placed around the gravitational lens as image sources. The mapping of these background objects reveals distortions due to gravitational light deflection and a possible multiplicity of points in the image plane. In this way, it provides some information about the structure of the caustics.

We propose a second technique which targets at a more systematic analysis of the caustic surfaces. The deficiency of the first method is that the background objects are only two-dimensional and thus cannot visualize the caustic surfaces embedded in three-dimensional space. This problem can be overcome by a three-dimensional volumetric object which determines the image mul-

tiplicity for points inside and thus samples the volume for caustic structures.

The procedure is as follows. In *RayViS*, both surface and volume objects are supported. A standard volume object is subclassed to additionally store the number and the initial directions of the light rays crossing a voxel of the object. Whenever a voxel is traversed by a ray, a counter is incremented and the position of the pixel on the image plane corresponding to the current ray is attached to this voxel. In a post processing step, each single voxel is evaluated and the number of rays coming from different areas of the image plane are accumulated. In this way, unintentional counting of nearby rays which cross the same voxel is avoided. The minimal required distance on the image plane is specified by the user; usual values are some ten pixels. Currently, only a regular grid is implemented as a caustic finder.

The scalar field containing the image multiplicities is written to a file and visualized by an external program. There exist numerous techniques for volume visualization. We tested isosurface representations based on the marching cube algorithm, and direct volume rendering based on ray casting or, alternatively, shear warp factorization. Isosurfaces directly indicate a change of multiplicity and thus are useful for representing caustic surfaces. Conversely, volume rendering is able to show several caustic structures embedded in one another. Here, shear warp rendering is mainly used for interactive explorations, whereas the ray casting program provides images of higher quality, as for illustrations.

In contrast to general relativistic ray tracing of the previous section, the caustic finder provides coordinate-dependent data. This might give interpretation problems in regions of high curvature. Therefore, this visualization technique is best suited for almost flat parts of spacetime, for example behind the gravitational lens at adequate distance. High computational and memory costs for a fine sampling of the volume grid are another problem, which could be solved by utilizing an adaptive grid.

6 Application: Rigidly Rotating Disk of Dust

The first application presented in this paper is the visualization of the so-called general relativistic rigidly rotating disk of dust, which is a simple model for a galaxy or a galaxy cluster. This project is joint work with the group for gravitational theory at the University of Jena, in particular, with M. Ansorg.

In 1995, Neugebauer and Meinel[15] from Jena succeeded in finding the global, analytical solution of Einstein’s equations for the gravitational field of a rigidly rotating (i.e., the angular velocity is independent of the radial position) pressure-free ideal fluid disk—the rigidly rotating disk of dust. The researchers in Jena studied the properties of the corresponding geometry of spacetime, for example, by investigating the trajectories of particles[2].

The cooperation between the theoretical relativists from Jena and our visualization group is motivated by the following reasons. First, there is great interest in “seeing” the results of theoretical work in order to gain some intuitive feeling. Secondly, visualization allows a compact representation of a vast number of null geodesics which are used as another means of probing the gravitational field. Thirdly, the communication of the theoretical research to colleagues and to the public should be facilitated.

Results[20] of the cooperation were presented to the relativity community at the Journées Relativistes ’99[11], an international conference on gravitation. The film shown at the Journées Relativistes ’99 is also included in the accompanying video. Several visualization techniques which were applied to the rigidly rotating disk of dust are presented in the following.

6.1 Outside View

The first and straightforward approach to visualizing a given gravitational field is to adopt an outside position. Figure 2 illustrates such an outside view. The three images show the disk with varying parameter μ. This parameter describes the relativistic “character” of the disk. For $\mu = 0$ the Newtonian, non-relativistic limit is obtained, for $\mu \approx 4.6$ the ultra-relativistic limit. The parameter μ is defined in [15].

The left image presents an almost Newtonian, classical situation with $\mu = 0.1$. The top side of the disk is colored blue. An artificial “pie slice” texture is applied in order to visualize rotational distortions. The middle image shows a slightly relativistic case with $\mu = 0.7$. Due to gravitational light bending, both the top and the bottom faces are simultaneously visible. The bottom side is colored green and brown. The right image shows a more relativistic situation with $\mu = 3$. Here, multiple images of the top and the bottom emerge. Moreover, rotational distortions which are caused by frame dragging (a general relativistic effect) and by the finite speed of light and the rotation of the disk are prominent.

The outside view gives a first, intuitive approach to the gravitating object. This visualization technique can easily be used for any metric and provides a coordinate-independent result. Furthermore, it is most useful for presenting the theoretical research to the public. For example, pictures of the rigidly rotating disk of dust were published in a scientific calendar[6].

6.2 Parameter Study

After these first visualization steps a systematic investigation of the properties of the light rays in the metric of the rigidly rotating disk of dust is required in order to obtain reliable scientific results. Therefore, a sampling of the parameter space for the null geodesics has to be considered.

The null geodesics are determined by two types of parameters. Parameters of the first kind describe the gravitational source. The properties of the disk of dust are completely determined by the parameter μ. The position of the observer and the direction of the incoming light constitute parameters of the second kind. The sampling of the direction of the light rays is implemented in the form of a 4π sterad camera, i.e., an observer looking in all directions simultaneously. Here, the projection onto a virtual sphere surrounding the observer is used instead of the standard projection onto an image plane. Therefore, the parameter space is completely sampled by generating 4π sterad images for various values of μ and positions of the observer.

The produced panorama images are viewed with a simple, external, OpenGL-based rendering program which maps these images onto a sphere. The viewpoint is located at the center of the sphere.

The parameter study confirms the qualitative results from the previous subsection, i.e., multiple images of the top and the bottom side and rotational distortions. In addition, new interesting results were found for disks with sufficiently large values of μ. These results are described in the following subsection.

6.3 Fractal Structure

The most interesting finding of the parameter study is the existence of fractal structures created by the gravitational field of the rigidly rotating disk of dust. Figure 3 shows a typical example. Here, the position of the observer and the parameter $\mu = 3$ are fixed. The observer is located on the axis of symmetry and looking towards the edge of the disk. The leftmost picture shows a snapshot with a wide angle field of view. Parts of the top side of the disk are visible in the lower part of the picture. An image of the bottom side is found directly above this first image of the top side. Further above, alternating images of the top and the bottom faces follow. The pictures

to the right document increasing zooming in on the original picture, whereas the rightmost image shows a part of the leftmost image which has a size approximately ten orders of magnitude smaller than the original image. This series reveals self-similarity and a fractal structure.

6.4 Caustics

Figure 4 shows the structure of the caustic surfaces for $\mu = 0.3$, based on the volumetric method from Sect. 5. The regular grid of the caustic finder has a size of 256^3 voxels. The red colors represent regions with many image multiplicities, the green colors represent regions with fewer image multiplicities, and the blue colors show regions with an image multiplicity of one.

7 Application: Warp Drive

The second application presented in this paper is the visualization of the warp drive metric. Alcubierre’s solution[1] of Einstein’s field equations allows to travel faster than the speed of light, as measured in an outside, flat region of spacetime. Ford and Roman[8] give a comprehensible introduction the warp metric and a discussion of some issues related to energy conditions and causality.

Basically, the warp drive constructs a warp bubble which separates two flat parts of spacetime. The warp bubble is able to move faster than the speed of light with respect to an outside, flat region of spacetime. A spaceship which is at rest inside the warp bubble would then travel faster than the speed of light.

The visualization of the warp drive was produced for “Seven Hills”[3]. This exhibition intends to give an inkling of what the future of mankind may look like in the next millennium. A leading-edge topic of physics like the visualization of the warp metric is very well suited for such an exhibition and allows to bring aspects of a complex scientific content to a wide public.

Figure 5 and the accompanying video show examples of the visualization of the warp metric. Here, the warp spaceship travels in front of the earth and moon, and Saturn. The light deflection at its warp bubble causes astonishing visual distortions on the background objects. In addition to this outside view, a position inside the warp bubble can be adopted. Respective images are shown at the exhibition “Seven Hills”. The view from inside the warp spaceship was independently investigated by Clark et al.[5] on a more theoretical footing.

8 Conclusion and Future Work

In this paper, non-linear ray tracing has been presented as a tool for gravitational physics. It has been shown how standard three-dimensional ray tracing can be extended to general relativistic ray tracing. Furthermore, a parallel implementation has been described, which is extremely useful for extensive parameter studies or production of movies.

General relativistic ray tracing offers several important features. First, it gives an intuitive approach to the structure of a gravitational field and allows a simple and straightforward use. Secondly, the generated images are coordinate-independent and can be regarded as the result of an experiment. This is of great importance in the context of general relativity because many properties of spacetime can be hidden by the normally used coordinate-dependent representation. Many other visualization techniques are based on specific coordinate systems, e.g., the visualization of geodesics with respect to pseudo-Euclidean coordinates in [4]. Thirdly, the ray-traced images are a compact representation of a vast number of null geodesics. These null geodesics probe the properties of spacetime, especially its causal structure. Moreover, an extension has been proposed to visualize the caustic surfaces of a gravitational lens.

By means of two applications the usability of general relativistic ray tracing has been demonstrated both for obtaining further insight by the researcher and for presenting results to colleagues and the public.

In future work, the change of color due to the Doppler effect and gravitational redshift, as well as the change of intensity of the incoming light will be implemented. Furthermore, adaptive algorithms and data structures for the caustic finder will be investigated.

Acknowledgments

This work was supported by the Deutsche Forschungsgemeinschaft (DFG) and is part of the project D4 within the Sonderforschungsbereich 382. Thanks to M. Ansorg and D. Moran for their cooperation and the friendly reception in Jena. The production of the warp drive visualization was supported by the Berliner Festspiele GmbH; thanks to R. Bülow for the kindly collaboration.

References

[1] M. Alcubierre. The warp drive: hyper-fast travel within general relativity. *Classical and Quantum Gravity*, 11:L73–L77, 1994.

[2] M. Ansorg. Timelike geodesic motions within the general relativistic gravitational field of the rigidly rotating disk of dust. *Jounal of Mathematical Physics*, 39(11):5984–6000, 1998.

[3] Berliner Festspiele GmbH. *Seven Hills. Images and Signs of the 21st Century.* Exhibition, 14 May to 29 October 2000, Berlin. Web Site: http://www.berlinerfestspiele.de/berlinzweitausend/seven.html.

[4] S. Bryson. Virtual spacetime: An environment for the visualization of curved spacetimes via geodesic flows. In *Proceedings of Visualization ’92*, pages 291–298, 1992.

[5] C. Clark, W. A. Hiscock, and S. L. Larson. Null geodesics in the Alcubierre warp-drive: the view from the bridge. *Classical and Quantum Gravity*, 16:3965–3972, 1994.

[6] Deutsche Forschungsgemeinschaft (DFG). Kalender 2000 (calendar 2000), Bonn, 2000.

[7] T. Ertl, F. Geyer, H. Herold, U. Kraus, R. Niemeier, H.-P. Noller, A. Rebetzky, H. Ruder, and G. Zeller. Visualization in astrophysics. In *Eurographics ’89 Proceedings*, pages 149–158, 1989.

[8] L. H. Ford and T. A. Roman. Negative energy, wormholes and warp drive. *Scientific American*, pages 30–37, Jan. 2000.

[9] E. Gröller. Nonlinear ray tracing: Visualizing strange worlds. *The Visual Computer*, 11(5):263–276, 1995.

[10] A. Gröne. *Entwurf eines objektorientierten Visualisierungssystems auf der Basis von Raytracing*. PhD thesis, University of Tübingen, 1996.

[11] *Journées Relativistes ’99.* International European Conference on Gravitation. Web Site: http://www.tpi.uni-jena.de/tpi/journees-relativistes.html.

[12] *Message Passing Interface Forum*. Web Site: http://www.mpi-forum.org.

[13] C. W. Misner, K. S. Thorne, and J. A. Wheeler. *Gravitation*. Freeman, New York, 1973.

[14] R. J. Nemiroff. Visual distortions near a neutron star and black hole. *American Journal of Physics*, 61(7):619–632, july 1993.

[15] G. Neugebauer and R. Meinel. General relativistic gravitational field of a rigidly rotating disk of dust: Solution in terms of ultraelliptic functions. *Physical Review Letters*, 75:3046, 1995.

[16] H.-P. Nollert, H. Ruder, H. Herold, and U. Kraus. The relativistic “looks” of a neutron star. *Astronomy and Astrophysics*, 208:153, 1989.

[17] W. H. Press, S. A. Teukolsky, W. T. Vetterling, and B. P. Flannery. *Numerical Recipes in C*. Cambridge University Press, second edition, 1994.

[18] P. Schneider, J. Ehlers, and E. E. Falco. *Gravitational Lenses*. Springer, Berlin, 1992.

[19] S. Weinberg. *Gravitation and Cosmology: Principles and Applications of the General Theory of Relativity*. John Wiley & Sons, New York, 1972.

[20] D. Weiskopf and M. Ansorg. Visualization of the general relativistic rigidly rotating disk of dust. *Annalen der Physik*, 9:SI179–SI185, 2000.

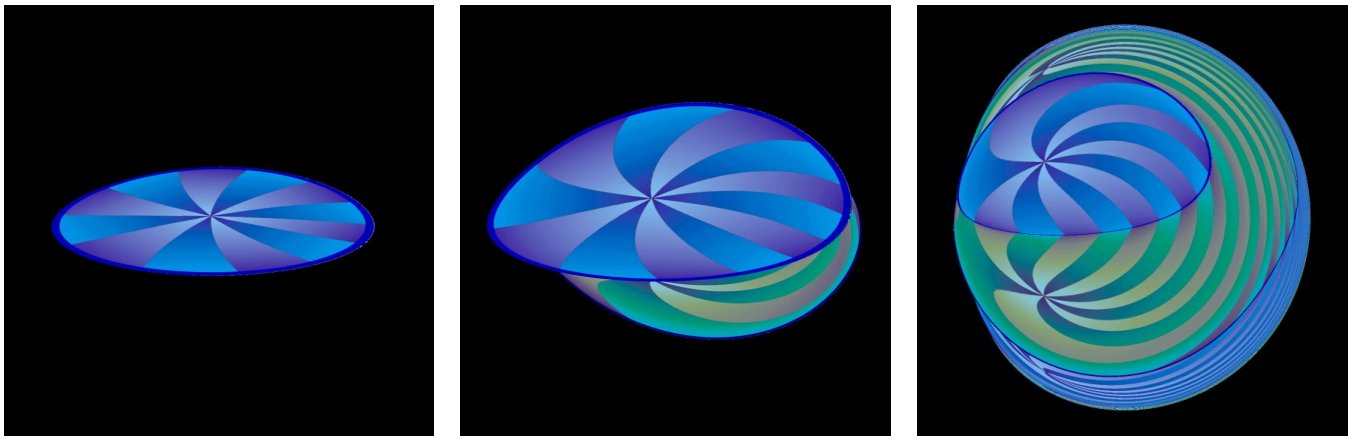

Figure 2: Visualization of the rigidly rotating disk of dust. The relativistic parameter μ is $0.1, 0.7, 3$, from left to right.

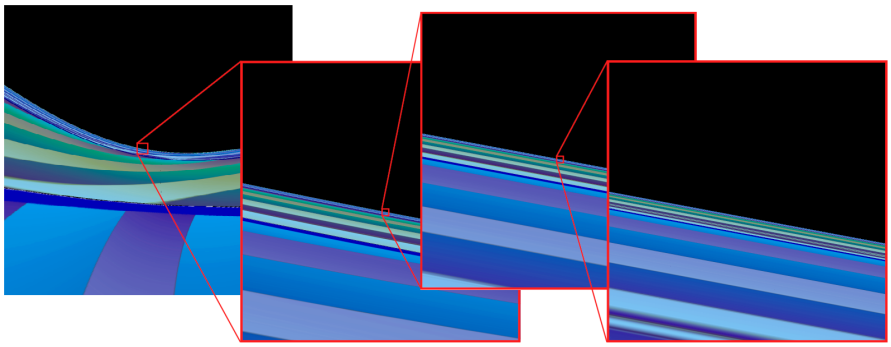

Figure 3: Fractal structures and self-similarity in the gravitational field of the rigidly rotating disk of dust with $\mu = 3$. The observer is located on the symmetry axis and is zooming in on the image.

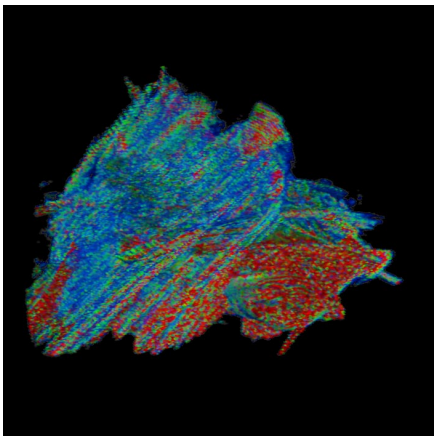

Figure 4: Caustic structure for $\mu = 0.3$.

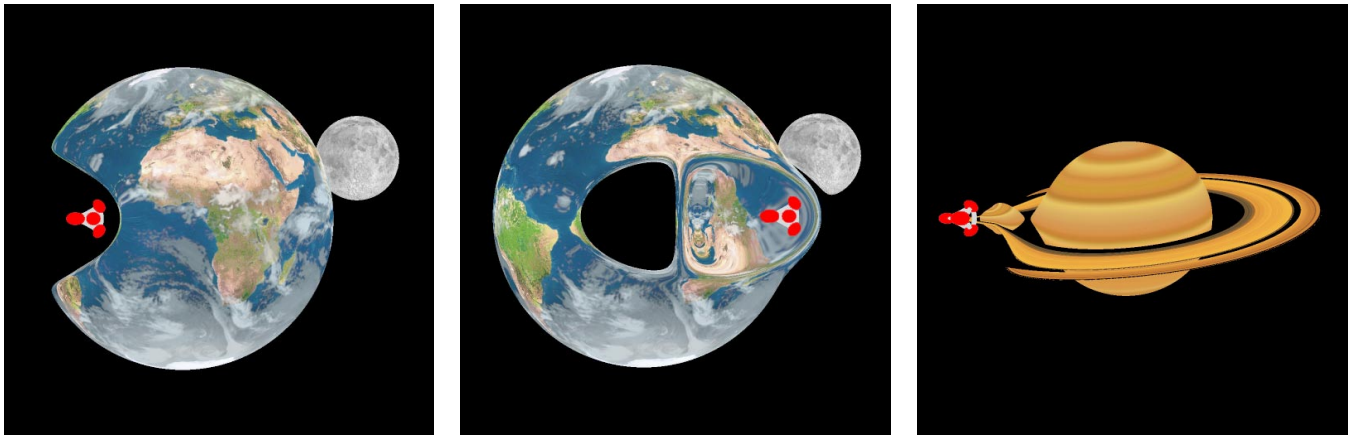

Figure 5: Visualization of the warp metric. The warp bubble and the spaceship are moving at a speed of $v = 1.5c$ in the left and middle image, and $v = 2.5c$ in the right image.

Color Plates

Special Relativistic Flight to Saturn

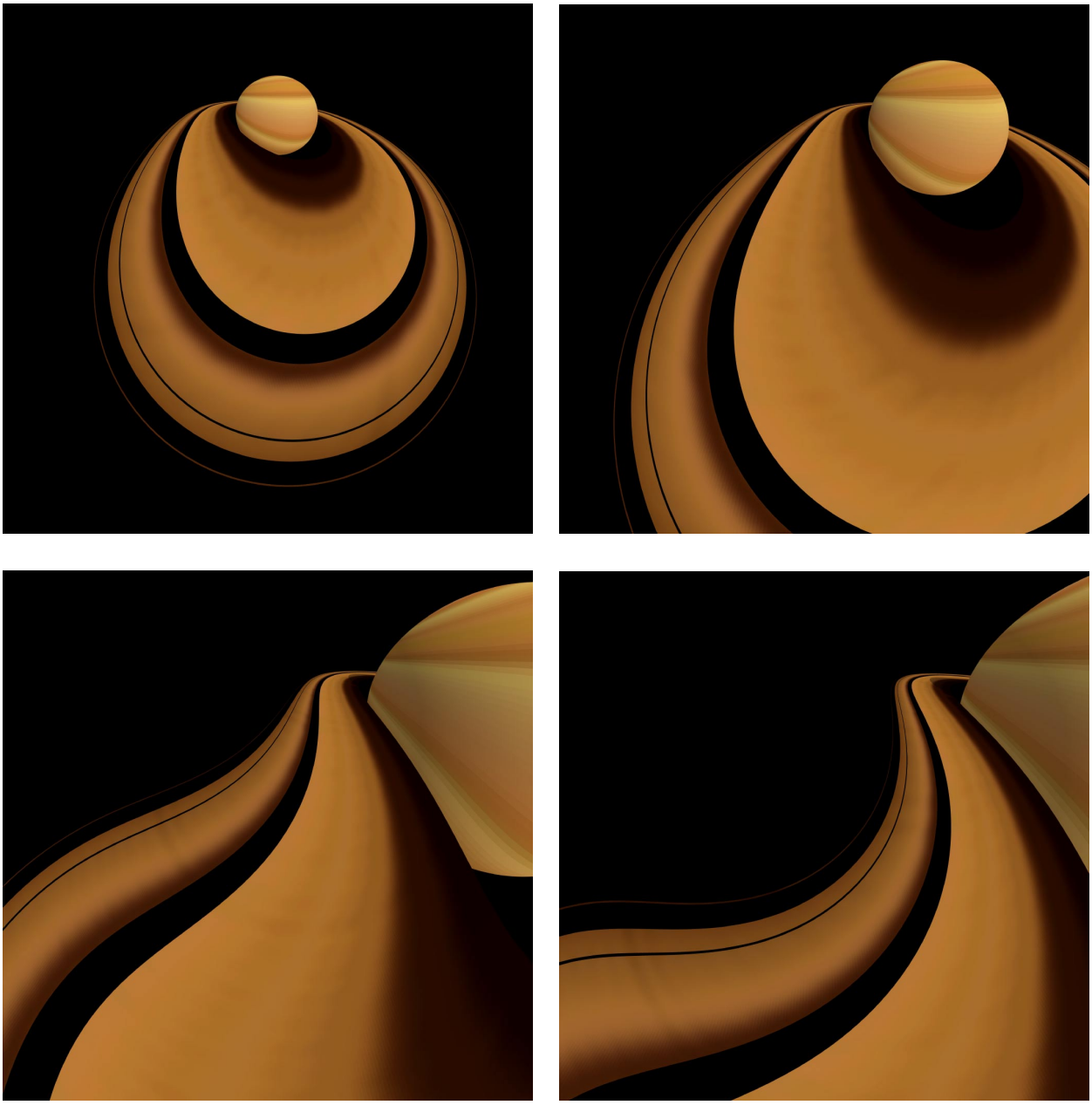

Special relativistic visualization of apparent geometry. The observer is moving at 99 percent of the speed of light.

Special Relativistic Radiosity

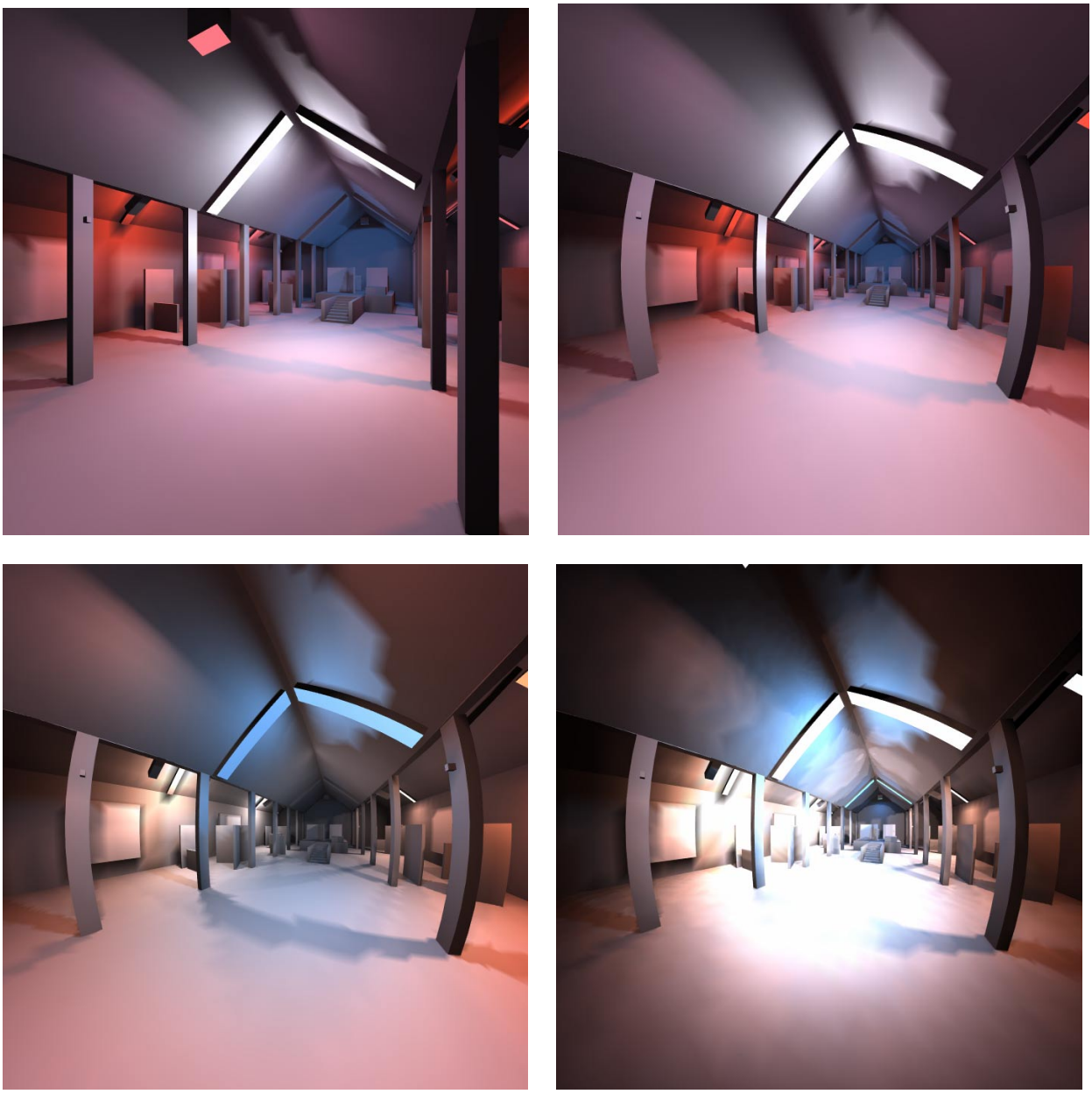

Special relativistic radiosity. The objects are illuminated at temperatures of 2600 Kelvin, 5800 Kelvin, and 15000 Kelvin. The upper left image shows the scene at low speed, the upper right image visualizes apparent geometry at v=0.6c, the lower left image adds the visualization of the Doppler effect, and the lower right image shows completely relativistic rendering. In this last image, the overall brightness is reduced to ten percent of that in the other images.

Special Relativistic Image-Based Rendering

Non-relativistic view

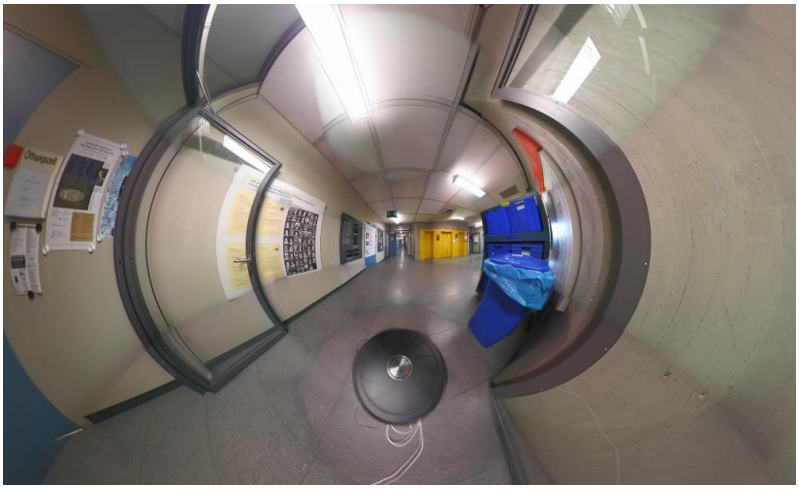

Visualization of apparent geometry. The observer is moving at v=0.99c

Visualization of apparent geometry and illumination. The observer is moving at v=0.3c. Here, the overall brightness is reduced to one half of that in the other images.

Acceleration in Special Relativistic Visualization

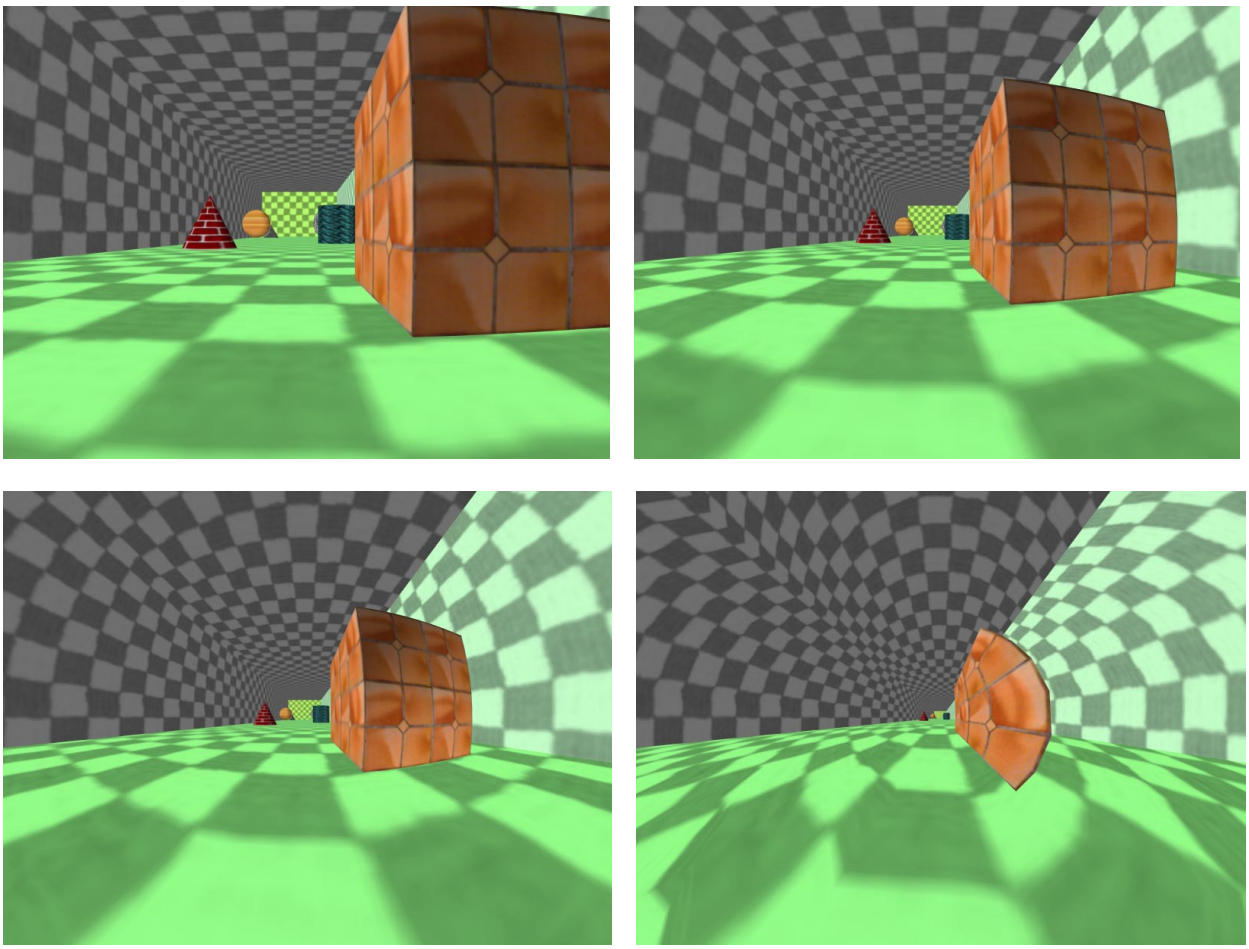

Visualization of an accelerated motion of the camera. From left to right and top to bottom, the speed of the observer is increased from v=0.3c to v=0.623c, v=0.817c, and v=0.975c, respectively.

The “Real” Einstein Ring

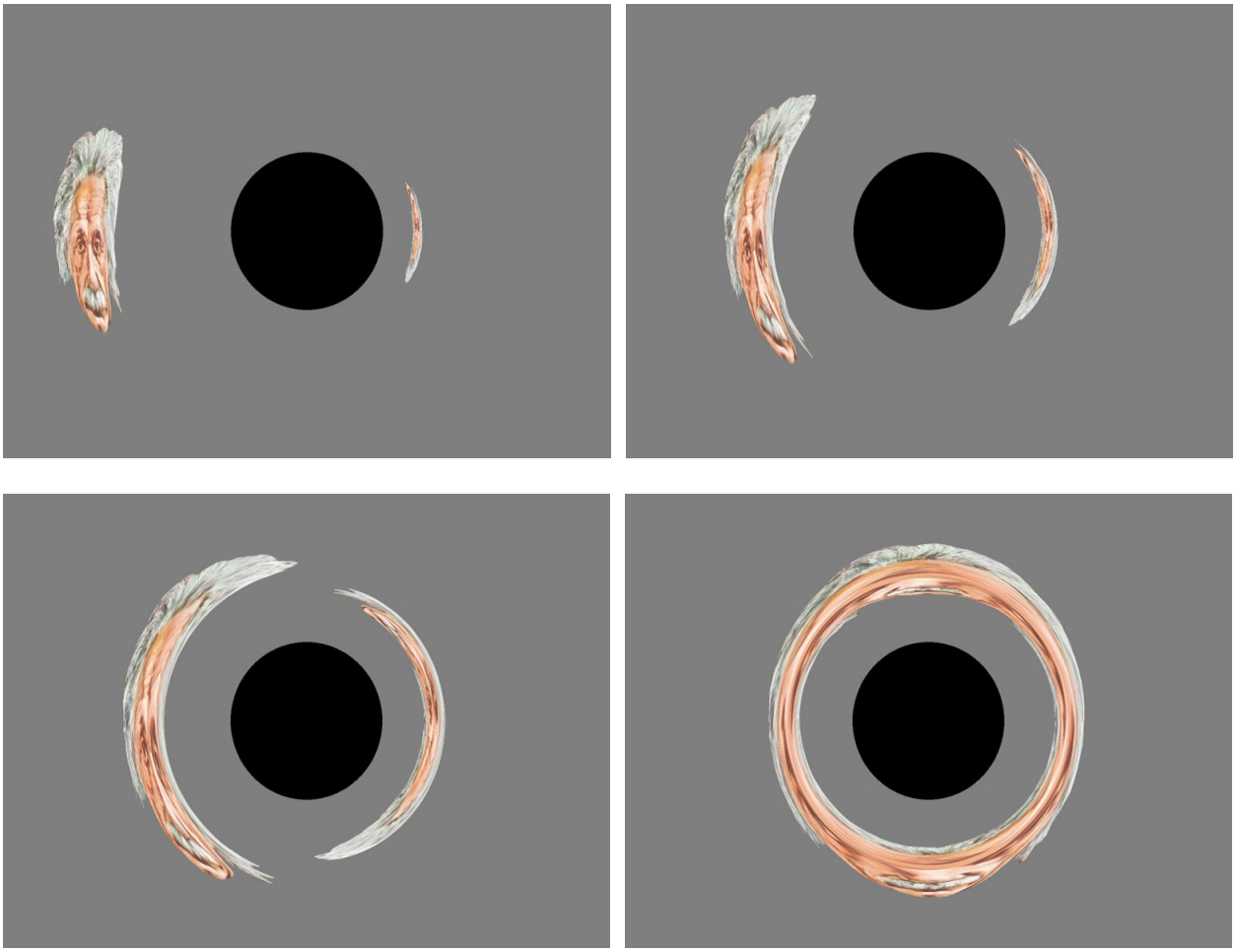

Visualization of the Schwarzschild metric. A portrait of Einstein is moving behind a black hole; due to gravitational light bending, an Einstein ring is generated.

Visualization of the Warp Metric

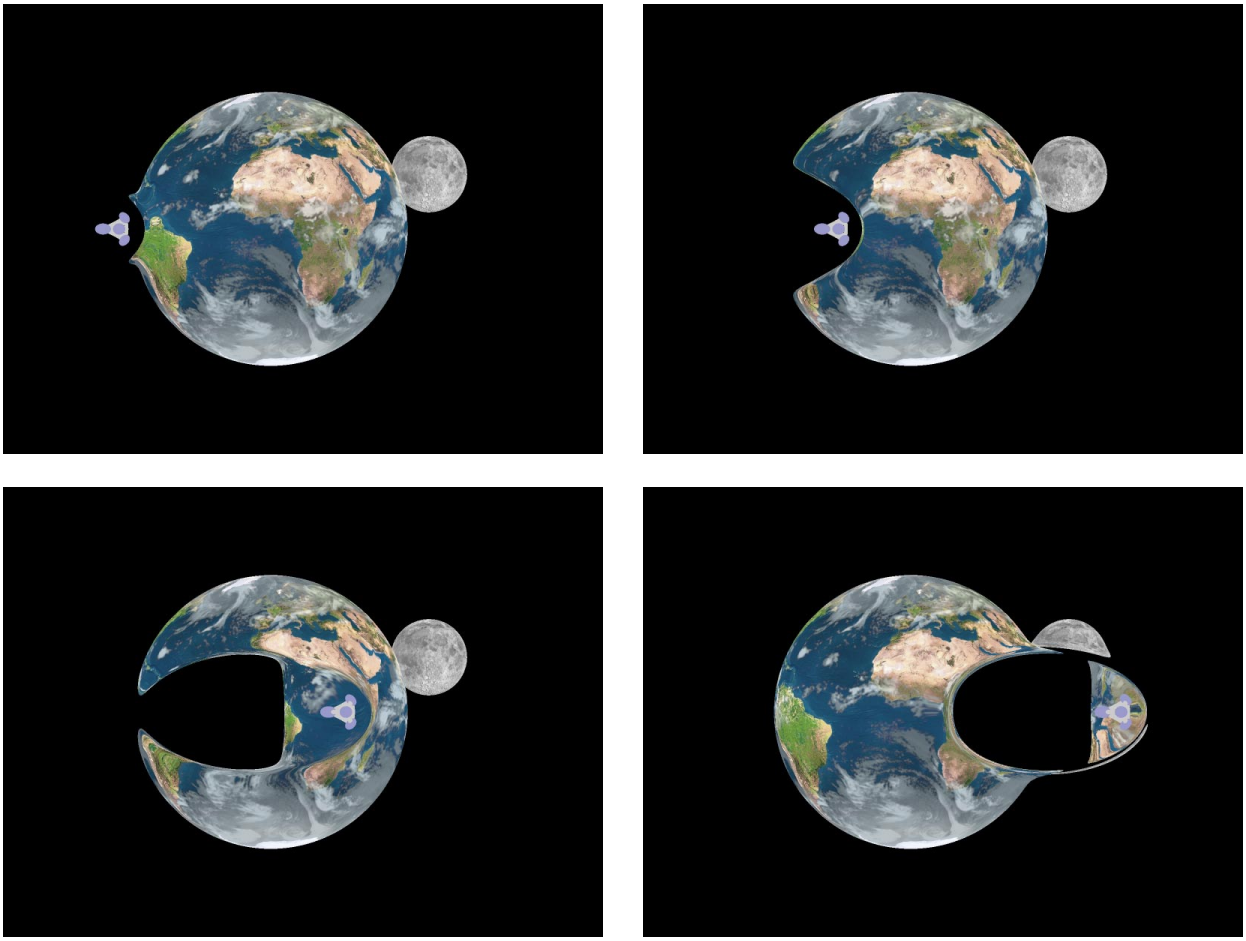

A spaceship is traveling inside a warp bubble at a speed of v=1.5c.

Visualization of the Rigidly Rotating Disk of Dust

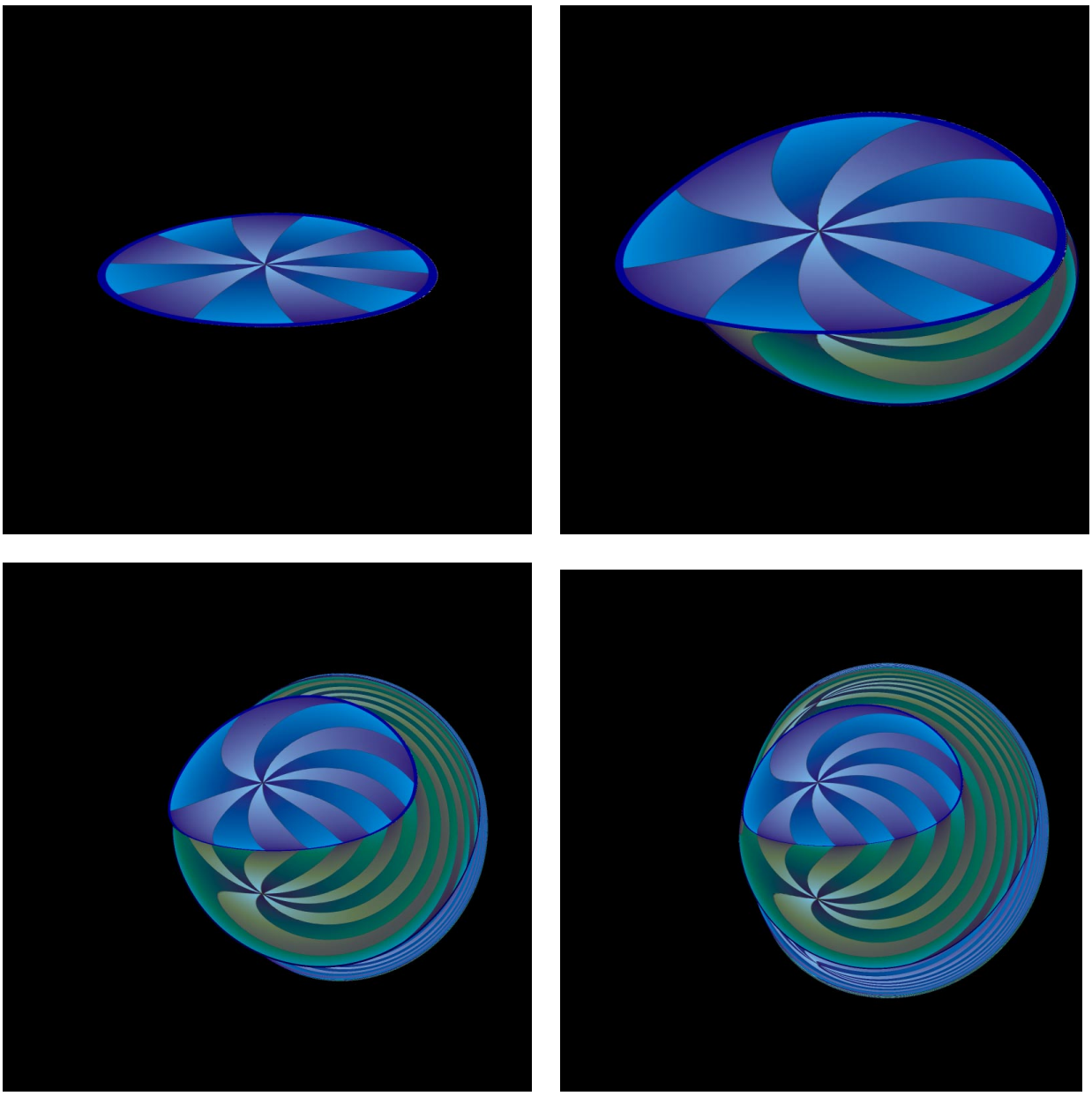

Visualization of the rigidly rotating disk of dust. The relativistic parameter μ is 0.1, 0.7, 2, 3, from left to right and top to bottom. For small values of μ, the Newtonian (classical) limit is obtained. Higher values for μ indicate a more relativistic situation: Multiple images of the top and the bottom side emerge due to gravitational light bending; rotational distortions are caused by frame dragging—a general relativistic effect. Detailed information on the physics of the rigidly rotating disk of dust can be found in: G. Neugebauer, R. Meinel, Phys. Rev. Lett. 75:3046 (1995).